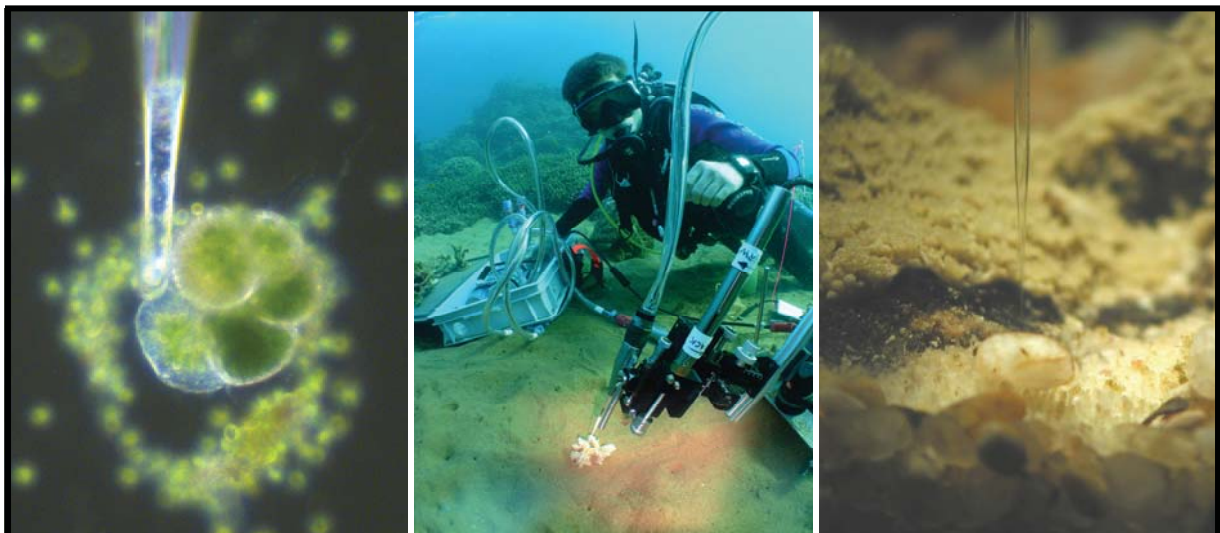# The importance of microgradients for marine calcifiers

Dissertation zur Erlangung des Doktorgrades der

Naturwissenschaften

(Doktor rerum naturalium, Dr. rer. nat.)

dem Fachbereich 2 Biologie / Chemie der Universität Bremen vorgelegt

von Martin Glas,

Bremen, Juli 2012

Die vorliegende Arbeit wurde von September 2009 bis Juli 2012 angefertigt und ist kumulativ verfasst. Die Dissertation wurde in englischer Sprache verfasst. Eine Zusammenfassung in deutscher Sprache ist beigefügt. Der experimentelle Teil der Arbeit besteht aus Kooperationsprojekten mit den folgenden Instituten:

1. Max Planck Institut für Marine Mikrobiologie in Bremen, Bremen, Deutschland
2. Australian Institute of Marine Science, Townsville, Queensland, Australien.
3. Alfred-Wegener-Institut für Polar- und Meeresforschung Bremerhaven, Bremen, Deutschland

Gutacher:

Prof. Dr. Kai Bischof

Dr. Björn Rost

Prüfer:

Dr. Dirk de Beer

Prof. Dr. Thomas Brey

Weitere Mitglieder des Prüfungsausschusses:

Dr. Gertraud Schmidt

B. Sc. Artur Fink

Datum des Promotionskolloquiums: 14.08.2012

Table of contents

Table of contents

Summary

This thesis describes the importance of microgradients around organic tissue of calcifiers in comparison to bulk seawater conditions. The objective of this work was to investigate extracellular microenvironments of marine calcifiers, how the metabolism of calcifiers drives microchemical gradients and how these gradients are coupled via carbonate system changes.

In Chapter 1 the effects of calcification on microenvironments of foraminifera were investigated (Figure 1, blue arrow). Microsensor measurements around calcifying and non-calcifying individuals revealed that calcification strongly decreases microenvironmental pH around these benthic symbiont-free foraminifera (*Ammonia* sp.) for extended periods of time (> 1 h). The foraminifera actively regulate H^+-discharge, thus microenvironmental acidification, to maintain cellular pH homeostasis. The dataset provides for the first time experimental evidence that calcification significantly reduces the pH microenvironment in unicellular calcifying organisms.

Chapter 2 studied the effects of metabolically induced low pH microenvironments on corals and bivalves (Figure 1, red arrows). The chapter illustrates how detrimental microchemical gradients can develop under increased diffusional resistance. It is shown that if detrimental microchemical conditions are trapped close to the tissue of calcifiers, due to the absence of turbulence and increased diffusional resistance, micro-chemical conditions adversely influence calcifiers. The coral disease 'black band disease' (BBD), in comparison to an earlier phase of the lesion termed 'cyanobacterial patch' (CP), traps deleterious micro-chemical conditions, namely low pH, hypoxia, and high levels of sulphide in a micro-volume (< 3 mm distance) at the coral-microbial mat interphase. This results in coral tissue necrosis. Additionally, levels of hypoxia and sulphide linearly correlate with the virulence, i.e. migrations speeds, of the lesions. Hence it was demonstrated, that the microbial mats as a whole, rather than a defined pathogen, create deleterious microchemical conditions that are lethal for the underlying coral tissue. We also measured microchemical dynamics within the enclosed extrapallial fluid (EPF) of the bivalve *Arctica islandica.* This fluid, between the mantle and shell of the bivalve, is hypothesized to be the site of calcification / shell formation in bivalves. However, respiratory input of CO_2 from the surrounding tissue resulted in a continuously low pH, thus carbonate saturation state (Ω) of the EPF. This fluid can therefore not sustain high rates of calcium carbonate precipitation and is not the site of calcification / shell formation as previously hypothesized.

Chapter 3 investigated the effects of bulk seawater carbonate system changes, i.e. 'ocean acidification' conditions, on microchemical O_2, pH and Ca^{2+} dynamics around foraminifera (Figure 1, green arrow). We could show that elevated pCO_2 did not change net photosynthesis of photosymbiotic foraminifera, but resulting H^+-microgradients were significantly enlarged, due to the decreased H^+-buffering-capacity of the seawater. In comparison, symbiont-free species exhibited only very weak O_2 and pH microgradients and microchemical O_2 and pH conditions deviated only marginally from bulk seawater conditions. Neither photosymbiotic nor symbiont-free foraminifera were thus able to compensate for bulk seawater pH decreases within their microenvironments at elevated pCO_2. Hence, foraminifera will most likely experience strongly decreased microenvironmental pH conditions at future pCO_2 concentrations, which makes them quite susceptible to the effects of ocean acidification.
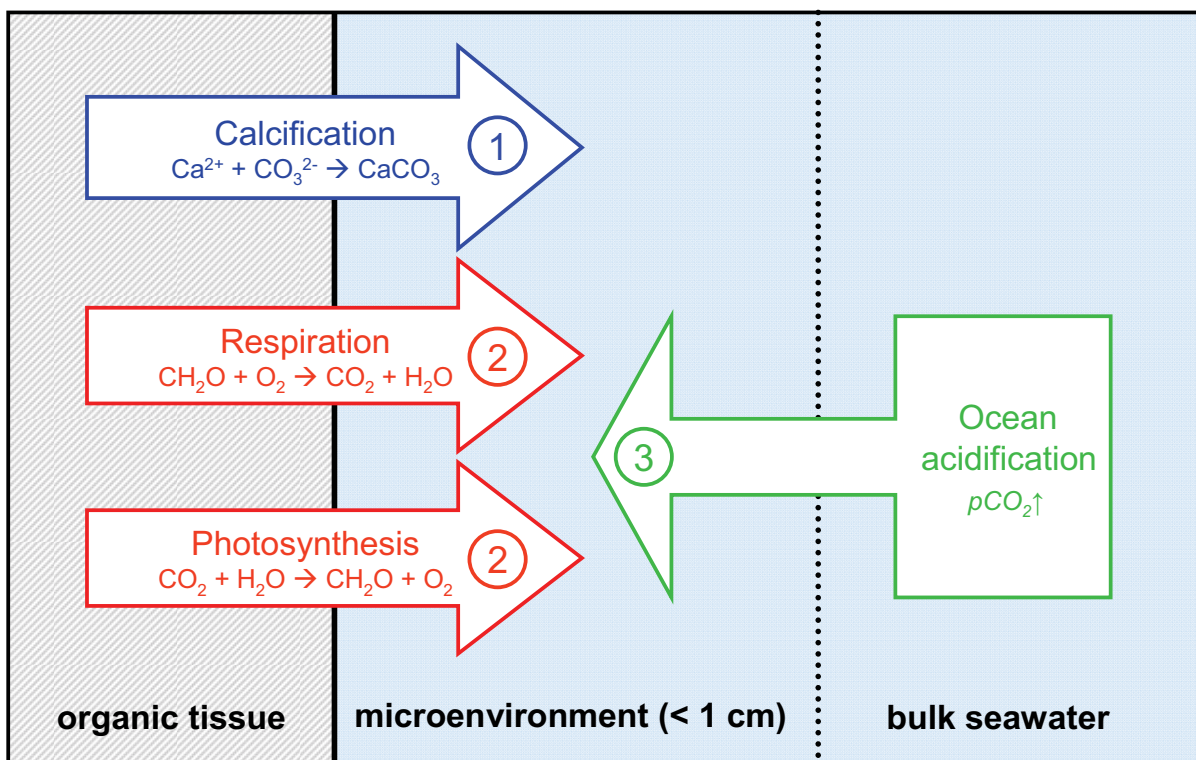
Figure 1: Metabolic and pCO_2 effects on the microenvironments of marine calcifiers. Chapter 1 (blue arrow): effects of calcification on microenvironments. Chapter 2 (red arrows): effects of metabolically induced low pH microenvironments on calcifiers. Chapter 3 (green arrow): ocean acidification effects on microgradients.

The thesis concludes that it is largely the metabolism of calcifiers (Chapter 1-3), rather than bulk seawater carbonate system changes (Chapter 3), which determines microchemical O_2, pH and Ca^{2+} dynamics. Yet, increased pCO_2 levels and ensuing carbonate system changes, are likely to severely alter microenvironmental H^+ concentrations and variability.

It is shown that microenvironmental acidification around calcifiers can result from various causes, such as calcification (Chapter 1), microbial mat or sediment exposure (Chapter 2), respiration (Chapter 2) or ocean acidification conditions (Chapter 3). Some calcifiers, like sediment dwelling foraminifera and bivalves, are naturally adapted to low pH and hypoxic conditions (Chapter 1, 2). Yet, microenvironmental low pH, hypoxia and high levels of sulphide resulted in tissue necrosis of corals, but only if those conditions were trapped close to the tissue of corals for extended periods of time (Chapter 2). The performance of some calcifiers under low pH and hypoxic conditions thus depends upon the duration of the exposure, as well as the diffusional resistance between the bulk seawater and their tissues. If diffusivity around their organic tissues is significantly reduced, some calcifiers may not be able to maintain pH homeostasis and thus severely suffer from extended exposure to low pH, hypoxia and high levels of sulphide (Chapter 2).

Zusammenfassung

Diese Arbeit beschreibt die Bedeutung von Mikrogradienten, welche das organische Gewebe von Kalzifizierern umgeben, vergleichend zu den in der Wassersäule vorherrschenden Bedingungen. Ziel dieser Arbeit war es, extrazelluläre Mikroumgebungen mariner, kalzifizierender Lebewesen zu untersuchen und zu verstehen, inwieweit ihr Metabolismus mikrochemische Gradienten erzeugt und wie diese Gradienten durch Änderungen des Karbonat-Systems gekoppelt sind.

In Kapitel 1 wurden die Auswirkungen der Kalzifizierung auf die Mikroumgebungen von Foraminiferen untersucht (Abbildung 1, blauer Pfeil). Mikrosensor Messungen rund um kalzifizierende und nicht kalzifizierende Individuen ergaben, dass Kalzifizierung den pH-Wert in der Mikroumgebung benthischer, symbiont-freier Foraminiferen (*Ammonia* sp.) für längere Zeit (> 1 h) stark senkt. Die Foraminiferen regulieren die Ausstoßung von H^+, und somit die Ansäuerung ihrer Mikroumgebung aktiv, um zelluläre pH-Homeostase aufrecht zu erhalten. Der Datensatz liefert zum ersten Mal experimentellen Nachweis dafür, dass Kalzifizierung den pH-Wert in der Mikroumgebung von einzelligen, kalzifizierenden Organismen signifikant reduziert.

Kapitel 2 untersuchte die Auswirkungen von metabolisch induzierten, niedrigen pH-Mikroumgebungen auf Korallen und Muscheln (Abbildung 1, rote Pfeile). Das Kapitel veranschaulicht wie sich, unter stark erhöhtem Diffusionswiderstand, für Kalzifizierer nachteilige, mikrochemische Gradienten entwickeln können. Es wird gezeigt, dass, wenn nachteilige mikrochemische Bedingungen nahe dem Gewebe kalzifizierender Lebewesen aufgrund fehlender Turbulenz und erhöhtem Diffusionswiderstand stabil gehalten werden, diese stark auf die Kalzifizierer rückwirken. In der Korallenkrankheit ‚black band disease' (BBD), im Gegensatz zu einer Vorstufe der Läsion welche ‚cyanobacterial patch' (CP) genannt wurde, werden schädliche mikrochemische Bedingungen, nämlich niedriger pH-Wert, Hypoxie, und ein hohes Maß an Sulfid in einem Mikrovolumen (< 3 mm Abstand) an der Grenzschicht zwischen der Koralle und der mikrobiellen Matte festgehalten. Dies führt zur Nekrose des Korallengewebes. Auch korrelieren Zunahme von Hypoxie und Sulfidkonzentration positiv linear mit der Virulenz, d.h. der Ausbreitungsgeschwindigkeit der Läsionen. Somit konnte gezeigt werden, dass die mikrobiellen Matten als Ganzes - anstatt eines einzelnen Erregers – schädliche, mikrochemische Bedingungen erzeugen, welche tödlich für das darunter liegende Korallengewebe sind. Wir haben auch mikrochemische Dynamiken innerhalb des eingeschlossenen, extrapallialen Fluids der Muschel *Arctica islandica*, untersucht. Man nimmt an, dass diese Flüssigkeit, welche sich zwischen dem

Mantel und der Schale der Muschel befindet, den Ort der Schalenbildung, d.h. der Kalzifizierung darstellt. Jedoch führt der Eintrag von CO_2 aus der Atmung des umgebenden Gewebes, zu einem dauerhaft niedrigen pH-Wert, und somit Karbonat-Sättigungszustand (Ω) des EPFs. Diese Flüssigkeit kann daher keine hohen Fällungsraten von Kalziumkarbonat aufrechterhalten und ist somit nicht, wie bisher angenommen, der Ort an welchem Kalzifizierung, bzw. die Schalenbildung stattfindet.
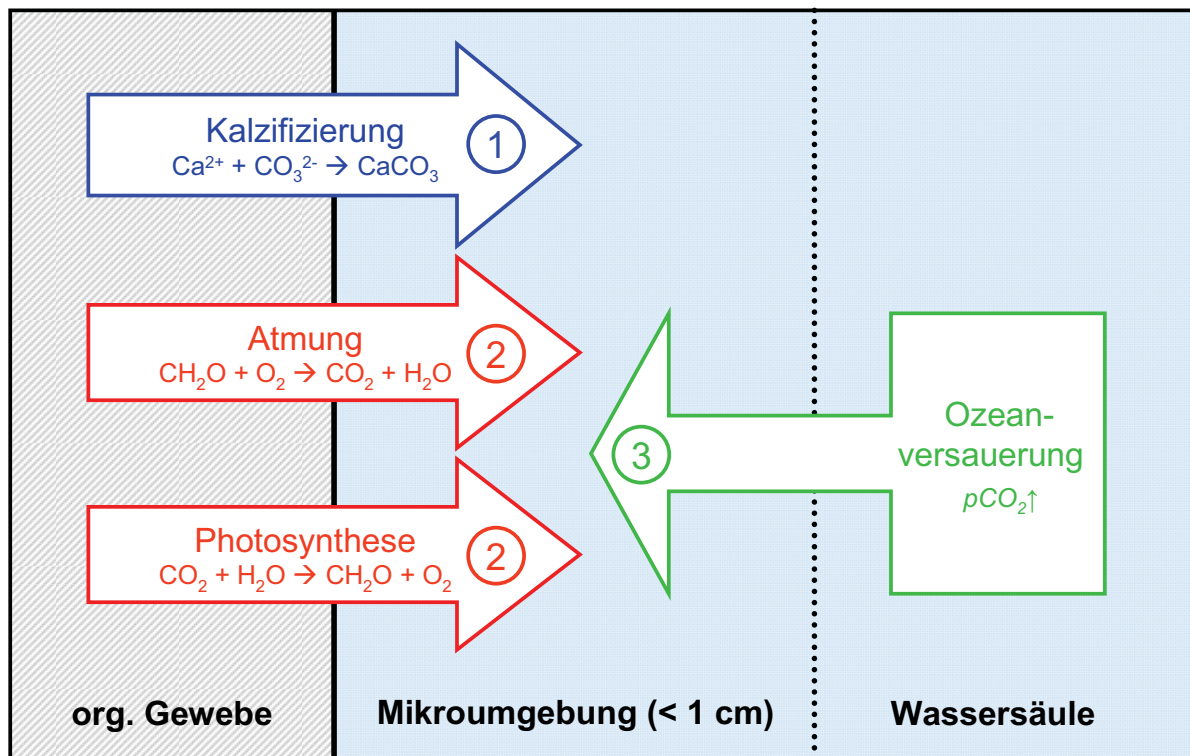
Abbildung 1: Stoffwechsel und *pCO$_2$* Effekte auf die Mikroumgebung mariner Kalzifizierer. Kapitel 1 (blauer Pfeil): Auswirkungen der Kalzifizierung auf Mikroumgebungen. Kapitel 2 (rote Pfeile): Auswirkungen von metabolisch induzierten, niedrig-pH Mikroumgebungen auf Kalzifizierer. Kapitel 3 (grüner Pfeil): Auswirkungen der Ozeanversauerung auf die Mikrogradienten.

Kapitel 3 untersucht Auswirkungen von Karbonat-System Veränderungen - genauer gesagt von 'Ozeanversauerungsbedingungen' - innerhalb der Wassersäule auf mikrochemische O_2, pH und Ca^{2+} Dynamiken rund um Foraminiferen (Abbildung 1, grüner Pfeil). Wir konnten zeigen, dass erhöhte *pCO$_2$* Bedingungen die Netto-Photosyntheserate photo-symbiontischer Foraminiferen nicht verändert. Die daraus resultierenden H^+-Mikrogradienten verstärkten sich jedoch signifikant, aufgrund der verringerten H^+-Pufferkapazität des Meerwassers unter erhöhten *pCO$_2$* Bedingungen. Im Vergleich dazu waren die O_2 and pH Mikrogradienten um symbiont-freie Arten herum nur sehr schwach ausbildet. Mikrochemische O_2 und pH Bedingungen wichen daher nur geringfügig von den

Konzentrationen innerhalb der Wassersäule ab. Weder photo-symbiontische noch symbiont-freie Foraminiferen sind somit in der Lage, erniedrigte pH-Bedingungen aufgrund des erhöhtem pCO_2 Gehalts, durch ihre Mikroumgebung zu kompensieren. Somit werden Foraminiferen unter zukünftigen pCO_2 Bedingungen höchstwahrscheinlich auch stark erniedrigte pH-Werte innerhalb ihrer Mikroumgebung erfahren, was sie sehr anfällig für Auswirkungen der Ozeanversauerung macht.

Die Studie kommt zu dem Schluss, dass es weitestgehend der Stoffwechsel von Kalzifizierern ist (Kapitel 1-3), welcher die mikrochemischen O_2, pH und Ca^{2+} Dynamiken bestimmt und nicht Änderungen des Karbonatsystems der Wassersäule (Kapitel 3). Jedoch ist es wahrscheinlich, dass erhöhte pCO_2 Bedingungen und die damit verbundenen Veränderungen des Karbonat-Systems, die H^+ Konzentrationen sowie ihre Variabilität innerhalb der Mikroumgebung stark verändern werden.

Es wird gezeigt, dass die Mikroumgebungen mariner Kalzifizierer aufgrund verschiedener Ursachen einen erniedrigten pH-Wert besitzen können – genannt werden beispielsweise Kalzifizierung (Kapitel 1), Kontakt mit mikrobiellen Matten oder Sedimenten (Kapitel 2), Atmung (Kapitel 2) oder Ozeanversauerungsbedingungen (Kapitel 3). Einige Kalzifizierer, wie Sediment bewohnende Foraminiferen oder Muscheln, sind natürlicher Weise an erniedrigte pH Bedingungen und Hypoxie angepasst (Kapitel 1, 2). Jedoch führten erniedrigter pH, Hypoxie und hohe Sulfidkonzentrationen in der Mikroumgebung von Korallen zum Absterben des Gewebes. Dies jedoch nur, wenn diese Bedingungen aufgrund erhöhten Diffusionswiderstands in der Nähe des Gewebes für längere Zeit stabil gehalten wurden (Kapitel 2). Die Fähigkeit einiger Kalzifizierer, unter erniedrigten pH Bedingungen sowie Hypoxie zu bestehen, hängt somit sowohl von der Dauer der Exposition, als auch den bestehenden Diffusionswiderständen zwischen der Wassersäule und ihrem Gewebe ab. Wenn die Diffusivität um organisches Gewebe herum stark reduziert ist, sind einige Kalzifizierer nicht mehr in der Lage pH Homeostase zwischen ihrem Gewebe und der umliegenden Wassersäule aufrecht zu erhalten und leiden somit stark unter länger anhaltendem, niedrigem pH, Hypoxie und hohen Sulfidkonzentrationen (Kapitel 2).

Danksagung

Abbreviations, acronyms and symbols

ADP	= adenosine diphosphate
AMP	= adenosine monophosphate
atm	= atmosphere (= 1.01325×10^5 Pa)
ATP	= adenosine triphosphate
BBD	= black band disease
CA	= carbonate alkalinity
CCA	= crustose coralline algae
CCD	= carbonate concentration depth
CCM	= carbonate concentration mechanism
$CO_{2(aq)}$	= dissolved fraction of CO_2
CO_2SYS	= program for CO_2 system calculations
CP	= cyanobacterial patch
DBL	= diffusive or diffusion boundary layer
DBS	= delimited biomineralization space
DIC	= dissolved inorganic carbon
ENSO	= El Nino-Southern Oscillation
EPF	= extrapallial fluid
GLM	= generalized linear model
H^+	= concentration of all hydrated proton forms
HC	= hard corals
IM	= intermediate / transition stage between BBD and CP
IPCC	= Intergovernmental Panel on Climate Change
LC50	= median lethal concentration
LGM	= last glacial maximum
LIX	= liquid ion exchange (microelectrodes)
OA	= ocean acidification
OPE	= outer protective envelope
PAR	= photosynthetic active radiation
pCO_2	= partial pressure of CO_2
PETM	= Paleocene–Eocene Thermal Maximum
PIC	= particulate inorganic carbon
POC	= particulate organic carbon
POS	= primary organic sheet
ppm	= parts per million
SC	= soft corals
SD	= standard deviation of the mean
SE	= standard error of the mean
SOM	= supplementary online material
SRB	= sulphate reducing bacteria
SRM	= standard metabolic rate
t_{90}	= time it takes a system to reach 90 % of the steady state signal
TA	= total alkalinity
WSRT	= Wilcoxon signed rank test
Z_δ	= thickness of diffusive boundary layer
α	= CO_2 solubility coefficient
Ω	= carbonate saturation state

Introduction

Introduction

This thesis focuses on processes, such as photosynthesis, respiration or calcification, affecting extracellular microenvironments of marine calcifiers. Organisms that were used to study these processes included various taxa such as foraminifera, corals, microbial mats, bivalves and crustose coralline algae (CCA). The introduction will therefore address the unifying concepts, rather than the specific metabolic mechanisms of the different studied organisms, as this would divert from the leading themes (Chapters) and go beyond the scope of this thesis. These unifying concepts of microenvironments, diffusive boundary layers (DBLs), seawater carbonate chemistry, as well as the significance of calcifiers in the global carbon cycle and the associated problem of ocean acidification are introduced in this chapter in more detail. Since microsensors represented the major experimental tools used in this work, a short methodological introduction about microsensors is given.

1. Microgradients form microenvironments

The term 'microenvironment' is not uniformly defined in the literature. In this thesis the term microenvironment is defined as a small, extracellular volume around organic tissue, distinguished from the surrounding seawater by its strong physicochemical gradients, such as analyte concentration-, flow- or light-gradients. These microgradients often differ profoundly from the conditions in the water column. Commonly, the microenvironment extends < 1 cm in distance around organic tissue (Summary – Figure 1). The term will be used to describe areas of coral-microbial-mat interactions, coral-sediment interactions (Chapter 2), as well as DBLs at low flow conditions (< 0.3 cm s^{-1}) around organic tissue (Chapter 1), compared to bulk seawater conditions. The microenvironment therefore encompasses extracellular substrates (microbial mats, sediments), the DBL, as well as the viscous sublayer around organic tissue.

Flow and turbulence, created mainly by winds and density gradients, as well as molecular diffusion are ever-present in aquatic systems. These processes cause mixing and consequently tend to homogenize the distribution of gases, dissolved and particulate matter in the water column. However, metabolic processes of marine organisms maintain concentration gradients of gases and dissolved substances, such as O_2, CO_2, Ca^{2+} and other metabolites across their surfaces and the surrounding seawater. Microchemical gradients thus emerge in response to these metabolic processes and the prevailing conditions in the water column. Prominent metabolic processes influencing microenvironmental conditions are respiration, photosynthesis, calcium carbonate formation and dissolution. These processes have been shown to cause large concentration gradients of either O_2, CO_2, CO_3^{2-}, Ca^{2+} or pH between the

bulk seawater and the tissue- and carbonate-surfaces of marine calcifiers, such as corals (Shashar et al. 1993, Kühl et al. 1995, Al-Horani et al. 2003a,b, de Beer et al. 2000), foraminifera (Jørgensen et al. 1985, Rink et al. 1998, Köhler-Rink and Kühl 2000, 2005), bivalves (Crenshaw and Neff 1969, Crenshaw 1972, Hurd et al. 2011), phytoplankton (Flynn et al. 2012, Wolf-Gladrow and Riebesell 1997) and calcareous algae (Hurd et al. 2011, de Beer and Larkum 2001). These metabolic processes and the associated development of microchemical gradients are all linked and ultimately depend on carbonate system changes, as explained in section 4.1.. It is the microenvironmental gradients that directly interact with the organic tissue of calcifiers, rather then the bulk seawater conditions. Microgradients determine ion-availability and transport limitations of gases and solutes between the tissues and the surrounding seawater, as shown in the following sections.

2. Diffusive boundary layer (DBL)

The term boundary layer was first introduced in fluid mechanics by Prandtl (1904). His basic theory applies to both gases and non compressible fluids (such as seawater). In his definition, the boundary layer divides the flow field of a moving fluid above a solid surface into two areas. The upper area lies outside the boundary layer and is uninfluenced by friction. The lower area close to the solid surface, where flow is influenced by friction, depicts the boundary layer (Figure 2).
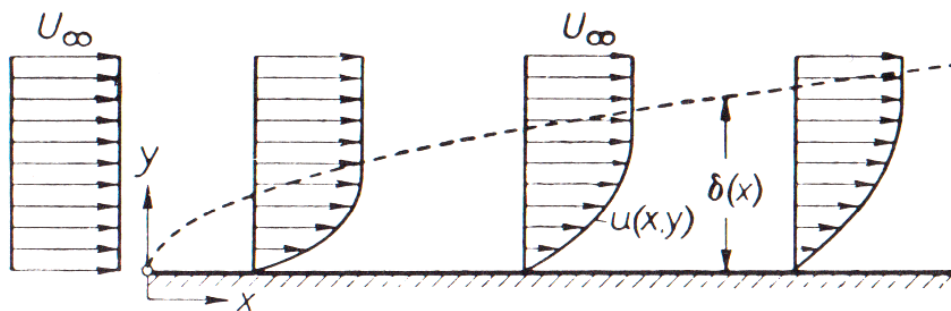
Figure 2: Velocity scheme of boundary layer development on a flat surface plane. The dashed line indicates the height of the boundary layer (δ) and U_∞ depicts the free-stream velocity (reproduced from Schlichting 1979, Chapter II).

Fluid particles always interact with the surface of a solid, thus creating friction. Flow at the fluid-solid boundary consequently equals zero. This condition is termed the 'no-slip condition' (Schlichting 1979, Chapter I). Figure 2 depicts the successive development of a flow field starting from a uniform free-stream velocity. When the flow field impacts on the leading edge of a solid surface, the lowest part of the field is affected by strong friction, i.e.

shear stress. Since shear stress is transmitted up the flow field, the boundary layer thickness (δ) continuously increases with increasing distance from the leading edge (Figure 2).

The same hydrodynamic concepts apply for flowing seawater in the marine environment. Here, the term 'benthic boundary layer' has been introduced, classifying the lowermost part of the water column that is affected by friction of the seafloor and therefore develops a velocity gradient. The boundary layer can further be separated into: 1) the Ekman layer, the water column above the sediment surface being affected by the Coriolis-force of the earth; 2) the logarithmic layer (~1 m thick), where flow is relatively unaffected by the Coriolis-force and flow-velocities decrease logarithmically with depth; 3) the viscous sub-layer (~1 cm thick), where the greatest and (mostly) linear changes in flow-velocity occur and vertical turbulence strongly decreases; 4) the diffusive boundary layer (~10 – 1000 μm thick), where flow is strictly laminar and vertical transport consequently takes place by molecular-diffusion only. This layer is also termed the 'diffusive sub layer'. A quite tangible definition of the DBL is "a film of water that sticks to the solid surface due to viscous forces, and therefore does not participate in the turbulent mixing of the water column" (Røy 2003). Under steady state conditions, a constant net production or consumption of an analyte (e.g. O_2 or Ca^{2+}) in the solid part underlying the flow (e.g. the seafloor or an organism), causes concentration differences between the surface (c_s) and the bulk seawater (c_{sw}). As there is usually no analyte production or consumption within the DBL and due to the diffusive nature of transport across the DBL, chemical concentration gradients develop linearly across the DBL (Figure 3). These concepts have been reviewed in Boudreau and Jørgensen (2001), Dade et al. (2001) and Jørgensen (2001).

The thickness of an idealized DBL gradient (dashed blue line, Figure 3) has been termed the effective DBL, also known as the hypothetical DBL (Z_δ; Jørgensen and Revsbech 1985). While the viscous sub-layer is dominated by turbulent mixing, turbulent transport ('eddy diffusion') continuously decreases with depth towards the DBL and molecular diffusion becomes more and more prominent (Figure 3; Boudreau and Guinasso 1982). The upper limit of the effective DBL depicts the plane where eddy-diffusion equals molecular-diffusion (line B in Figure 3; Røy 2003). In this transition layer between turbulence- and molecular-diffusion-dominated transport regimes, concentration gradients do not develop as a straight line but display a certain curvature (solid blue line, Figure 3). Two additional DBL thicknesses can therefore be defined, the 'outer DBL thickness', also known as the mass boundary layer, and the 'true DBL thickness' (Figure 3). In reality, the outer and true DBL thicknesses are however poorly defined, since small variability in flow causes these

boundaries to fluctuate. Extrapolation of linear DBL gradients, and determination of the effective DBL are more robust and were therefore applied in the presented work to determine DBL thicknesses.
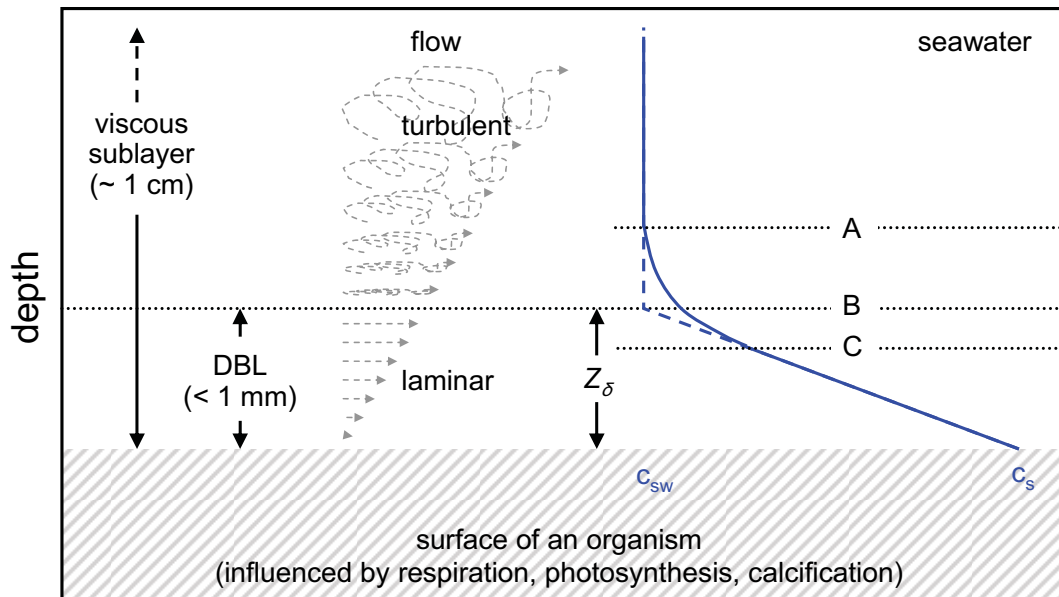
Figure 3: Conceptual representation of the viscous sublayer, diffusive boundary layer (DBL) and associated flow regimes. Grey lines indicate transitions of the flow field in the viscous sublayer towards the DBL. The blue lines depict an idealized (dashed line) and an actual (solid line) analyte concentration profile. c_{sw} = analyte concentration in the water column, c_s = analyte concentration on the surface, Z_δ = effective DBL thickness, A = 'outer limit of DBL', B = 'outer limit of effective DBL', C = 'true DBL thickness' (Jørgensen and Revsbech 1985).

Molecular diffusional fluxes (*J*) across the DBL can be determined by Fick's first law of diffusion:

$$J = D \frac{(c_{sw} - c_s)}{Z_\delta} = \beta (c_{sw} - c_s) \qquad \text{(Eq. 1)}$$

where *D* represents the molecular diffusion coefficient, $(c_{sw} - c_s)/Z_\delta$ the concentration gradient and *β* the mass transfer coefficient. Hence, the flux of an analyte from or to the surface of an organism scales linearly with the molecular diffusion coefficient of the analyte (Jørgensen 2001). In contrast, eddy diffusion in the viscous sublayer is largely constant for different molecules. Consequently, changes in *D* shift the thickness of the effective DBL (Z_δ), since equality between molecular- and eddy-diffusion will be reached at different depths (Jørgensen and Revsbech 1985, Santschi et al. 1983). The DBL thickness is therefore different for different molecules or analytes (Jørgensen 2001). Gradients of non-inert analytes are additionally influenced by interactions with their medium. For example, protons are buffered

in seawater, mainly by ions of the carbonate system. Hence, resulting DBL proton gradients do not necessarily develop as a straight line, as they depend on both proton diffusion and proton buffering effects (see also 4.1.).

3. Microsensors - a tool for studying microgradients

Microsensors (definition after Revsbech and Jørgensen 1986) were the major tool used in this thesis to elucidate microenvironmental dynamics, because they offer several advantages compared to other analytical techniques. For example, microsensors compared to macro-sensors, have very small sensing areas and tips (~0.1-3 µm in Ø). This strongly decreases analyte consumption and diffusional distances towards their sensing areas (reviewed in Heinze 1993). Hence, diffusive analyte supply to the sensing area of microsensors is very fast in relation to convective transport. Consequently, microsensors have very fast response times, a high spatial resolution and low stirring sensitivities. The time needed to reach ~90 % of the steady-state signal, can be as short as < 0.2 s for fast-responding microsensors like the O_2 sensor (Revsbech and Jørgensen 1986). Therefore, they are suitable for measuring both high–spatial-resolution concentration profiles and rapid concentration changes, such as photosynthetic O_2 production during light-dark shifts. Microsensor measurements in currents / convective transport fluids only give 1-5 % signal differences compared to stagnant fluids (Revsbech and Jørgensen 1986). Additionally, microsensors are minimally invasive due to their small tip sizes. Microbial mats, biofilms, sediments, and even organic tissues can be penetrated by microsensors with minimal disturbance. In return, the small tip sizes of microsensors only create small measurement artifacts (themselves), compared to macro-sensors (discussed in Glud et al. 1994). In contrast to fluorescent dyes, chemical interactions with the organism's physiology can also be excluded. Another advantage compared to imaging systems (e.g. planar optodes, fluorescence-imaging) is that microsensors can be applied in opaque matrices.

In this thesis, DBL dynamics were measured under ecologically realistic flow-conditions (Chapter 1-3), resulting in typical DBL thicknesses of ~10–1000 µm. Microsensors allowed the measurement of concentration profiles in steps of < 50 µm and thus detected concentration gradients within very thin DBLs (Chapter 1, 3). Measurements of profiles on coral- and foraminiferal-microenvironments were performed through different flow regimes of the viscous sublayer, the DBL and into low diffusivity matrices, such as microbial mats on corals, rhizopodial networks and / or organic tissue (Chapter 1, 2). The low stirring sensitivity of microsensors was thus very important. In addition, their ability to penetrate low mechanical

strength substrates and measure in opaque matrices allowed recordings within foraminiferal rhizopodial networks (Chapter 1), within and at the base of microbial mats and sediments around coral tissue (Chapter 2), and within the bivalve shell of *Arctica islandica* (Chapter 2). The minimal chemical and mechanical interferences of the microsensors allowed monitoring of the very sensitive life stage of chamber formation in foraminifera, which can easily be interrupted by chemical and mechanical disturbances (Chapter 1).

Both amperometric and potentiometric microsensors were used in the following work. The measurement principle of amperometric microsensors is based on a redox-reaction, its rate being proportional to the concentration of the analyte (reviewed in Gieseke and de Beer 1999). The analyte is either reduced or oxidized inside the polarized microsensor tip, resulting in the development of a current over the measuring circuit (Figure 4).
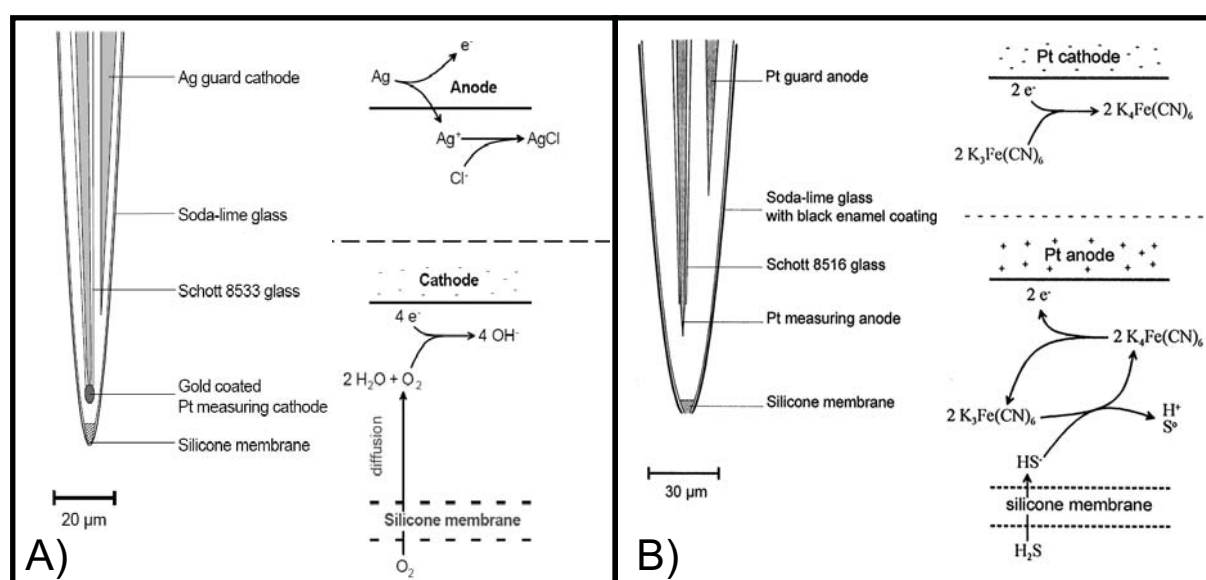
Figure 4: Scheme of an amperometric A) Clark-type O_2 and B) H_2S microsensor and associated redox-reactions (modified after Kühl and Revsbech 2001).

In the case of a Clark-type O_2 microsensor, O_2 diffuses across a gas-permeable silicone membrane into the polarized (-0.8 V) sensor tip, where it is reduced to OH^- at the negatively charged cathode. Ag is consequently oxidized at the anode forming AgCl. H_2S sensors work along the same principle, yet, via a redox-mediator system of iron-cyanide (Figure 4 B). The gas H_2S, but not the ions HS^- and S^{2-}, can diffuse through the silicone membrane and therefore H_2S sensors measure the concentration of H_2S, rather than that of total sulphide (discussed in Chapter 2).

In potentiometric microsensors, a charge (potential) difference (ΔE) develops at the electrode tip, which is measured against a second reference electrode. This potential is created by ion-selective materials, which can be in the form of full glass (e.g. in glass-pH-sensors) or

liquid ion-exchange (LIX) membranes (Figure 5). In the case of glass-pH-sensors, a lithium-silicate-glass constitutes the outer tip (50-100 μm in length), which is H^+-selective in its hydrated form (Hinke 1969). The tip of LIX-microsensors is filled with a chemical membrane cocktail containing ionophores (ion-exchangers), which specifically bind to a certain ion species (reviewed in Bühlmann et al. 1998). All other ions are excluded from binding, thereby creating a boundary potential at the outside and inside of the membrane. The different analyte concentrations, between the outside and inside of the membrane, result in a potential difference across the membrane (ΔE), which is proportional to the concentration difference according to the Nernst equation (Eq. 2, Figure 5 B):

$$\Delta E = \frac{RT}{zF} \ln\left(\frac{a_e}{a_i}\right) \qquad\qquad \text{(Eq. 2)}$$

where R depicts the gas constant, T the absolute temperature, z the charge of the ion, F the Faraday constant and a_i and a_e the internal and external ion activity, respectively. As the internal concentration can be considered constant, the response of the sensors is due to the external concentration and Eq. 2 can be simplified to:

$$\Delta E = E_0 + k \log(a_e) \qquad\qquad \text{(Eq. 3)}$$

where E_0 is the offset potential and k a constant (slope factor). These concepts are reviewed in Gieseke and de Beer (1999).
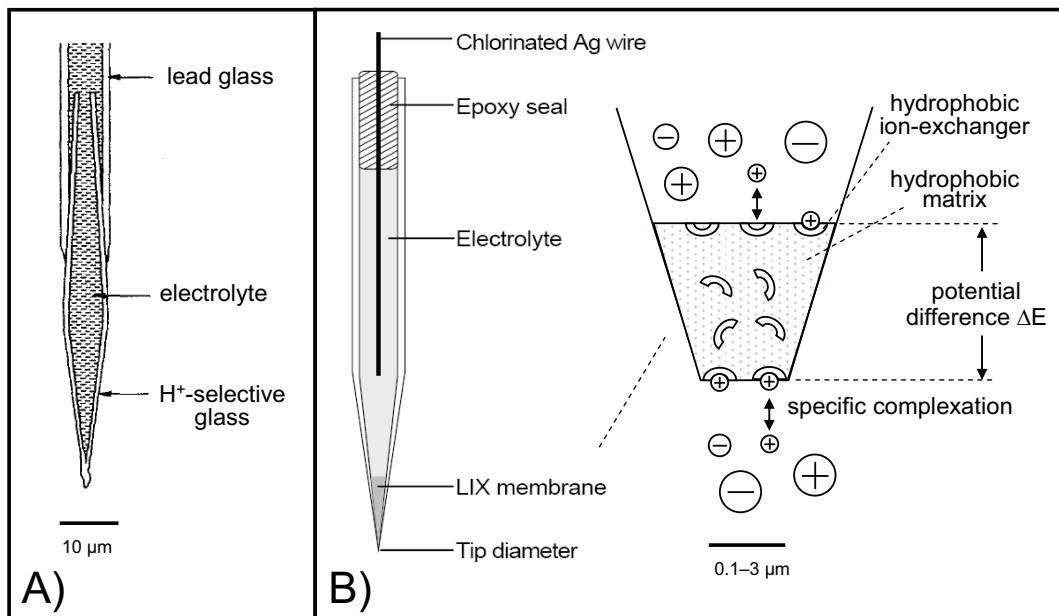
Figure 5: Scheme of potentiometric A) pH-glass and B) liquid ion-exchange (LIX) microsensors (modified after Revsbech and Jørgensen 1986 and Kühl and Revsbech 2001).

LIX and pH-glass microsensors were built with an outer coaxial shielding filled with 3 M KCl to better insulate the sensor from electrical disturbances. The Ca^{2+} sensors used in this work were of LIX-type (Chapter 1-3), while pH-sensors were built in the form of both LIX- and glass-pH-sensors (Chapter 1-3). One advantage of LIX sensors is that they can be prepared with very small tip diameters (< 3 μm), as was necessary for the small-scale measurements on foraminifera (Chapter 1). Also, they are cheaper and easier to make than glass-pH-sensors. This is particularly important when sensors are prone to breaking during measurements inside organisms and microbial mats, where sensor tips are concealed from view (Chapter 1-2), and on top of hard coral and foraminiferal skeletons, i.e. near carbonates (Chapter 1-3). On the other hand, glass-pH-sensors possess a longer life-expectancy and show less signal drift over long periods of time compared to LIX sensors. Therefore, glass-pH sensors were used for time series measurements lasting > 3 h that were not concealed from direct observations (Chapter 1).

4. Global carbon cycle

Marine calcifiers significantly contribute to oceanic carbon sequestration and cycling, due to their large biomass and continuous formation of biogenic carbonates (Fabry et al. 2008). Chemical microgradients and DBL thicknesses around calcifiers determine both ion speciation and transport limitations for solute and gas exchanges from the surrounding seawater into the organic tissue (Figure 3). The marine carbonate system strongly influences the development of these micro-gradients, due to the high concentrations of dissolved inorganic carbon (DIC) and its chemical properties in seawater. Hence, the basic principles of the global carbon cycle, seawater carbonate chemistry and the significance of calcifiers in the global carbon cycle, i.e. the biological pumps, are explained in the following section in more detail.

Carbon is one of the most important elements of our earth's biosphere. It is cycled between the atmosphere, biosphere, hydrosphere and lithosphere. There are presently about 800 Gt of carbon in the form of CO_2 within the atmosphere, and ~38 000 Gt as dissolved inorganic carbon (DIC) in the oceans (Riebeek 2011). Due to its ability to absorb infrared radiation, CO_2 significantly contributes to the warming of the atmosphere and is therefore a greenhouse gas. After water vapor, CO_2 is the most abundant greenhouse gas in the atmosphere with a present concentration of 396 μatm (measured while writing this thesis at May 18th 2012, Mauna Loa Observatory, NOAA-ESRL 2012). Hence, earth's climate-changes are coupled to a certain extend to atmospheric CO_2 concentrations (Royer et al. 2007).

On geological time scales, atmospheric and oceanic carbon budgets have changed significantly (Berner and Kothavala 2001, Bergman et al. 2004, reviewed in Doney and Schimel 2007). Some of these fluctuations are associated with biological mass extinction events like the Palaeocene-Eocene Thermal Maximum (PETM; Zachos et al. 2008) or the Eocene-Oligocene climate transition (Pearson et al. 2009). The coupling of CO_2 and temperature is also represented in recent historical climate events, like the El Nino-Southern Oscillation (ENSO; Bousquet et al. 2000), or glacial interglacial oscillations (Petit et al. 1999). The ocean represents the major sink of atmospheric CO_2 concentrations. Understanding the physicochemical basics of oceanic uptake and carbonate chemistry are thus important and introduced in the following section.

4.1. Seawater carbonate system

The uptake of CO_2 by the ocean surface waters follows Henry's law:

$$\left[CO_2\right] = \alpha \cdot pCO_2 \qquad\qquad\qquad \text{(Eq. 4)}$$

where α depicts the temperature- and salinity- dependent CO_2 solubility coefficient and pCO_2 the partial pressure of CO_2 in the atmosphere. CO_2 dissolves in seawater, but in contrast to other gases, such as oxygen and nitrogen, $CO_{2(aq)}$ further reacts with seawater forming carbonic acid (H_2CO_3), which immediately dissociates into bicarbonate (HCO_3^-), carbonate (CO_3^{2-}) and protons (H^+; Zeebe and Wolf-Gladrow 2001):

$$CO_{2(aq)} + H_2O \leftrightarrow H_2CO_3 \leftrightarrow HCO_3^- + H^+ \leftrightarrow CO_3^{2-} + 2H^+ \qquad \text{(Eq. 5)}$$
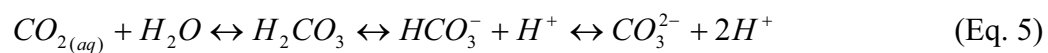
The sum of all inorganic carbon species is termed dissolved inorganic carbon (DIC), sum of CO_2 ($\sum CO_2$) or total CO_2 (TCO_2). The terminology DIC is used throughout this thesis. Oceanic DIC concentrations are much higher than atmospheric CO_2 concentrations (explained by Eq. 5). If CO_2 is in excess within the atmosphere, it will continuously be taken up by the ocean to establish equilibrium. Generated H^+ ions (Eq. 5) do not exist in free form in seawater, but immediately form larger complexes mainly with H_2O and SO_4^{2-} ions, such as H_3O^+, $H_5O_2^+$, $H_7O_3^+$, $H_9O_4^+$ and HSO_4^- (Marx et al. 1999, Stoyanov et al. 2010). The sum of all H^+-complexes is expressed by the total hydrogen ion scale, and will be referred to as H^+ in the following. The speciation of DIC dictates the pH of seawater. At lowered concentrations of $CO_{2(aq)}$ and higher concentrations of CO_3^{2-}, the carbonate system shifts towards elevated pH. At elevated $CO_{2(aq)}$ and lowered CO_3^{2-} concentrations, it shifts towards lowered pH (Figure 6).
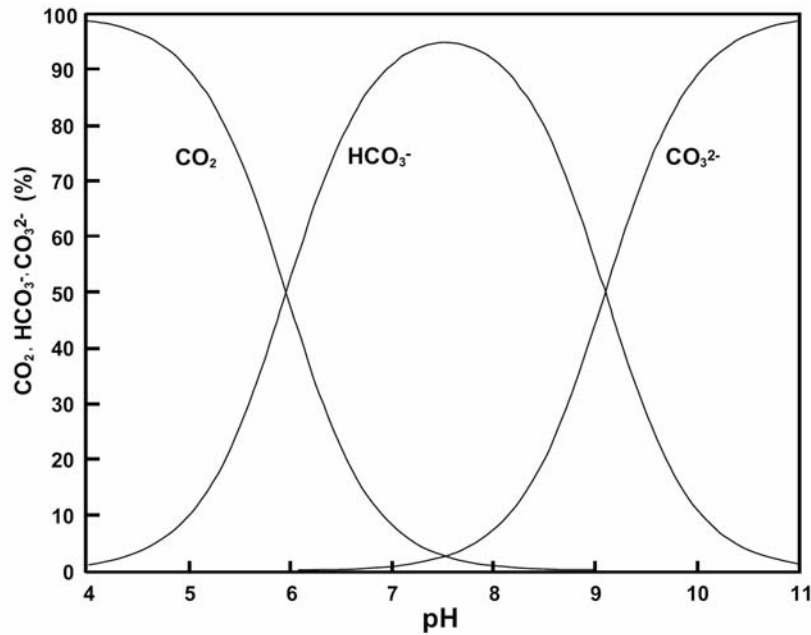
Figure 6: DIC speciation in seawater (15°C, S=35, P = 1 µatm) as a function of pH (reproduced from Rost 2003).

Another important concept for the determination of the carbonate system is total alkalinity (TA). In normal seawater, strong cations (Na^+, Mg^{2+}, Ca^{2+}, K^+, etc.) predominate over strong anions (Cl^-, SO_4^{2-}, Br^-, F^-, etc.). This surplus in charge is electrochemically balanced by weaker ions, being defined as TA (Rost 2003).

$$TA = \left[HCO_3^-\right] + 2\left[CO_3^{2-}\right] + \left[B(OH)_4^-\right] + \left[OH^-\right] - \left[H^+\right] + minor\ ions \qquad (Eq.\ 6)$$

Total alkalinity thus constitutes the electrochemical charge balance of seawater. Total alkalinity is analysed in seawater by strong acid titration. Since changes in H^+-concentrations are chemically buffered within the carbonate system, due to the uptake and release of H^+ by CO_3^{2-} and HCO_3^- (Figure 6, Eq. 5), TA can be regarded as the buffering capacity of seawater. With concentrations of roughly 2200 µM in ocean surface waters, DIC concentrations are highest compared to all other gases and weak ions. Therefore, carbonate alkalinity (CA) depicts a good approximation for the TA (Zeebe and Wolf-Gladrow 2001).

$$CA = \left[HCO_3^-\right] + 2\left[CO_3^{2-}\right] \qquad (Eq.\ 7)$$

Factors of the carbonate systems (DIC, TA, pH and DIC-speciation) are interrelated, which is described by the following scheme (Zeebe and Wolf-Gladrow 2001):
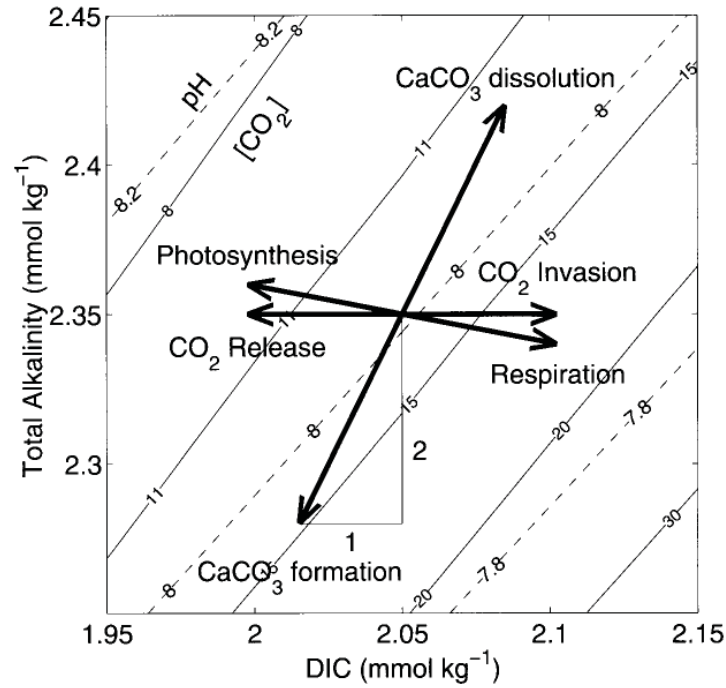
Figure 7: Metabolic and *pCO₂* effects on the carbonate system. Ratio changes of TA and DIC are depicted as arrows. Dashed and solid lines indicate changes of pH (total scale) and CO$_{2(aq)}$ (μM) (reproduced from Zeebe and Wolf-Gladrow 2001).

This interrelation is expressed by the following equations (Zeebe and Wolf-Gladrow 2001):

$$\left[CO_2\right] = DIC \left/ \left(1 + \frac{K_1}{\left[H^+\right]} + \frac{K_1 K_2}{\left[H^+\right]^2}\right)\right. \qquad \text{(Eq. 8)}$$

$$\left[HCO_3^-\right] = DIC \left/ \left(1 + \frac{\left[H^+\right]}{K_1} + \frac{K_2}{\left[H^+\right]}\right)\right. \qquad \text{(Eq. 9)}$$

$$\left[CO_3^{2-}\right] = DIC \left/ \left(1 + \frac{\left[H^+\right]}{K_2} + \frac{\left[H^+\right]^2}{K_1 K_2}\right)\right. \qquad \text{(Eq. 10)}$$

K_1 and K_2 depict the equilibrium constants of carbonic acid. Due to the above equations, all system parameters can be calculated if two of the parameters, pH, TA, *pCO₂* or DIC are known at a given pressure, temperature and salinity. For example, at a *pCO₂* of 396 μatm, a pH of 8.10 (total scale), S = 35 and T = 25°C, ~87 % of the total DIC concentration are in the form of HCO$_3^-$, ~12 % in the form of CO$_3^{2-}$ and < 1 % in the form of dissolved CO$_2$ (CO₂SYS calculation, Pierrot et al. 2006).

4.2. The oceanic carbon pumps

The input of DIC into the ocean surface waters, is partly compensated by uptake from the so-called 'carbon pumps'. These pumps govern the physical and biological uptake and transport of DIC from the ocean surface waters into the deep sea and are thus differentiated into the physical and biological carbon pump (Volk and Hoffert 1985). In reality these pumps do not occur separately, however, for a better understanding they are described individually in the following section.

The physical pump relates to the vertical carbon flux as a consequence of seawater temperature-solubility differences of CO_2, and is thus also referred to as the 'solubility-' or 'solution-pump' (Figure 8). Due to the thermohaline circulation, warm water is transported from low to high latitudes. This results in cooling of surface waters and consequently increased uptake of CO_2 in high latitudes. DIC-rich water is then transported into the deep sea and later back to lower latitudes, where it partly upwells and releases CO_2 back into the atmosphere (Raven and Falkowski 1999). The biological pump relates to the phototrophic fixation of $CO_{2(aq)}$ in the photic zone, which is consequently transferred up the food chain and finally sinks into the deep sea (Figure 8; Chisholm 2000). Biological fixation results in the formation of organic matter, as well as inorganic carbonates, such as coccoliths, coral skeletons or foraminiferal tests. Sarmiento et al. (1995) estimated that about 75 % of the total vertical DIC flux is biologically mediated, and that only ~25 % account for physical transport (Rost 2003). Depending on the biogenic product formed, the biological carbonate pump can further be differentiated into the 'organic carbon pump' and the '$CaCO_3$ counter pump' (Figure 8, Heinze et al. 1991). The 'organic carbon pump' also known as the 'soft tissue pump', transports particulate organic carbon (POC) into intermediate and deep waters, where it is remineralized by bacterial activity (< 1 % of POC reaches the ocean floor) and DIC is released (Chisholm 2000). This leads to the formation of DIC rich intermediate and deep waters, which are partly upwelled to the surface and release CO_2 back into the atmosphere. The '$CaCO_3$ counter pump' on the other hand, refers to the production of particulate inorganic carbon (PIC). Due to the uptake of CO_3^{2-}, the formation of $CaCO_3$ (i.e. calcification) causes TA and therefore pH reduction and an increase of $CO_{2(aq)}$ concentrations (Figure 7). This results in a net CO_2 out-gassing of ocean surface waters in areas of net calcification (Figure 8). PIC later sinks into the deep ocean, below the carbonate concentration depth (CCD), where it dissolves and CO_3^{2-} is released, thus increasing TA (Figure 8).
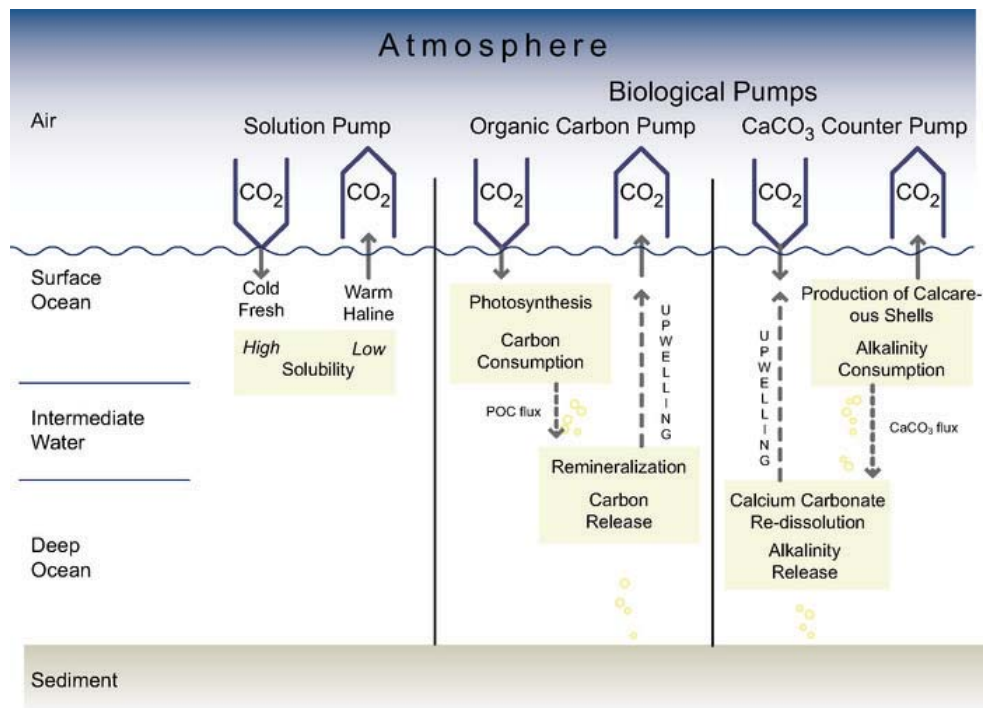
Figure 8: Schematic drawing of physical (solution pump) and biological carbon pumps (reproduced from IPCC AR4 WG1 (2007), modified after Heinze et al. 1991).

Anthropogenic CO_2 increases currently change the global carbon budget and seawater carbon chemistry at a very fast rate (Orr et al. 2005). The resulting consequences for marine calcifiers are likely to significantly alter this vertical DIC flux.

4.3. Ocean acidification

Since the last glacial maximum, atmospheric CO_2 concentrations have been relatively constant (Monnin et al. 2001). Yet, from the beginning of the industrial revolution, human activity on the planet has started to increase these concentrations (Figure 9). Anthropogenic CO_2 increases include changes in land use, such as deforestation, desertification, as well as increased fossil fuel combustion or cement construction (Canadell and Dhakal 2012). Not only is CO_2 a potent greenhouse gas in the atmosphere resulting in global warming, but approximately one third of the anthropogenic CO_2 increase is taken up by the ocean surface water (Sabine et al. 2004, Doney et al. 2009). Considering Figure 7, the anthropogenic enhanced input of CO_2 into the oceans will directly decrease surface seawater pH and increase DIC concentrations (Figure 9).
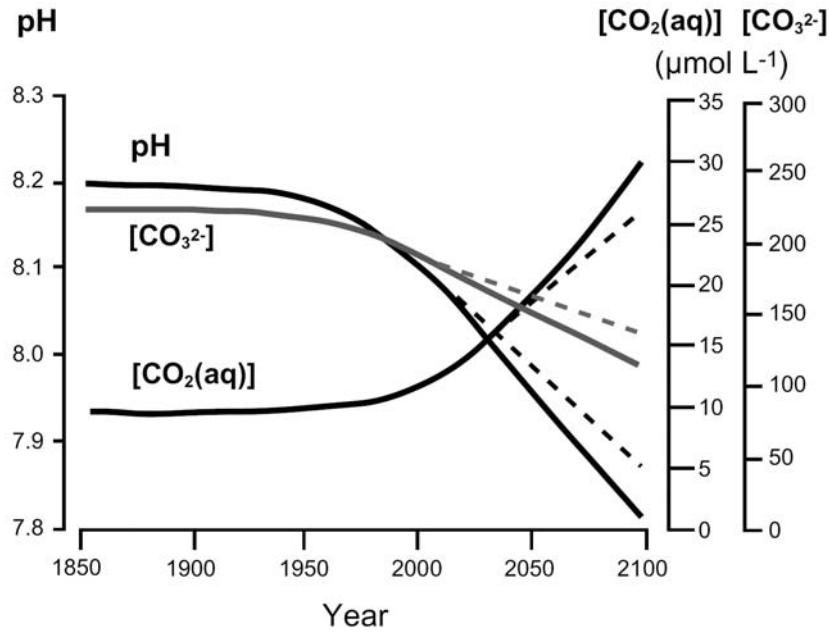
Figure 9: Changes of seawater dissolved carbon dioxide [CO$_{2(aq)}$] and carbonate ion [CO$_3^{2-}$] concentrations in the ocean surface waters under the IPCC (IS92a) 'business as usual' CO$_2$ emission scenario (IPCC 2007). Dashed lines represent possible scenarios considering global compliance of the Kyoto Protocol (reproduced from Rost 2003, modified after Wolf-Gladrow et al. 1999b).

This process is termed 'ocean acidification' (OA). A consequence of OA is that the carbonate saturation state (Ω) of the ocean surface waters is reduced (Eq. 11). The carbonate saturation being defined as:

$$\Omega = \frac{\left[Ca^{2+}\right]_{sw} \cdot \left[CO_3^{2-}\right]_{sw}}{K_{sp}}$$
(Eq. 11)

K_{sp} hereby represents the stoichiometric solubility product for the different crystal forms of calcite or aragonite at a given temperature, pressure and salinity (Mucci 1983).

5. Evolution of the hypotheses of the individual chapters

This section is intended to supply the reader with the evolution of ideas that led to the formulation of the individual hypotheses / objectives of the thesis.

5.1. Calcification in foraminifera (Chapter 1)

Foraminifera are protists found in almost all marine habitats. The shells of calcareous benthic foraminifera are used as index fossils and their (trace) element and stable isotope compositions are widely used as proxies for paleoceanographic reconstructions. A process

based understanding of foraminiferal calcification is therefore essential to better understand incorporation of (trace) element and stable isotopes for shell proxy interpretation. Chapter 1 investigates chamber formation in benthic, symbiont-free foraminifera and provides experimental evidence about the extracellular microchemistry around calcifying and non calcifying individuals.

Benthic, symbiont-free foraminifera represent a suitable model organism to study the effects of calcification on microenvironments for the following reasons. First, they calcify or grow in discrete steps of new chambers additions (reviewed in Goldstein 2003). Calcification, i.e. chamber formation can thus be detected and timed visually (< 20 min accuracy), which is not possible for other calcifiers such as corals, bivalves or coccolithophores. Second, chamber formation can be stimulated by simple seawater manipulations (elevated temperatures and reduced salinity), which allows predicting time-periods of calcification to some extent in younger individuals. Third, benthic-foraminifera remain immotile during chamber formation, locked to the base of the culturing vessel in a spatially stable measurement position (Angell 1967, reviewed in Hemleben et al. 1986). Fourth, the absence of photosynthetic symbionts makes interpretations of calcification related microenvironmental pH changes easier, since photosynthesis influences the pH microenvironment of foraminifera considerably (Rink et al. 1998, Köhler-Rink and Kühl 2000). Fifth, they are of sufficient size (> 50 μm in Ø) to warrant the development of detectable pH gradients around the organisms, as DBL thicknesses correlate with the radius of circular shaped protists (Wolf-Gladrow and Riebesell 1997).

Several models describing calcification in benthic calcareous foraminifera have been proposed (e.g. Erez 2003, Bentov et al. 2009, de Nooijer et al. 2009). The basic theory underlying those models includes the concentration of Ca^{2+} and DIC in intracellular vesicles (Figure 10). DIC-vesicle pH is elevated by the active removal of protons, shifting the DIC equilibrium within towards very low percentage of $CO_{2(aq)}$ (Figure 6). This mechanism is believed to work as a DIC trap by facilitating the diffusion of metabolic CO_2 into the vesicles. The vesicles are then exocytosed at the site of calcification, facilitating calcite precipitation on a micro-scale, on top of an organic layer, by elevating Ca^{2+}, DIC, pH and consequently Ω_{Ca} (de Nooijer et al. 2009). The model proposed by de Nooijer et al. (2009) thus led to the hypothesis that microenvironment pH levels, around the newly forming chamber on top of the organic layer, are elevated, due to the exudation of high pH vesicles in this region (Figure 10).
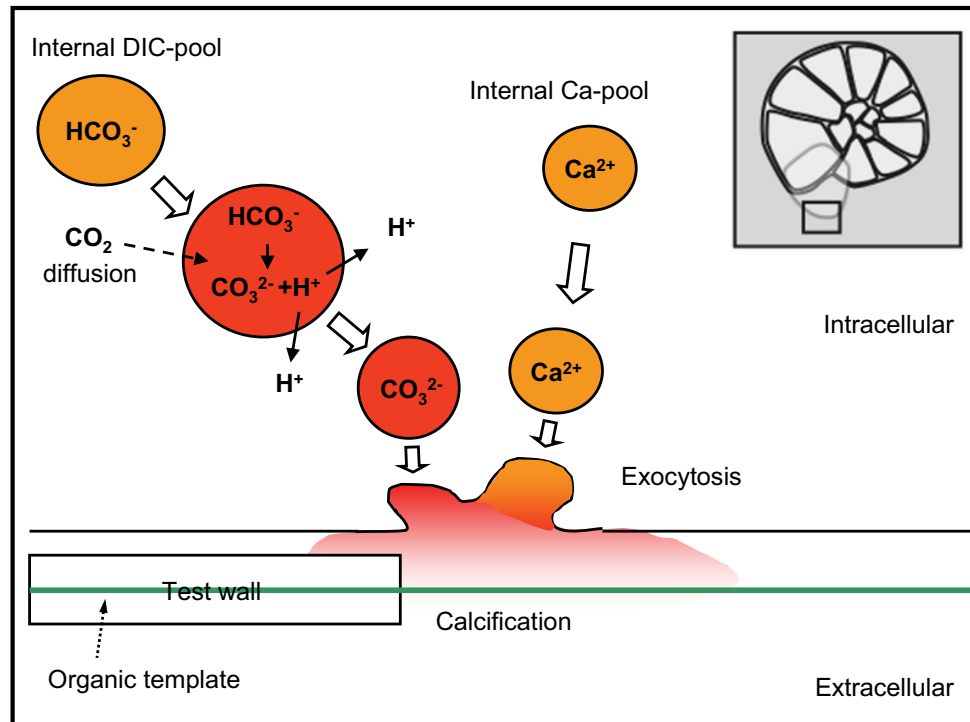
Figure 10: Calcification pathway scheme of benthic, hyaline foraminifera. Red = high pH vesicles, orange = intermediate pH vesicles (modified after de Nooijer et al. 2009).

However, through the consumption of CO_3^{2-} ions, calcification decreases TA and DIC of any calcifying fluid in a ratio of 2 : 1, which causes pH reduction of the fluid (Figure 7; Zeebe and Wolf-Gladrow 2001). Compared to inorganic carbonate precipitation, biological controlled calcification like in foraminifera, produces very delicate endo- and exoskeletal structures. To fabricate such fragile forms, calcium carbonate precipitation must be highly regulated, which necessitates a strict control over the carbonate chemistry of the calcifying fluid and thus its carbonate saturation state (Ω; reviewed in Nielsen 1964, and Lowenstam and Weiner 1989). One way to achieve such control is by calcifying in delineated compartments. In corals and coccolithophores, these compartments exhibit active pH control (Jokiel 2011, Taylor et al. 2011). A similar mechanism has been suggested, but not proven, for foraminifera (reviewed in Erez 2003). The resulting acidification can however not be allowed to remain uncontrolled intra- or intercellular, outside these delineated compartments (Alberts 2002). Biological calcification happening internally within the organism in delineated compartments, must therefore develop 'H$^+$-transport-pathways' to channel H$^+$-transport within the organism. The protons can either be metabolized or externalized. The latter mechanism implies that the proton discharge should result in an acidification of the microenvironment around the organism, while precipitating calcite.

We tested these two hypotheses by measuring pH and Ca^{2+} dynamics within the microenvironment of calcifying and non-calcifying foraminiferal specimens at different life stages with microsensors.

5.2. Microenvironmental conditions in black band disease and cyanobacterial patch lesions (Chapter 2)

Black band disease (BBD) is a poly-microbial mat that migrates over host scleractinian corals, killing the underlying coral tissue and exposing bare skeleton (Figure 11, A). First identified within coral reefs in the Caribbean in the early 70's, this darkly pigmented microbial mat is recognized as playing some role in continued degradation of reef ecosystems worldwide (Antonius 1973, Sutherland et al. 2004).
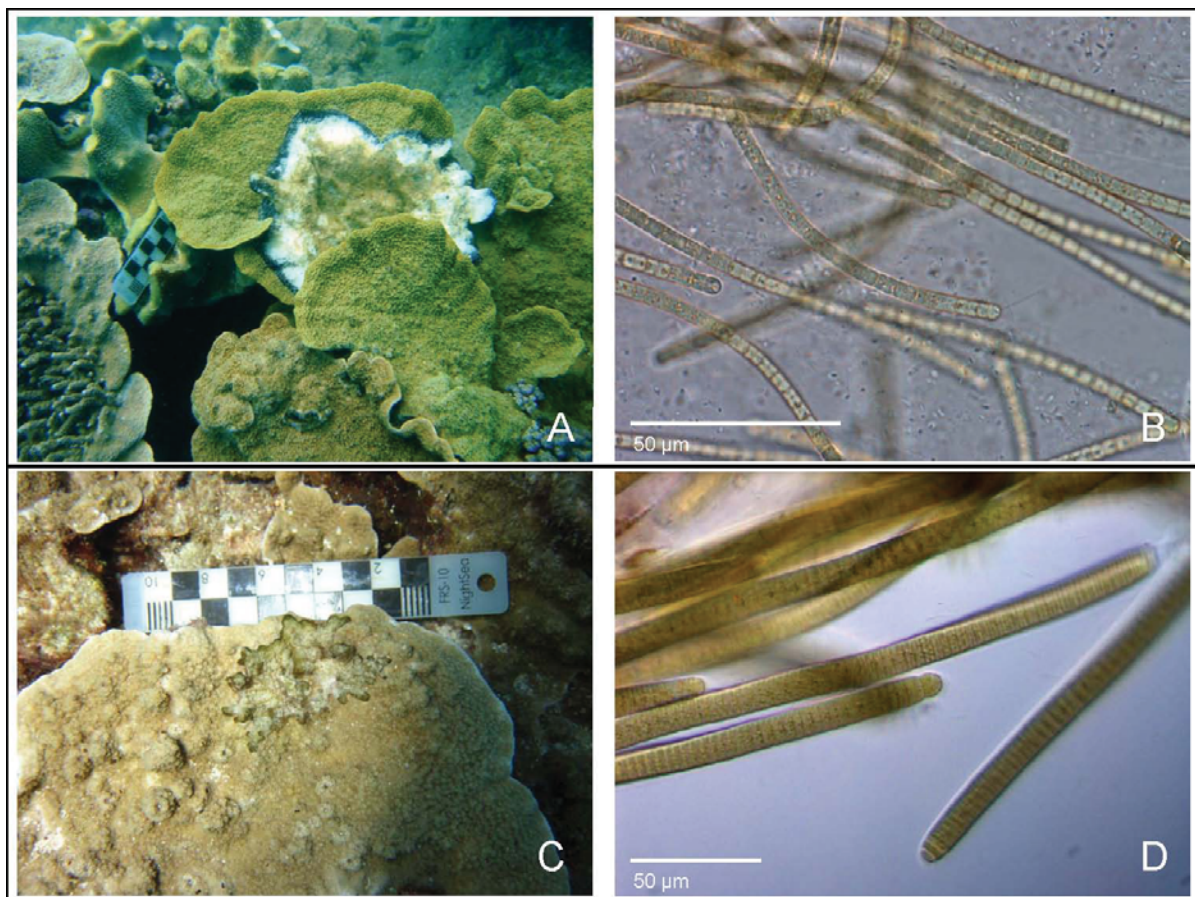
Figure 11: A) BBD and C) CP lesions on *Montipora* sp.. Meter scales = 1 cm. Microscopic images of B) BBD and D) CP associated dominant *Oscillatoria* and *Blennothrix* cyanobacterial species (photographs A, C with permission from Y. Sato, photographs B, D made by the author).

Early classification of BBD as a coral 'disease' led to the assumption that the onset and outbreak of this lesion might be triggered by a single, clearly defined pathogen, according to Koch's postulate (reviewed in Richardson 1998). The BBD microbial community is highly

diverse, with large differences in community structure identified for lesions from different geographical locations (Miller and Richardson 2011). This makes sense, considering that the colonization of the microbial mat by microbes must happen from the surrounding water-column and reef-biota communities, which likely change for different geographic locations and temporal periods. However, the microbial community of BBD lesions are comprised of similar functional groups, including phototrophic motile filamentous cyanobacteria, sulphate reducing bacteria (SRB) and other heterotrophic bacteria (e.g. Cooney et al. 2002, Frias-Lopez et al. 2004, Sekar et al. 2008, Sato et al. 2010). The BBD community structure is thus similar to other complex microbial mats, including hypersaline mats, which are stratified into an upper-phototrophic zone and lower anoxic sulphidic zone (e.g. Jonkers et al. 2003, Ludwig et al. 2005, Dupraz et al. 2009). Investigations of chemical micro-gradients within BBD revealed that the base of the microbial mat is anoxic and contains high concentrations of sulphide, both conditions are highly detrimental to the underlying coral tissue and contribute directly to tissue necrosis (Carlton and Richardson 1995). These findings provide evidence that not one single pathogen, but the functional microbial community as a whole, creates microchemical conditions at the coral-microbial mat interphase that are toxic to the living tissues. In addition, BBD is highly infectious and can be transmitted from one coral species to another (Kuehl et al. 2011), indicating that the host-lesion interaction is not species specific (Miller and Richardson 2011).

At a study site on reefs around Orpheus Island in the central Great Barrier Reef, an ongoing monitoring program recorded recurring summer outbreaks of BBD, causing significant mortality in susceptible coral populations (Sato et al. 2009). The monitoring program identified cyanobacterial-dominated disease lesions termed 'cyanobacterial patches (CP)' on coral assemblages, which acted as a precursor to BBD infections (Sato et al. 2010). CP lesions were less virulent and typically developed into BBD over 1-2 months *in situ*. Temperature and light were major environmental drivers of increased disease prevalence at these sites (Sato et al. 2009). A shift in the bacterial communities during the onset of BBD from CP was also documented (Sato et al. 2010). Stereo-microscope observations of BBD and CP surface topographies showed that BBD surfaces, dominated by *Oscillatoria* cyanobacterial species (Figure 11 A, B; Glas et al. 2010), consist of tightly inter-woven filaments. This smooth, blanket like surface structure might hamper solute and gas exchange of the underlying coral tissue with the surrounding seawater. In contrast, CP surfaces, dominated by *Blennothrix* cyanobacterial species (Figure 11 C, D; Glas et al. 2010), consist of disorganized cyanobacterial filaments, and thus show a rough surface structure. By creating

strong friction and turbulence, this surface structure might result in a deeper penetration of solutes and gases from the water column into the CP mats than the BBD mats. This might result in stronger chemical microgradients and thus stratification in BBD when compared with CP.

The above observations led to the hypothesis that not a single pathogen, but the microbial mat of BBD as whole, creates and traps microchemical conditions that are lethal to the underlying coral tissue.

5.3. Microchemical conditions around foraminifera at elevated pCO_2 (Chapter 3)

Ocean acidification has become a major threat to marine calcifiers (Fabry et al. 2008, Doney et al. 2009). It has been argued that net photosynthesis of calcifiers, which relies on the utilization of $CO_{2(aq)}$, may be enhanced by future pCO_2 concentrations by shifting the carbonate system towards higher levels of $CO_{2(aq)}$ (Riebesell et al. 2009). On the other hand, decreases in CO_3^{2-} concentration adversely affect calcification in predominant calcifiers, such as foraminifera and coccolithophores (Riebesell et al. 2009).

The effects of ocean acidification on marine calcifiers are ultimately mediated through their pH microenvironments. Phototrophic or photosymbiotic calcifiers, in comparison to non-phototrophic calcifiers, are known to elevate their external O_2 and pH microenvironment in daylight, due to photosynthetic oxygen production and uptake of $CO_{2(aq)}$ (and possibly HCO_3^-; e.g. Shashar et al. 1993, Kühl et al. 1995, Rink et al. 1998, de Beer and Larkum 2001, Köhler-Rink and Kühl 2000, 2005). Photosynthesis thus increases microenvironmental CO_3^{2-} concentrations, which is believed to enhance calcification in daylight (Figure 12, Wolf-Gladrow et al. 1999a). This suggests that phototrophic calcifiers - compared to non-phototrophic calcifiers - might profit from increased $CO_{2(aq)}$ concentrations at elevated pCO_2, via increased rates of net photosynthesis (Riebesell et al. 1993, Hein and Sand-Jensen 1997) and / or calcification. Additionally, increased net photosynthesis at elevated pCO_2 and associated microenvironmental pH elevations, could shield phototrophic calcifiers from the physiological effects of low pH in daylight (Figure 12). This led us to the hypothesis that pH elevation within the DBL in daylight, over the surface of photosymbiotic calcifiers, might partly or fully counteract ambient pH decreases predicted by future ocean acidification. It is consequently hypothesized that phototrophic calcifiers are more resistant towards the effects of ocean acidification, compared to non-phototrophic calcifiers.
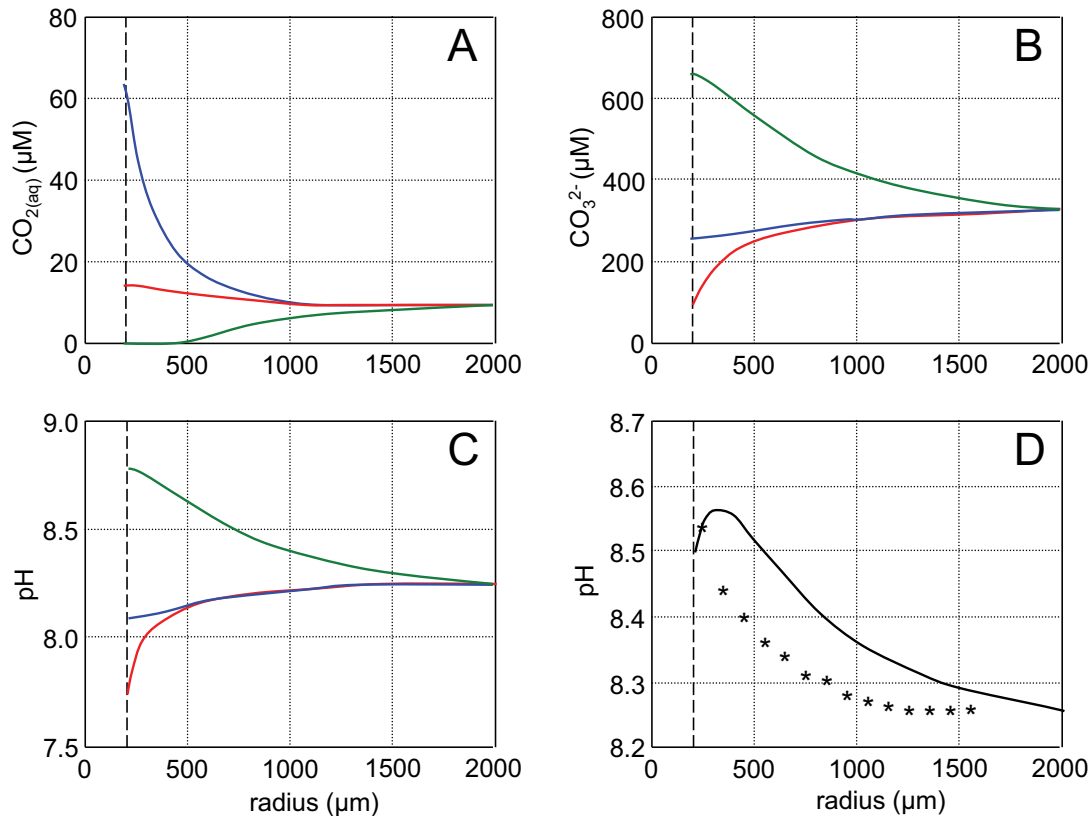
Figure 12: Modelled steady state profiles of A) $CO_{2(aq)}$, B) CO_3^{2-} and C) pH for photosynthesis (green line), respiration (blue line) and calcification (red line) of photosymbiotic planktonic foraminifera, as a function of the distance from the center of the shell (radius). D) pH gradient in *Globigerinoides sacculifer,* resulting from the combination of photosynthesis, respiration and calcification in light. The stars represent a pH profile measured with microelectrodes (Jørgensen unpublished data; modified after Wolf-Gladrow et al. 1999a).

We used benthic foraminifera to study this hypothesis, since they display several advantages compared to other calcifiers. First, both symbiotic and symbiont free foraminiferal species exist, which facilitates an inter-comparison of the effects of photosynthesis and respiration on pH microenvironments. Second, adult individuals are of sufficient size (> 500 µm in Ø) to warrant the development of detectable pH and O_2 gradients (see also 5.1.). Third, the process of chamber formation can be detected visually and is too sensitive to occur whilst experimental handling, thus effects of calcification on pH microenvironments can be excluded (Chapter 1, see also Chapter 3 - discussion).

We tested these hypotheses by measuring the O_2 and pH microenvironment of 4 photosymbiotic and 2 symbiont-free, benthic, tropical foraminiferal species under different ocean acidification scenarios in light and dark conditions.

6. Objectives of the thesis

This thesis is divided into three chapters. The objectives of the individual chapters were the following:

Chapter 1 - Effects of calcification on microenvironments (Summary - Figure 1, blue arrow):

- To investigate, how microchemical Ca^{2+} and pH dynamics are related to the different stages of chamber formation around a benthic non-symbiotic foraminifer (*Ammonia* sp.)

Chapter 2 - Effects of metabolically induced low pH microenvironments on calcifiers (Summary - Figure 1, red arrows):

- To investigate, to which extent physicochemical microgradients directly back-influence calcifiers, such as corals and bivalves.
    - o To investigate, how physicochemical microgradients are related to the virulence of the coral diseases BBD and CP.
    - o To study the involvement of the extrapallial fluid of the bivalve *Arctica islandica* in its shell formation / calcification.
    - o To examine the effects of sediment-microgradients on the calcification of corals, foraminifera and crustose coralline algae (CCA).

Chapter 3 - Ocean acidification effects on microgradients (Summary - Figure 1, green arrow):

- To study, to which degree metabolically induced microchemical dynamics are going to change, due to bulk seawater carbonate system changes, i.e. 'ocean acidification' conditions in foraminifera.
    - o To test, if phototrophic calcifiers can counteract bulk seawater acidification in daylight by elevating their surface pH, due to photosynthetic uptake of DIC.

7. References

Al-Horani FA, Al-Moghrabi SM, de Beer D (2003a). Microsensor study of photosynthesis and calcification in the scleractinian coral, *Galaxea fascicularis*: active internal carbon cycle. Journal of Experimental Marine Biology and Ecology 288: 1-15.

Al-Horani FA, Al-Moghrabi SM, de Beer D (2003b). The mechanism of calcification and its relation to photosynthesis and respiration in the scleractinian coral *Galaxea fascicularis*. Marine Biology 142: 419-426.

Alberts B, Johnson A, Lewis J, Raff M, Roberts K, Walter P (2002). Molecular biology of the cell, 4th edn. Garland Science Taylor & Francis Group: New York.

Angell RW (1967). The process of chamber formation in the foraminifer *Rosalina floridana* (Cushman). Journal of Eukaryotic Microbiology 14: 566-574.

Antonius A (1973). New observations on coral destruction in reefs. Association of island marine laboratories of the caribbean: 3.

Bentov S, Brownlee C, Erez J (2009). The role of seawater endocytosis in the biomineralization process in calcareous foraminifera. Proceedings of the National Academy of Sciences of the United States of America 106: 21500-21504.

Bergman NM, Lenton TM, Watson AJ (2004). COPSE: A new model of biogeochemical cycling over Phanerozoic time. American Journal of Science 304: 397-437.

Berner RA, Kothavala Z (2001). Geocarb III: A Revised Model of Atmospheric CO_2 over Phanerozoic Time. American Journal of Science 301: 182-204.

Boudreau PB, Guinasso NL (1982). The influence of a diffusive sublayer on accretion, dissolution, and diagenesis at the sea floor. In K. A. Fanning and F.T. Manheim [eds.], The dynamic environment at the ocean floor. Lexington. pp. 115-145

Boudreau PB, Jørgensen BB (2001). Introduction. In: Boudreau PB, Jørgensen BB (eds). The benthic boundary layer. Oxford University Press: Oxford. pp 1-3.

Bousquet P, Peylin P, Ciais P, Le Quéré C, Friedlingstein P, Tans PP (2000). Regional Changes in Carbon Dioxide Fluxes of Land and Oceans Since 1980. Science 290: 1342-1346.

Bühlmann P, Pretsch E, Bakker E (1998). Carrier based ion-selective electrodes and bulk optodes. Chem Rev 98: 1593-1687.

Canadell P, Dhakal S (2012). Global carbon project. CSIRO Marine and Atmospheric Research: Canberra. electronic document: http://www.globalcarbonproject.org/, accessed 16.05.2012

Carlton RG, Richardson LL (1995). Oxygen and sulfide dynamics in a horizontally migrating cyanobaterial mat: black band disease of corals. Fems Microbiology Ecology 18: 155-162.

Chisholm SW (2000). Oceanography: Stirring times in the Southern Ocean. Nature 407: 685-687.

Cooney RP, Pantos O, Le Tissier MDA, Barer MR, O'Donnell AG, Bythell JC (2002). Characterization of the bacterial consortium associated with black band disease in coral using molecular microbiological techniques. Environmental Microbiology 4: 401-413.

Crenshaw MA, Neff JM (1969). Decalcification at the Mantle-Shell Interface in Molluscs. American Zoologist 9: 881-885.

Crenshaw MA (1972). The inorganic composition of molluscan extrapallial fluid. The Biological Bulletin 143: 506-512.

Dade WB, Hogg AJ, Boudreau PB (2001). Physics of flow above the sediment-water interface. In: Boudreau PB, Jørgensen BB (eds). The benthic boundary layer. Oxford University Press: Oxford. pp 4-43.

de Beer D, Kühl M, Stambler N, Vaki L (2000). A microsensor study of light enhanced Ca2+ uptake and photosynthesis in the reef-building hermatypic coral *Favia* sp. Marine Ecology Progress Series 194: 75-85.

de Beer D, Larkum AWD (2001). Photosynthesis and calcification in the calcifying algae *Halimeda discoidea* studied with microsensors. Plant Cell and Environment 24: 1209-1217.

de Nooijer LJ, Toyofuku T, Kitazato H (2009). Foraminifera promote calcification by elevating their intracellular pH. Proceedings of the National Academy of Sciences of the United States of America 106: 15374-15378.

Doney SC, Schimel DS (2007). Carbon and climate system coupling on timescales from the Precambrian to the anthropocene. Annual Review of Environment and Resources 32: 31-66.

Doney SC, Fabry VJ, Feely RA, Kleypas JA (2009). Ocean acidification: the other CO_2 problem. Annual Review of Marine Science 1: 169-192.

Dupraz C, Reid RP, Braissant O, Decho AW, Norman RS, Visscher PT (2009). Processes of carbonate precipitation in modern microbial mats. Earth-Science Reviews 96: 141-162.

Erez J (2003). The source of ions for biomineralization in foraminifera and their implications for paleoceanographic proxies. Biomineralization 54: 115-149.

Fabry VJ, Seibel BA, Feely RA, Orr JC (2008). Impacts of ocean acidification on marine fauna and ecosystem processes. Ices Journal of Marine Science 65: 414-432.

Flynn KJ, Blackford JC, Baird ME, Raven JA, Clark DR, Beardall J et al (2012). Changes in pH at the exterior surface of plankton with ocean acidification. Nature Climate Change, advanced online publication: doi:10.1038/nclimate1489

Frias-Lopez J, Klaus JS, Bonheyo GT, Fouke BW (2004). Bacterial community associated with black band disease in corals. Applied and Environmental Microbiology 70: 5955-5962.

Gieseke A, de Beer D (1999). Use of microelectrodes to measure in situ microbial activities in biofilms, sediments, and microbial mats. In: Akkermans ADL, van Elsas JD, de Bruyn FJ (eds). Molecular Microbial Ecology Manual, 2 edn. Kluwer: Dordrecht (Nl). pp 1-23.

Glas MS, Motti CA, Negri AP, Sato Y, Froscio S, Humpage AR et al (2010). Cyanotoxins are not implicated in the etiology of coral black band disease outbreaks on Pelorus Island, Great Barrier Reef. Fems Microbiology Ecology 73: 43-54.

Glud RN, Gundersen JK, Revsbech NP, Jorgensen BB (1994). Effects on the benthic diffusive boundary-layer imposed by microelectrodes. Limnology and Oceanography 39: 462-467.

Goldstein S (2003). Foraminifera: A biological overview. In: Sen Gupta B (ed). Modern Foraminifera. Springer Netherlands: New York, Boston, Dordrecht, London, Moscow. pp 37-55.

Hein M, Sand-Jensen K (1997). CO_2 increases oceanic primary production. Nature 388: 526-527.

Heinze C, Maier-Reimer E, Winn K (1991). Glacial pCO_2 reduction by the world ocean: experiments with the Hamburg carbon cycle model. Paleoceanography 6: 395-430.

Heinze J (1993). Elektrochemie mit Ultramikroelektroden. Angewandte Chemie 105: 1327-1349.

Hemleben C, Anderson OR, Berthold W, Spindler M (1986). Calcification and chamber formation in foraminifera - a brief overview. In: Leadbeater BSC, Riding R (eds). Biomineralization in lower plants and animals. Oxford University Press: Oxford. pp 237-249.

Hinke J (1969). Glass microelectrodes for the study of binding and compartmentalisation of intracellular ions. In: Lavallee M, Schanne OF, Herbert NC (eds). Glass microelectrodes. Wiley: New York. pp 349-375.

Hurd CL, Cornwall CE, Currie K, Hepburn CD, McGraw CM, Hunter KA et al (2011). Metabolically induced pH fluctuations by some coastal calcifiers exceed projected 22nd century ocean acidification: a mechanism for differential susceptibility? Global Change Biology 17: 3254-3262.

IPCC (2007). Climate change 2007: synthesis report. Cambridge University Press: Cambridge. pp. 23-74

Jokiel PL (2011). The reef coral two compartment proton flux model: A new approach relating tissue-level physiological processes to gross corallum morphology. Journal of Experimental Marine Biology and Ecology 409: 1-12.

Jonkers HM, Ludwig R, De Wit R, Pringault O, Muyzer G, Niemann H et al (2003). Structural and functional analysis of a microbial mat ecosystem from a unique permanent hypersaline inland lake: 'La Salada de Chiprana' (NE Spain). FEMS Microbiology Ecology 44: 175-189

Jørgensen BB, Erez J, Revsbech NP, Cohen Y (1985). Symbiotic photosynthesis in a planktonic foraminiferan, *Globigerinoides-Sacculifer* (Brady), studied with microelectrodes. Limnology and Oceanography 30: 1253-1267.

Jørgensen BB, Revsbech NP (1985). Diffusive boundary-layers and the oxygen-uptake of sediments and detritus. Limnology and Oceanography 30: 111-122.

Jørgensen BB (2001). Life in the diffusive boundary layer. In: Boudreau PB, Jorgensen BB (eds). The benthic boundary layer. Oxford University Press: Oxford. pp 348-373.

Köhler-Rink S, Kühl M (2000). Microsensor studies of photosynthesis and respiration in larger symbiotic foraminifera. I The physico-chemical microenvironment of *Marginopora vertebralis*, *Amphistegina lobifera* and *Amphisorus hemprichii*. Marine Biology 137: 473-486.

Köhler-Rink S, Kühl M (2005). The chemical microenvironment of the symbiotic planktonic foraminifer *Orbulina universa*. Marine Biology Research 1: 68-78.

Kuehl K, Jones R, Gibbs D, Richardson L (2011). The roles of temperature and light in black band disease (BBD) progression on corals of the genus *Diploria* in Bermuda. Journal of Invertebrate Pathology 106: 366-370.

Kühl M, Cohen Y, Dalsgaard T, Jørgensen BB, Revsbech NP (1995). Microenvironment and photosynthesis of zooxantella in scleractinian corals studied with microsensors for O_2, pH and light. Mar Ecol Prog Ser 117: 159-172.

Kühl M, Revsbech NP (2001). Biogeochemical microsensors for boundary layer studies. In: Boudreau PB, Jørgensen BB (eds). The benthic boundary layer. Oxford University Press: Oxford. pp 180-210.

Lowenstam HA, Weiner S (1989). On biomineralization. Oxford University Press: Oxford, New York, Toronto.

Ludwig R, Al-Horani FA, de Beer D, Jonkers HM (2005). Photosynthesis-controlled calcification in a hypersaline microbial mat. Limnology and Oceanography 50: 1836-1843.

Marx D, Tuckerman ME, Hutter J, Parrinello M (1999). The nature of the hydrated excess proton in water. Nature 397: 601-604.

Miller AW, Richardson LL (2011). A meta-analysis of 16S rRNA gene clone libraries from the polymicrobial black band disease of corals. Fems Microbiology Ecology 75: 231-241.

Monnin E, Indermühle A, Dällenbach A, Flückiger J, Stauffer B, Stocker TF et al (2001). Atmospheric CO_2 concentrations over the last glacial termination. Science 291: 112-114.

Mucci A (1983). The solubility of calcite and aragonite in seawater at various salinities, temperatures, and one atmosphere total pressure. American Journal of Science 283: 780-799.

Nielsen AE (1964). Kinetics of precipitation. Pergamon Press [distributed in the Western Hemisphere by Macmillan]: Oxford, New York.

NOAA-ESRL (2012). Atmospheric CO_2 for May 2012. In: Laboratory NOaAA-ESR (ed). Pro Oxygen: Mauna Loa Observatory. electronic document: http://co2now.org/, accessed 18.05.2012.

Orr JC, Fabry VJ, Aumont O, Bopp L, Doney SC, Feely RA et al (2005). Anthropogenic ocean acidification over the twenty-first century and its impact on calcifying organisms. Nature 437: 681-686.

Pearson PN, Foster GL, Wade BS (2009). Atmospheric carbon dioxide through the Eocene-Oligocene climate transition. Nature 461: 1110-1113.

Petit JR, Jouzel J, Raynaud D, Barkov NI, Barnola JM, Basile I et al (1999). Climate and atmospheric history of the past 420,000 years from the Vostok ice core, Antarctica. Nature 399: 429-436.

Pierrot DE, Lewis E, Wallace DWR (2006). MS exel program developed for CO_2 system calculations. ORNL/CDIAC-105a Carbon Dioxide Information Analysis Centre. Oak Ridge National Laboratory, US Department of Energy.

Prandtl L (1928). Über Flüssigkeitsbewegungen sehr kleiner Reibung. Proc. 3rd Intern. Math. Congr. Heidelberg 1904, 484 – 491. Reprinted in: Vier Abhandlungen zur Hydrodynamik und Aerodynamik, Göttingen, 1927; see also Coll. Works II, 575 – 584; Engl. Transl. NACA TM 452 (1928).

Raven JA, Falkowski PG (1999). Oceanic sinks for atmospheric CO_2. Plant, Cell & Environment 22: 741-755.

Revsbech NP, Jørgensen BB (1986). Microelectrodes - Their Use in Microbial Ecology. Advances in Microbial Ecology 9: 293-352.

Richardson LL (1998). Coral diseases: what is really known? Trends in Ecology and Evolution 13: 438-443.

Riebeek H (2011). The carbon cycle. NASA earth observatory. electronic document: http://earthobservatory.nasa.gov/Features/CarbonCycle/, accessed 18.05.2012.

Riebesell U, Wolf-Gladrow DA, Smetacek V (1993). Carbon dioxide limitation of marine phytoplankton growth rates. Nature 361: 249-251.

Riebesell U, Körtzinger A, Oschlies A (2009). Sensitivies of marine carbon fluxes to ocean change. Proceedings of the National Academy of Sciences 106: 20602-20609.

Rink S, Kühl M, Bijma J, Spero HJ (1998). Microsensor studies of photosynthesis and respiration in the symbiotic foraminifer *Orbulina universa*. Marine Biology 131: 583-595.

Røy H (2003). Dynamic structure and function of the diffusive boundary layer at the seafloor. PhD thesis, Universität Bremen, Bremen.

Rost B (2003). Inorganic carbon acquisition and isotope fractionation of marine phytoplankton with emphasis on the coccolithophore *Emiliania huxleyi*. PhD thesis, Universität Bremen, Bremen.

Royer DL, Berner RA, Park J (2007). Climate sensitivity constrained by CO_2 concentrations over the past 420 million years. Nature 446: 530-532.

Sabine CL, Feely RA, Gruber N, Key RM, Lee K, Bullister JL et al (2004). The oceanic sink for anthropogenic CO_2. Science 305: 367-371.

Santschi PH, Nyffeler UP, Azevedo WS, Broecker WS (1983). Estimates of the resistance to chemical transport posed by the deep-sea boundary layer. Limnology & Oceanography 28: 899-912.

Sarmiento JL, Murnane R, Quere CL, Keeling R, Williams RG (1995). Air-sea CO_2 transfer and the carbon budget of the North Atlantic. Philosophical Transactions of the Royal Society of London Series B: Biological Sciences 348: 211-219.

Sato Y, Bourne DG, Willis BL (2009). Dynamics of seasonal outbreaks of black band disease in an assemblage of *Montipora* species at Pelorus Island (Great Barrier Reef, Australia). Proceedings of the Royal Society B-Biological Sciences 276: 2795-2803.

Sato Y, Willis BL, Bourne DG (2010). Successional changes in bacterial communities during the development of black band disease on the reef coral, *Montipora hispida*. ISME Journal 4: 203-214.

Schlichting H (1979). Boundary layer theory, 7th edition edn. McGraw-Hill New York.

Sekar R, Kaczmarsky LT, Richardson LL (2008). Microbial community composition of black band disease on the coral host *Siderastrea siderea* from three regions of the wider Caribbean. Marine Ecology-Progress Series 362: 85-98.

Shashar N, Cohen Y, Loya Y (1993). Extreme diel fluctuations of oxygen in diffusive boundary-layers surrounding stony corals. Biological Bulletin 185: 455-461.

Stoyanov ES, Stoyanova IV, Reed CA (2010). The Structure of the Hydrogen Ion (H_{aq}^+) in Water. Journal of the American Chemical Society 132: 1484-1485.

Sutherland KP, Porter JW, Torres C (2004). Disease and immunity in Caribbean and Indo-Pacific zooxanthellate corals. Marine Ecology-Progress Series 266: 273-302.

Taylor AR, Chrachri A, Wheeler G, Goddard H, Brownlee C (2011). A voltage-gated H^+ channel underlying pH homeostasis in calcifying coccolithophores. PLoS Biol 9: e1001085, advanced online publication: doi:10.1371/journal.pbio.1001085

Volk T, Hoffert MI (1985). Ocean carbon pumps: analysis of relative strengths and efficiencies in ocean-driven atmospheric CO_2 changes. The carbon cycle and atmospheric CO_2: natural variations archean to present. AGU: Washington DC. pp 99-110.

Wolf-Gladrow D, Riebesell U (1997). Diffusion and reactions in the vicinity of plankton: A refined model for inorganic carbon transport. Marine Chemistry 59: 17-34.

Wolf-Gladrow DA, Bijma J, Zeebe RE (1999a). Model simulation of the carbonate chemistry in the microenvironment of symbiont bearing foraminifera. Marine Chemistry 64: 181-198.

Wolf-Gladrow DA, Riebesell ULF, Burkhardt S, Bijma J (1999b). Direct effects of CO_2 concentration on growth and isotopic composition of marine plankton. Tellus B 51: 461-476.

Zachos JC, Dickens GR, Zeebe RE (2008). An early Cenozoic perspective on greenhouse warming and carbon-cycle dynamics. Nature 451: 279-283.

Zeebe RE, Wolf-Gladrow D (2001). CO_2 in Seawater: Equilibrium, Kinetics and Isotopes., 1st edition edn, vol. 65. Elsevier: Amsterdam.

8. Overview of manuscripts

I) *Original research article*: **Martin S. Glas**, Gerald Langer, Nina Keul. Calcification acidifies the microenvironment of a benthic foraminifer (*Ammonia* sp.). This article is published in the Journal of Experimental Marine Biology and Ecology (*JEMBE*) 424-425: 53 – 58. doi:10.1016/j.jembe.2012.05.006

Contributions: M. Glas and N. Keul planned the study. All authors performed the culturing. M. Glas performed the microsensor measurements, sample analyses and analyzed all data. M. Glas and G. Langer interpreted the data. M. Glas wrote the manuscript with help of all co-authors.

II) *Original research article*: **Martin S. Glas**, Yui Sato, Karin E. Ulstrup, David G. Bourne. Biogeochemical conditions determine virulence of black band disease in corals. This article is published in the *ISME Journal*: advanced online publication, February 9th 2012; http://dx.doi.org/10.1038/ismej.2012.2

Contributions: M. Glas, D. Bourne and K. Ulstrup planned the study. Y. Sato performed the field-sampling. D. Bourne performed the molecular work. M. Glas performed the microsensor measurements, lesion culturing, sampling, and analyzed all data. M. Glas wrote the manuscript with help of all co-authors.

III) *Original research article*: Kristina Stemmer, **Martin S. Glas**, Dirk de Beer, Martin Beutler, Thomas Brey. The extrapallial fluid of the bivalve *Arctica islandica* is not the site of shell formation. This work will be submitted to a peer-reviewed scientific journal. A manuscript is currently in preparation by K. Stemmer. An abstract is supplied as a supplement to this thesis.

Contributions: K. Stemmer and M. Glas planned the study. K. Stemmer performed the field-sampling. K. Stemmer and M. Glas performed the microsensor measurements and carbonate chemistry analyses. K. Stemmer, M. Beutler and M. Glas performed the fluorescence imaging. K. Stemmer performed the radiotracer studies. M. Glas and K. Stemmer analyzed the data.

IV) *Original research article*: Miriam Weber, Craig Humphrey, **Martin S. Glas**, Dirk de Beer, Katharina E. Fabricius. The impacts of sediment-microgradients on the calcification of corals, foraminifera and crustose coralline algae. The dataset is

currently analyzed. This work will be submitted to a peer-reviewed scientific journal. An abstract is supplied as a supplement to this thesis.

Contributions: M. Weber, K. Fabricius and Dirk de Beer planned this study. M. Weber, M. Glas and K. Fabricius performed the field work. M. Weber, C. Humphrey and M. Glas performed the lab work.

V) *Original research article:* **Martin S. Glas**, Katharina E. Fabricius, Dirk de Beer, Sven Uthicke. The O_2, pH and Ca^{2+} microenvironment of benthic foraminifera in a high CO_2 world. This manuscript is currently in review with *PLosONE*. This dataset was selected by the ASLO conference 2012 in Japan for a student travel award.

Contributions: M. Glas and S. Uthicke planned and designed the study. M. Glas and S. Uthicke performed the field sampling. M. Glas performed all measurements, analyses and analyzed all data with statistical help from K. Fabricius. M. Glas wrote the manuscript with help of all co-authors.

VI) *Original research article*: Katharina E. Fabricius, Chris Langdon, Sven Uthicke, Craig Humphrey, Sam Noonan, Glenn De'ath, Remy Okazaki, Nancy Muehllehner, **Martin S. Glas** and Janice M. Lough. This article is published in *Nature Climate Change*: 1(3): 165-169. DOI: 10.1038/NCLIMATE1122

Contributions: K. Fabricius planned and designed the study. All co-authors beside G. De'ath and J. Lough, who were involved in the data and sample analyses, helped in the field work. K. Fabricius wrote the manuscript with help of all co-authors.

Chapter 1

Effects of calcification on microenvironments

Calcification acidifies the microenvironment of a benthic foraminifer (*Ammonia* sp.)

Martin S. Glas [a,*], Gerald Langer [b,c], Nina Keul [c]

[a] *Max Planck Institute for Marine Microbiology, Celsiusstr. 1, D-28359 Bremen, Germany*
[b] *Department of Earth Sciences, Cambridge University, Cambridge CB2 3EQ, United Kingdom*
[c] *Alfred Wegener Institute for Polar and Marine Research, Am Handelshafen 12, D-27570 Bremerhaven, Germany*

ARTICLE INFO

ABSTRACT

Calcareous foraminifera are well known for their $CaCO_3$ shells. Yet, $CaCO_3$ precipitation acidifies the calcifying fluid. Calcification without pH regulation would therefore rapidly create a negative feedback for $CaCO_3$ precipitation. In unicellular organisms, like foraminifera, an effective mechanism to counteract this acidification could be the externalization of H^+ from the site of calcification. In this study we show that a benthic symbiont-free foraminifer *Ammonia* sp. actively decreases pH within its extracellular microenvironment only while precipitating calcite. During chamber formation events the strongest pH decreases occurred in the vicinity of a newly forming chamber (range of gradient ~100 μm) with a recorded minimum of 6.31 (<10 μm from the shell) and a maximum duration of 7 h. The acidification was actively regulated by the foraminifera and correlated with shell diameters, indicating that the amount of protons removed during calcification is directly related to the volume of calcite precipitated. The here presented findings imply that H^+ expulsion as a result of calcification may be a wider strategy for maintaining pH homeostasis in unicellular calcifying organisms.

1. Introduction

Foraminifera are abundant marine calcifiers found in virtually all marine habitats. There are approximately 10,000 extant species (Vickerman, 1992) and calcareous wall structures radiated in the Paleozoic (Ross and Ross, 1991; Tappan and Loeblich, 1988) making their calcium carbonate shells important index fossils. Together with coccolithophores, foraminifera are the major pelagic producers of calcium carbonate (Baumann et al., 2004). Their fossilization, abundance and global distribution moreover make calcareous foraminifera an important model organism for paleoceanographic reconstructions. The (trace) element and stable isotope compositions of their calcite shells are used as proxies to estimate past seawater parameters, such as temperature (Lea, 2003), salinity (Rohling, 2000), pH (Spero et al., 1997; Spivack et al., 1993) and nutrients (Elderfield and Rickaby, 2000; Rickaby and Elderfield, 1999). A process-based understanding of foraminiferal calcification is therefore essential to better interpret proxy signals.

Foraminifera grow in discrete steps of new chamber additions. Calcite precipitation in benthic rotalid foraminifera is believed to proceed in a confined space termed delimited biomineralization space (DBS). This space is actively created by the rhizopodial network around the newly forming chamber during chamber formation events (Fig. 1, model based on Erez, 2003). $CaCO_3$ precipitation is catalyzed on the surface of an organic template termed primary organic sheet (POS), being formed after establishment of the DBS (reviewed in

Erez, 2003; Goldstein, 1999). In benthic rotalid foraminifera calcite wall thickening proceeds in two layers, termed 'primary calcite' on the POS of the newly forming chamber and a secondary layer termed 'secondary calcite' ((Angell, 1967), reviewed in Erez, 2003; Hansen, 1999). This secondary calcite is excreted over the complete shell surface of the foraminifera during chamber formation, resulting in a fine lamination of older chambers (Hansen, 1999).

Central to calcite precipitation by foraminifera (as in all calcifiers) is a strict control over the carbonate chemistry of the calcifying fluid. To promote $CaCO_3$ precipitation, super-saturation of the calcifying fluid needs to be maintained throughout the calcifying period. In addition, to form the delicate structures of foraminiferal shells, strict control of the timing, rate and geometry of precipitation as well as the degree of super-saturation is required (Nielsen, 1964).

It is well established that calcite precipitation strongly decreases the pH of the calcifying fluid (Zeebe and Wolf-Gladrow, 2001). Thus, biological regulated calcification, taking place in confined compartments (as in foraminifera), would rapidly shift the carbonate system towards a lower calcite saturation state without active pH compensation and thereby create a negative feedback for calcite precipitation.

We hypothesize that during chamber formation the degree of $CaCO_3$ super-saturation is controlled by active export of protons from the calcifying fluid. This excess acidification does not appear inside the cell as intracellular pH is highly regulated (reviewed in Alberts et al., 2002; Madshus, 1988). Therefore, the protons must either be neutralized or externalized. The latter mechanism implies that the proton discharge should result in an acidification of the microenvironment around the newly forming calcite.
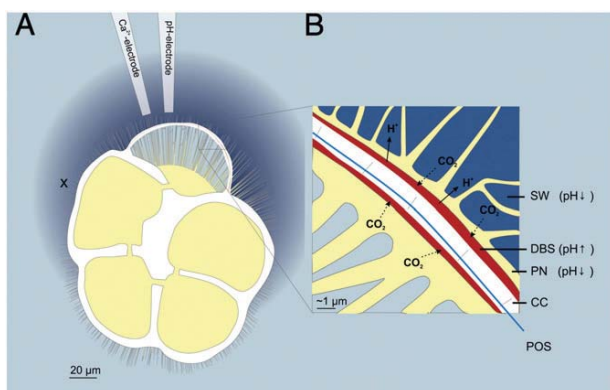
Fig. 1. A) Measurement settings for combined pH and Ca^{2+} measurements of *Ammonia* sp. during chamber formation. Area affected by low pH gradient (idealized shape) is colored in dark blue (thickness reduced to ~1/3 for clarity). Spikes indicate the fine pseudopodial network (PN = yellow) established during chamber formation and forming the delimited biomineralization space (DBS = red). B) Close up of calcifying fluid and DBS. Increased pH within the DBS and calcification (reduction of DIC) would strongly enhance the molecular diffusion of CO_2 into the DBS from both the cytosol and the surrounding seawater (SW). POS = primary organic sheet (light blue), CC = $CaCO_3$ (calcite), dashed arrows indicate molecular diffusion, solid arrows indicate the active transport of ions.

We tested this hypothesis by measuring pH and Ca^{2+} dynamics within the microenvironment of calcifying and non-calcifying foraminiferal specimens at different life stages with microsensors. To exclude the effect of photosynthesis, which is known to influence pH microenvironments (Rink et al., 1998), we conducted our experiments with specimens of the benthic, symbiont-free, non-phototrophic genus *Ammonia* (Cushman, 1926).

2. Materials and methods

2.1. Sampling and culturing

Specimens of a single morphotype of *Ammonia* were collected from North Sea tidal flats near Dorum, Germany (53°40′28″N 8°30′57″E) between August 2009 and June 2010. Sediments were sieved (mesh size 630 μm) to remove larger meiofauna and stored in seawater at 10 °C in the dark. Prior to experiments, adult individuals were isolated from the sediment by additional sieving through a 230 μm mesh. Reproduction was stimulated by cultivating these individuals at 25 °C and reduced salinity (to about 26) and by feeding them with sterile, heat-treated (photosynthetically inactive) microalgae of the species *Dunaliella salina*. Within 7 days about 10% of the adults reproduced asexually, yielding approximately 50–200 single-chambered juveniles (Ø~50 μm) per event, which were used for the experiments.

2.2. Experimental setup

Microsensor measurements were performed in a large Petri dish under a backlit microscope (ZeissAxiovert 200 M) equipped with a camera (AxioCamMRc5). The Petri dish was filled with natural seawater of reduced salinity (to about 26) and contained >30 individuals. The friction velocity at the bottom of the Petri dish was adjusted to 0.2 cm s^{-1} by measuring particle movement over the bottom and directing an air jet onto the water surface, to emulate natural flow conditions of tidal flat sediment surfaces (Huettel and Gust, 1992; Shimeta et al., 2001). Temperature and pH (total scale) in the bulk seawater were measured using a micro-thermometer and a handheld pH meter (WTW pH 330i), respectively.

pH LIX (precision 0.005), Ca^{2+} LIX (precision 5 μM), and glass pH microelectrodes (precision 0.001) were prepared, calibrated and used as previously described (Ammann et al., 1987; De Beer, 2000; De Beer et al., 2000; Revsbech and Jorgensen, 1986). A detailed description of the measurement setup can be found in Polerecky et al. (2007). Microsensors had a tip diameter of <20 μm and were positioned around foraminifera using a robotic arm (Eppendorf PatchManNP2 system) with a precision of 50 nm.

2.3. Experimental procedure

Microscale measurements of pH and Ca^{2+} were performed in close vicinity (<10 μm) around foraminifera and away from the calcite shell in the bulk seawater between and during chamber formation events (Fig. 2). Ca^{2+} measurements were done simultaneously with pH measurements, with sensor tips separated by ~10 μm (Fig. 1A). All time series recordings of pH and Ca^{2+} stated in Figs. 3, 4 and 5 were performed within the rhizopodial network for >30 min on top of the POS (<10 μm distance) as illustrated by Fig. 1A. Chamber formation was visually detected by observing pseudopodial retraction and gathering of food particles around the shell and space where the new chamber was going to be formed (reviewed in Goldstein, 1999). Throughout chamber formation, individuals remained in a fixed position attached to the bottom of the Petri dish, allowing accurate placement of the microsensor tips and ensuring a stable position of the electrode during chamber formation. The dimensions of the specimen and of the newly forming chambers were measured from the acquired time series images (software Zeiss, Axio-Vision 4.8.1).

2.4. Mass balance calculations

Calcification rates [μg h^{-1}] were estimated from the amount of precipitated calcite and duration of the individual chamber formation events that could be recorded completely ($n = 19$). The amount of calcite was calculated by assuming the newly formed chamber as 2/3 of an ellipsoid with radii derived from measured chamber dimensions, wall thickness of 3 μm (de Nooijer et al., 2009b) and tabulated calcite densities (DeFoe and Compton, 1925).

2.5. Data analyses

Linear regressions between specimen diameter (measured as largest possible diameter of individuals) and pH decreases, duration of pH decreases were assessed using Pearson product–moment correlation coefficient (R) and a general linear regression model. Regressions and statistical analyses were performed with the statistical analyses software SigmaPlot 10.0 (Systat Inc., USA).

3. Results

3.1. Microsensor measurements

During chamber formation strong pH decreases were detected near the primary organic sheet (POS) of newly calcifying chambers and in its vicinity (as illustrated by Fig. 1A) in all specimens (Fig. 2). The strongest pH decreases originated from the newly forming chambers but also extended to the neighboring chambers (Fig. 1A, indicated as point X). The difference between the maximum pH decreases recorded at the surface of the POS (Fig. 1A) and that of the surrounding seawater, denoted as ΔpH, was positively linearly correlated with the diameter of the individuals and ranged from −0.060 to −1.774 (Fig. 3). The pH decreases only occurred when chamber formation had progressed beyond the initial stage of rhizopodial network formation (~1 h) and construction of the primary organic sheet (POS; 1–3 h; Fig. 4). The onset of calcite precipitation could not be timed accurately (>3 min accuracy) by light microscopy, but was associated with an instant decrease in extracellular pH (<1 min precision, Fig. 4). The acidification persisted while the formation of pores within the calcite wall became apparent about 1–2 h
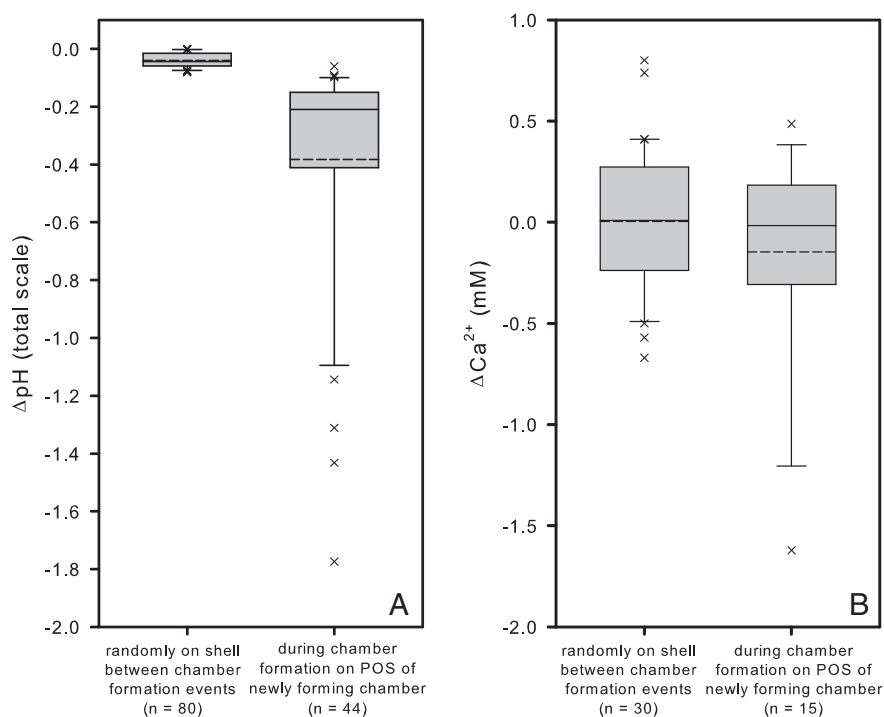
Fig. 2. Differences between A) pH- and B) Ca^{2+}-decreases and the bulk seawater (denoted as ΔpH and ΔCa^{2+}) recorded around (<10 μm from the shell) replicated (*n*) foraminiferal specimens between and during chamber formation events. Box plots show the 25th, 50th and 75th percentiles (horizontal bars). Error bars indicate the 90th and 10th percentiles. Means are indicated as dotted lines.

after the onset of calcification. The end of the chamber formation process was reached when foraminifera extended their pseudopodia and resumed movement. Shortly before and sometimes during the extension of larger rhizopodia the pH microenvironment around the foraminifera reverted back to seawater levels (Fig. 4). The timing of pH acidification of the foraminiferal microenvironment therefore exactly matched with visual signs of calcite precipitation (Fig. 4). Complete chamber formation events could be recorded in 19 cases and acidification lasted between 1 h 10 min and 7 h (Fig. 5). Durations also exhibited a positive linear correlation with the diameter of the individuals (Fig. 5). Thickness and form of the pH gradients measured from the POS surface and extending into the surrounding seawater (i.e. the 'diffusive boundary layers' = DBLs) were highly variable (50–500 μm) and strongly depended on the orientation of the new chamber in respect to flow
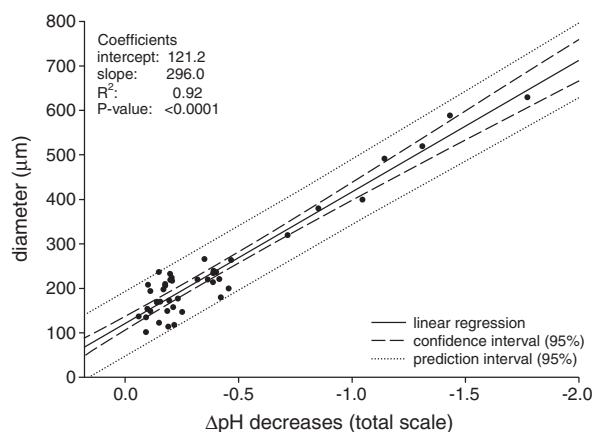
direction and gathering of food particles, which hampered and distorted linear diffusion (data not shown). Calcification rates derived from mass balance calculations (*n* = 19) were 0.028 ± 0.002 (SE) μg h^{-1} and ranged from 0.015 to 0.045 μg h^{-1}.

During periods between two chamber formation events only small pH variations (0 to −0.08) were detectable (−0.040 ± 0.003 (mean ± SE)). These small pH decreases were not localized specifically to the surface of the shell, but recorded on all plasma membranes including rhizopodia (Fig. 2).

The established proton flux was highly regulated by the foraminifera as disturbance of the POS by gently nudging the microsensors resulted in an instant pH increase (Fig. 4), thus interrupting H^+ pumping. A complete breakdown of H^+ pumping was observed if disturbances persisted or occurred near the end of the chamber formation process. Small oscillations in pH were present in about 1/3 of all chamber formation events and persisted throughout lowered pH conditions (Fig. 4).

ΔCa^{2+} measured on top of the POS was variable between (4 ± 65 μM (mean ± SE)) and during (−146 ± 135 μM (mean ± SE)) chamber formation (Fig. 2). In contrast to pH dynamics, Ca^{2+} did not change significantly during chamber formation when averaged over all tested individuals compared to the surrounding seawater (paired *t*-test: *t* = 1.081, *df* = 14, *P* = 0.298, *n* = 15).

4. Discussion

4.1. Acidification due to calcification

The exact congruence of timing of the measured microenvironmental acidification with visual signs of calcite precipitation (Fig. 4), together with the fact that acidification could not be detected in periods in between two chamber formation events (Fig. 2), indicates that the pH drops are a direct consequence of localized proton removal from the site of calcification during calcite precipitation (Fig. 1B).

Fig. 3. Relationship between foraminiferal diameter and decreases of pH during chamber formation events and their linear regression (*n* = 44).
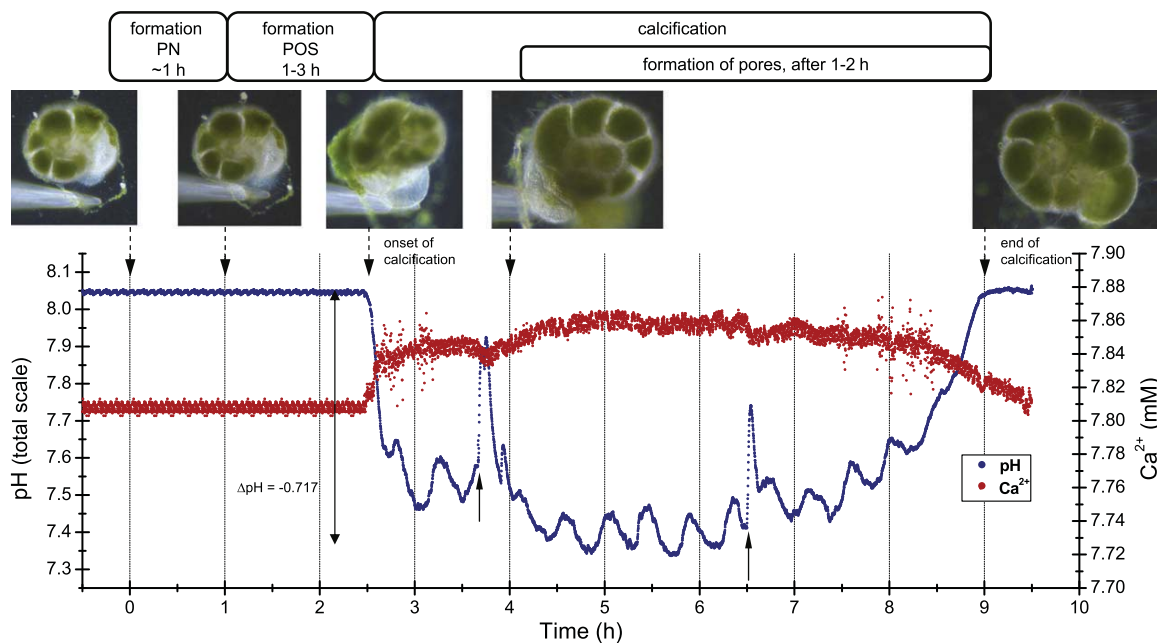
Fig. 4. Example of pH and Ca^{2+} dynamics of an adult *Ammonia* sp. individual (diameter 320 μm) during a chamber formation event. Upward arrows indicate the moments of deliberate nudging of the POS to trigger the interruption of active proton pumping for ~5 min. Ambient water conditions: salinity 26, temperature 18 °C; incident light: 10 μmol photons m^{-2} s^{-1}; friction velocity: 0.2 cm s^{-1}.

An additional indicator for this is the observed significant correlation between foraminiferal diameter and ΔpH changes (Fig. 3), following a trend of increased calcite precipitation with size. The microenvironmental acidification in the vicinity of neighboring chambers (Fig. 1A as indicated by point X) is most likely caused by secondary lamination of older chambers during chamber formation. Yet, the strongest pH drops radiated from the newly forming chamber, as a result of the high volumetric concentrations of calcite being precipitated in this region (Fig. 1A) (Hansen, 1999; Hansen and Reiss, 1971). Due to this fact, differentiating acidifications between primary and secondary layering around foraminifera was difficult.

4.2. Calcification rates

Calcification rates obtained by the measurements (0.028 ± 0.002 (mean ± SE) μg h^{-1}) represent, to the best of our knowledge, the first
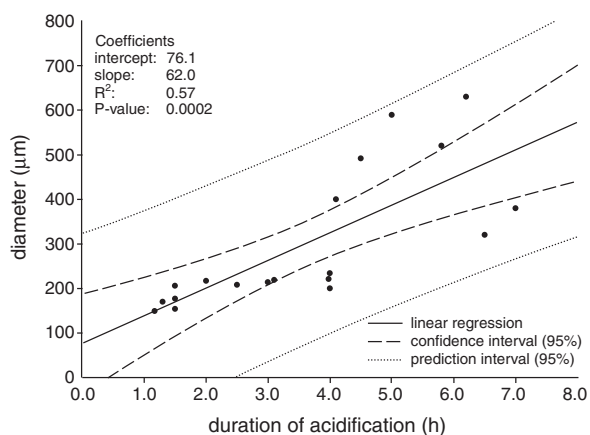
Fig. 5. Relationship between foraminiferal diameter and duration of pH decreases during chamber formation events that could be recorded completely and their linear regression ($n = 19$).

estimates of calcification rates for *Ammonia* sp. They are lower than rates obtained by Ca^{2+} labeling experiments of symbiotic planktonic foraminifera (0.04 μg h^{-1} (dark) to 0.11 μg h^{-1} (light) (Erez, 1983), 0.39 to 0.87 μg h^{-1} (light) (Anderson and Faber, 1984), 0.06 μg h^{-1} (dark) to 0.32 μg h^{-1} (light) (Lea et al., 1995)). Yet, cell diameters of *Ammonia* sp. are small compared to planktonic species, suggesting decreased calcification rates with decreasing size as in coccolithophores (Langer et al., 2006; Stoll et al., 2002). Also, compared to the above labeling experiments, calcification rates determined geometrically from the formation of the ultimate chamber did not take secondary layering of the complete shell into account and thereby underestimated the amount of total calcite precipitated. Yet, calcification rates are less variable than in symbiotic foraminifera, indicating that photosynthesis is most likely the cause for increased variability of calcification rates as suggested by Lea et al. (1995).

4.3. Calcium dynamics

The variability of ΔCa^{2+} between and during chamber formation events (Fig. 2) is in accordance with previous microsensor measurements, showing high spatial variability of Ca^{2+} microgradients in *Amphistegina lobifera* and *Marginopora vertebralis* (Koehler-Rink and Kuehl, 2000) and among specimens in *Orbulina universa* (Koehler-Rink and Kuehl, 2005). This indicates that Ca^{2+} uptake varies temporally and spatially over the shell surface of *Ammonia* sp. (Koehler-Rink and Kuehl, 2000). The absence of an overall significant calcium gradient during chamber formation in the microenvironment can be explained in two ways: 1) Ca^{2+} was not transported from the external seawater into the DBS via channel-pumping, but supplied via an intracellular calcium pool as shown by Anderson and Faber (1984), ter Kuile and Erez (1988) and ter Kuile et al. (1989). 2) Ca^{2+} was transported over the complete surface of the shell (Angell, 1979). Due to the high surface area, Ca^{2+} concentrations of North Sea seawater would only require a small concentration gradient to establish a high enough flux to sustain a constant rate of calcite precipitation at calcite supersaturated conditions ($\Omega_{calcite} > 1$). In both cases calcium

gradients measured within the foraminiferal microenvironment would be small, which is in accordance with the measurements.

4.4. Trans-membrane transport of H^+

We confirm that the site of calcification (i.e. the 'delimited biomineralization space') must be delineated from the bulk seawater (Angell, 1979; Be et al., 1979; Erez, 2003), as explained in the following. The microenvironment around the newly forming chamber is most likely low- or under-saturated in respect to calcite, due to the observed acidification (see also (Wolf-Gladrow and Riebesell, 1997; Wolf-Gladrow et al., 1999)). It is therefore unlikely that calcite precipitation proceeds directly from bulk seawater during chamber formation, considering the measured high calcification rates (see above). Also, if protons could diffuse freely between DBS and bulk seawater, so would other ions, e.g. Ca^{2+}, Mg^{2+} and Sr^{2+}. However, measured Mg- and Sr-fractionation factors in Ammonia sp. cannot be explained assuming inorganic fractionation (Dissard et al., 2010), but are consistent with the hypothesis that these ions are transported across membranes before entering the calcifying fluid. It is therefore inferred that trans-membrane transport across the pseudopodial network is the means of proton removal during chamber formation (Fig. 1B). Voltage gated H^+-channels have recently been discovered in the protoplasma membrane of coccolithophores and are present in a wide variety of eukaryotic protists (Taylor et al., 2011).

An instant halt of trans-membrane transport of protons can also explain the pH increase in the microenvironment upon mechanical disturbance of the individual during chamber formation (Fig. 4). Another explanation could be a temporary rupture of the pseudopodial network upon mechanical disturbance and a consequent efflux of pH elevated calcifying fluid into the surrounding seawater (Fig. 1B). Yet, the acidic characteristics near the newly forming chamber were equally rapidly restored if the mechanical disturbance was not prolonged or too severe (Fig. 4). This shows that foraminifera strongly regulate calcite precipitation and/or H^+ removal.

After the initial drop in pH during chamber formation, pH underwent cyclic changes (Fig. 4). It can only be speculated what this pH-fluctuation might be. One possibility could be a temporary opening of the pseudopodial network around the calcifying chamber causing mixing of the high pH fluid from the DBS with the lower pH fluid of the microenvironment. The function of such a temporary opening, however, remains unclear. A replenishment of the DBS with Ca^{2+} and/or dissolved inorganic carbon (DIC) cannot be the main function because such a Ca^{2+}-pathway would not fractionate strongly against Mg^{2+} and weakly for Sr^{2+} (Dissard et al., 2010), as discussed above. Another possibility could be the additional cyclic exocytosis of low pH fluid vesicles to maintain cellular pH homeostasis. Such low pH compartments have previously been identified in other benthic rotalid foraminifera during calcification (Bentov et al., 2009; de Nooijer et al., 2009a). A third explanation could be related to temporary ion transport across the plasma membrane of the pseudopodial network. Cyclic H^+ conductive transport pathways would hereby allow for short periods of net H^+-uptake and therefore extracellular temporal alkalization (reviewed in Lukacs et al., 1993).

Active H^+ removal from the DBS does not only result in a pH decrease in the microenvironment of a newly forming chamber, but also in a comparatively increased pH within the DBS (Fig. 1B). An advantage of such a pH increase within the DBS is related to the driving force for CO_2 transport. A twofold pH gradient established between the DBS, the external seawater and cytosol would strongly enhance molecular diffusion of CO_2 from the acidic cytosol (see also (Angell, 1979; Zeebe and Sanyal, 2002)) and external seawater into the DBS on a micro scale (0.1–5 μm distance, Fig. 1B). Such a mechanism has already been suggested for high pH seawater vacuoles during chamber formation in other species of benthic rotalid foraminifera (Bentov et al., 2009; de Nooijer et al., 2009a). Also, diffusion is the limiting factor for DIC uptake

in Amphistegina lobifera and calcification in Amphisorus hemprichii (ter Kuile et al., 1989). Hence, by maintaining an increased pH to increase super-saturation with respect to calcite within the DBS, a highly efficient DIC trap would be created at the same time, facilitating bilateral diffusion of CO_2 into the DBS (Fig. 1B).

5. Conclusions

Our results show that calcification during chamber formation strongly influences the extracellular pH in the microenvironment (range of gradient ~100 μm) of the benthic foraminifer Ammonia sp. Additionally, within their natural habitats, i.e. tidal flat surface sediments with strongly decreased diffusivity compared with natural seawater, this pH effect is expected to be more pronounced. The here presented findings might suggest that excess H^+ expulsion due to calcification could be a widespread strategy for maintaining pH homeostasis in other species of calcareous rotalid foraminifera.

References

Alberts, B., Johnson, A., Lewis, J., Raff, M., Roberts, K., Walter, P., 2002. Molecular biology of the cell, 4th ed. Garland Science Taylor & Francis Group, New York.
Ammann, D., Bührer, T., Schefer, U., Müller, M., Simon, W., 1987. Intracellular neutral carrier based Ca^{2+} microelectrode with sub-nanomolar detection limit. Pflugers Arch. 409, 223–228.
Anderson, O.R., Faber, W.W., 1984. An estimation of calcium carbonate deposition rate in a planktonic foraminifer Globigerinoides sacculifer using 45 Ca as a tracer; a recommended procedure for improved accuracy, pp. 303–308.
Angell, R.W., 1967. The test structure and composition of the foraminifer Rosalina floridana*. J. Eukaryot. Microbiol. 14 (2), 299–307.
Angell, R.W., 1979. Calcification during chamber development in Rosalina floridana. J. Foraminifer. Res. 9 (4), 341–353.
Baumann, K.H., Böckel, B., Frenz, M., 2004. Coccolith contribution to South Atlantic carbonate sedimentation. In: Hans, R., Thierstein, J.R.Y. (Eds.), Coccolithophores: from molecular processes to global impact. Springer, Berlin, pp. 367–402.
Be, A.W.H., Hemleben, C., Anderson, O.R., Spindler, M., 1979. Chamber formation in planktonic foraminifera. Micropaleontology (New York) 25 (3), 294–307.
Bentov, S., Brownlee, C., Erez, J., 2009. The role of seawater endocytosis in the biomineralization process in calcareous foraminifera. Proc. Natl. Acad. Sci. U. S. A. 106 (51), 21500–21504.
Cushman, J.A., 1926. Recent foraminifera from Porto Rico. Publ. Carnegie Inst. Wash. 342, 73–84.
De Beer, D., 2000. Potentiometric microsensors for in situ measurements in aquatic environments. In: Buffle, J., Horvai, G. (Eds.), In situ monitoring of aquatic systems: chemical analysis and speciation. Wiley & Sons, London, pp. 161–194.
De Beer, D., Kuehl, M., Stambler, N., Vaki, L., 2000. A microsensor study of light enhanced Ca^{2+} uptake and photosynthesis in the reef-building hermatypic coral Favia sp. Mar. Ecol. Prog. Ser. 194, 75–85.
de Nooijer, L.J., Toyofuku, T., Kitazato, H., 2009a. Foraminifera promote calcification by elevating their intracellular pH. Proc. Natl. Acad. Sci. U. S. A. 106 (36), 15374–15378.

de Nooijer, L.J., Langer, G., Nehrke, G., Bijma, J., 2009b. Physiological controls on seawater uptake and calcification in the benthic foraminifer *Ammonia tepida*. Biogeosciences 6 (11), 2669–2675.

DeFoe, O.K., Compton, A.H., 1925. The density of rock salt and calcite. Phys. Rev. 25 (5), 618–620.

Dissard, D., Nehrke, G., Reichart, G.J., Bijma, J., 2010. Impact of seawater pCO(2) on calcification and Mg/Ca and Sr/Ca ratios in benthic foraminifera calcite: results from culturing experiments with *Ammonia tepida*. Biogeosciences 7 (1), 81–93.

Elderfield, H., Rickaby, R.E.M., 2000. Oceanic Cd/P ratio and nutrient utilization in the glacial Southern Ocean. Nature 405 (6784), 305–310.

Erez, J., 1983. Calcification rates, photosynthesis and light in planktonic foraminifera. In: Westbroek, P., de Jong, E.W. (Eds.), Biomineralization and Biological Metal Accumulation. D. Reidel Publishing Company, Dordrecht, The Netherlands, pp. 307–312.

Erez, J., 2003. The source of ions for biomineralization in foraminifera and their implications for paleoceanographic proxies. Biomineralization 54, 115–149.

Goldstein, S.T., 1999. Foraminifera: A biological overview. In: Sen Gupta, B.K. (Ed.), Modern Foraminifera. Springer, Netherlands, pp. 37–55.

Hansen, H.J., 1999. Shell construction in modern calcareous Foraminifera. In: Sen Gupta, B.K. (Ed.), Modern Foraminifera. Springer, Netherlands, pp. 57–70.

Hansen, H.J., Reiss, Z., 1971. Electron microscopy of rotaliacean wall structures. Bull. Geol. Soc. Den. 20, 329–346.

Huettel, M., Gust, G., 1992. Impact of bioroughness on interfacial solute exchange in permeable sediments. Mar. Ecol. Prog. Ser. 89, 253–267.

Koehler-Rink, S., Kuehl, M., 2000. Microsensor studies of photosynthesis and respiration in larger symbiotic foraminifera. I The physico-chemical microenvironment of *Marginopora vertebralis*, *Amphistegina lobifera* and *Amphisorus hemprichii*. Mar. Biol. 137 (3), 473–486.

Koehler-Rink, S., Kuehl, M., 2005. The chemical microenvironment of the symbiotic planktonic foraminifer *Orbulina universa*. Mar. Biol. Res. 1 (1) ISSN 1745-1000 (print)|1745-1019(electronic).

Langer, G., Geisen, M., Baumann, K.H., Kläs, J., Riebesell, U., Thoms, S., Young, J.R., 2006. Species-specific responses of calcifying algae to changing seawater carbonate chemistry. Geochem. Geophys. Geosyst. 7 (9), Q09006.

Lea, D.W., 2003. 6.14 - Elemental and Isotopic Proxies of Past Ocean Temperatures. In: Holland, Heinrich D., Turekian, Karl K. (Eds.), Treatise on Geochemistry. Pergamon, Oxford, pp. 365–390.

Lea, D.W., Martin, P.A., Chan, D.A., Spero, H.J., 1995. Calcium uptake and calcification rate in the planktonic foraminifera *Orbulina universa*. J. Foramineferal Res. 25 (1), 14–23.

Lukacs, G.L., Kapus, A., Nanda, A., Romanek, R., Grinstein, S., 1993. Proton conductance of the plasma membrane: properties, regulation, and functional role. Am. J. Physiol. Cell Physiol. 265 (1), C3–C14.

Madshus, I.H., 1988. Regulation of intracellular pH in eukaryotic cells. Biochem. J. 250 (1), 1–8.

Nielsen, A.E., 1964. Kinetics of precipitation. Pergamon Press, Oxford.

Polerecky, L., Bachar, A., Schoon, R., Grinstein, M., Jorgensen, B.B., de Beer, D., Jonkers, H.M., 2007. Contribution of *Chloroflexus* respiration to oxygen cycling in a hypersaline microbial mat from Lake Chiprana, Spain. Environ. Microbiol. 9 (8), 2007–2024.

Revsbech, N.P., Jorgensen, B.B., 1986. Microelectrodes — their use in microbial ecology. Adv. Microb. Ecol. 9, 293–352.

Rickaby, R.E.M., Elderfield, H., 1999. Planktonic foraminiferal Cd/Ca: paleonutrients or paleotemperature? Paleoceanography 14 (3), 293–303.

Rink, S., Kuehl, M., Bijma, J., Spero, H.J., 1998. Microsensor studies of photosynthesis and respiration in the symbiotic foraminifer *Orbulina universa*. Mar. Biol. 131 (4), 583–595.

Rohling, E.J., 2000. Paleosalinity: confidence limits and future applications. Mar. Geol. 163 (1–4), 1–11.

Ross, C.A., Ross, J.R.P., 1991. Paleozoic foraminifera. Biosystems 25 (1–2), 39–51.

Shimeta, J., Starczak, V.R., Ashiru, O.M., Zimmer, C.A., 2001. Influences of benthic boundary-layer flow on feeding rates of ciliates and flagellates at the sediment-water interface. Limnol. Oceanogr. 46 (7), 1709–1719.

Spero, H.J., Bijma, J., Lea, D.W., Bemis, B.E., 1997. Effect of seawater carbonate concentration on foraminiferal carbon and oxygen isotopes. Nature 390 (6659), 497–500.

Spivack, A.J., You, C.F., Smith, H.J., 1993. Foraminiferal boron isotope ratios as a proxy for surface ocean pH over the past 21-Myr. Nature 363 (6425), 149–151.

Stoll, H.M., Klaas, C.M., Probert, I., Encinar, J.R., Alonso, J.I.G., 2002. Calcification rate and temperature effects on Sr partitioning in coccoliths of multiple species of coccolithophorids in culture. Glob. Planet. Chang. 34 (3–4), 153–171.

Tappan, H., Loeblich Jr., A.R., 1988. Foraminiferal evolution, diversification, and extinction. J. Paleontol. 62 (5), 695–714.

Taylor, A.R., Chrachri, A., Wheeler, G., Goddard, H., Brownlee, C., 2011. A voltage-gated H^+ channel underlying ph homeostasis in calcifying coccolithophores. PLoS Biol 9 (6), e1001085.

ter Kuile, B., Erez, J., 1988. The size and function of the internal inorganic carbon pool of the foraminifer *Amphistegina lobifera*. Mar. Biol. 99 (4), 481–487.

ter Kuile, B., Erez, J., Padan, E., 1989. Mechanisms for the uptake of inorganic carbon by two species of symbiont-bearing foraminifera. Mar. Biol. 103, 241–251.

Vickerman, K., 1992. The diversity and ecological significance of Protozoa. Biodivers. Conserv. 1 (4), 334–341.

Wolf-Gladrow, D., Riebesell, U., 1997. Diffusion and reactions in the vicinity of plankton: a refined model for inorganic carbon transport. Mar. Chem. 59 (1), 17–34.

Wolf-Gladrow, D.A., Bijma, J., Zeebe, R.E., 1999. Model simulation of the carbonate chemistry in the microenvironment of symbiont bearing foraminifera. Mar. Chem. 64 (3), 181–198.

Zeebe, R.E., Sanyal, A., 2002. Comparison of two potential strategies of planktonic foraminifera for house building: Mg^{2+} or H^+ removal? Geochim. Cosmochim. Acta 66 (7), 1159–1169.

Zeebe, R.E., Wolf-Gladrow, D., 2001. CO_2 in Seawater: Equilibrium, Kinetics and Isotopes. Elsevier, Amsterdam. 346 pp.

Chapter 2

Effects of metabolically induced low pH microenvironments on calcifiers

npg

ORIGINAL ARTICLE

Biogeochemical conditions determine virulence of black band disease in corals

Martin S Glas[1], Yui Sato[2,3], Karin E Ulstrup[4] and David G Bourne[2]

[1]Max Planck Institute for Marine Microbiology, Microsensor Group, Bremen, Bremen, Germany; [2]Centre of Marine Microbiology and Genetics, Australian Institute of Marine Science, PMB 3, Townsville, Queensland, Australia; [3]ARC Centre of Excellence for Coral Reef Studies and School of Marine and Tropical Biology, James Cook University, and AIMS@JCU, Townsville, Queensland, Australia and [4]DHI Water & Environment, West Perth, Western Australia, Australia

The microenvironmental dynamics of the microbial mat of black band disease (BBD) and its less virulent precursor, cyanobacterial patch (CP), were extensively profiled using microsensors under different light intensities with respect to O_2, pH and H_2S. BBD mats exhibited vertical stratification into an upper phototrophic and lower anoxic and sulphidic zone. At the progression front of BBD lesions, high sulphide levels up to 4977 μM were measured in darkness along with lower than ambient levels of pH (7.43 ± 0.20). At the base of the coral–BBD microbial mat, conditions were hypoxic or anoxic depending on light intensity exposure. In contrast, CP mats did not exhibit strong microchemical stratification with mostly supersaturated oxygen conditions throughout the mats at all light intensities and with levels of pH generally higher than in BBD. Two of three replicate CP mats were devoid of sulphide, while the third replicate showed only low levels of sulphide (up to 42 μM) present in darkness and at intermediate light levels. The level of oxygenation and sulphide correlated well with lesion migration rates, that is virulence of the mats, which were greater in BBD than in CP. The results suggest that biogeochemical microgradients of BBD shaped by the complex microbial community, rather than a defined pathogen, are the major trigger for high virulence and the associated derived coral mortality of this disease.
The ISME Journal advance online publication, 9 February 2012; doi:10.1038/ismej.2012.2
Subject Category: microbe–microbe and microbe–host interactions
Keywords: BBD; CP; pathogen; microsensor; anoxia; sulphide

Introduction

Black band disease (BBD) is a highly virulent coral disease that affects scleractinian corals, the major reef builders in tropical reef ecosystems around the world (Sutherland *et al.*, 2004). It manifests as a complex microbial mat that migrates over coral tissue, resulting in lysis and necrosis of the underlying coral tissue, leaving bare coral skeleton behind (Richardson, 2004). Despite being first identified in 1973 (Antonius, 1973), the aetiology and underlying mechanisms of pathogenesis and pathogenicity of BBD remain unresolved, as no primary pathogen has been identified and various causes for the disease's high virulence are still debated.

BBD comprises a complex microbial community including phototrophic cyanobacteria, sulphate-reducing bacteria (SRB), sulphide-oxidizing bacteria

and other heterotrophic bacteria (Cooney *et al.*, 2002; Frias-Lopez *et al.*, 2004; Barneah *et al.*, 2007; Voss *et al.*, 2007; Sekar *et al.*, 2008; Sato *et al.*, 2010). The BBD lesion therefore closely resembles that of other complex microbial mats, as suggested by Carlton and Richardson (1995), including hypersaline mats, which are vertically stratified into an upper phototrophic zone and a lower anoxic-sulphidic zone (Jonkers *et al.*, 2003; Dupraz *et al.*, 2004, 2009; Ludwig *et al.*, 2005; Dillon *et al.*, 2009). The stratification in hypersaline mats is mainly driven by gliding filamentous members (cyanobacteria, *Beggiatoa* sp.) that are highly motile and exhibit active diurnal migration (Fourcans *et al.*, 2006; Hinck *et al.*, 2007; Dillon *et al.*, 2009). The vertical orientation of functional groups within hypersaline mats results in the development of pronounced biogeochemical microgradients (e.g., O_2, light, pH, sulphate and sulphide), reciprocally influenced by and influencing their environment. Such conditions enable tight spatial coupling of matter cycling, further driving development of functionally differentiated, stratified communities. Similar modulations of biogeochemical microgradients in BBD lesions are likely (Carlton and Richardson, 1995)

2

and may be an important trigger for high virulence at the base of the mat (coral–microbial mat interphase), where healthy tissue, necrosing tissue and the microbial consortium interact.

Biogeochemical conditions at the base of the BBD mat are typically hypoxic or anoxic with high concentrations of sulphide lethal to the underlying coral tissue. Such detrimental biogeochemical conditions established within and at the base of the mat have previously been suggested as virulence factors for BBD (Richardson *et al.*, 1997). Yet, sulphide estimations within the microbial mat of BBD have focused on microsensor measurements of the S^{2-} fraction only, without taking pH variations within the mat into account (Carlton and Richardson, 1995). Importantly, the dissociation of the three sulphide species in seawater (H_2S, HS^- and S^{2-}) integrally depends on pH (Millero and Hershey, 1989) and the attained results therefore do not quantify total sulphide. Accurate measurements of the spatio-temporal dynamics of total sulphide is the key to understanding the onset and aetiology of BBD, as toxicity estimates for the coral tissue depend on the levels of total sulphide present (Vismann, 1991; Bagarinao, 1992; Richardson *et al.*, 1997).

An outbreak of BBD and an earlier less-virulent stage of the disease, termed 'cyanobacterial patch' (CP), has been documented on *Montipora* coral species around Orpheus Island, within the Great Barrier Reef Marine Park (Sato *et al.*, 2009, 2010). Transitions of CP-like lesions into developed BBD have also been observed on Indonesian reefs (B Willis, personal communication). In the field, BBD lesions develop from CP approximately 62 days following the onset of the CP lesion (Sato *et al.*, 2010). Shifts in the microbial community structure as CP transitioned into BBD (Glas *et al.*, 2010; Sato *et al.*, 2010) included increases in sulphate-reducing bacterial (SRB) populations, namely *Desulfovibrio* sp. (Bourne *et al.*, 2011). This disease outbreak around Orpheus Island also provided the opportunity to examine biogeochemical microgradients within the microbial mats, and the role microenvironmental conditions play in the virulence of BBD as well as the onset of BBD from CP.

To investigate if the high virulence of BBD is driven by the dynamic microenvironmental conditions within and at the base of the mat, we extensively profiled coral fragments infected with BBD and CP under controlled laboratory conditions with O_2, pH and H_2S (measuring the dissolved H_2S fraction) microsensors. The microsensor measurements were complemented with molecular quantification of sulphate reducers within the mat. The main aim of this study was therefore to further our understanding of virulence of CP and BBD by determining the spatio-temporal dynamics of pH, total sulphide and oxygen within and at the base of CP and BBD microbial mats and relate these results to the typical fast directional migration (virulence) of the corresponding lesions.

Materials and methods

Sampling and culturing
Samples of the scleractinian coral *Montipora hispida* infected with either CP or BBD ($n = 3$ colonies each, labelled as BBD no. 1–3 and CP no. 1–3) were collected in March 2010, using a hammer and chisel along the northeast coast of Pelorus Island (18°32′S, 146°30′E; central region of the Great Barrier Reef Marine Park, east coast of Australia), at depths of 3.5–4.5 m (for a detailed description of the study site, see Sato *et al.*, 2009). Coral fragments infected with lesions of CP or BBD were carefully placed in separate 70-l cooling boxes containing ambient seawater, and immediately transported to the Australian Institute of Marine Science in Townsville. Samples were maintained in an indoor aquarium facility at 26 °C to avoid thermally induced transition of CP into BBD due to prevalent high summer temperatures (Glas *et al.*, 2010). The facility provided a flow of freshly filtered seawater (3 cm s⁻¹) and light intensities of $\sim$100 μmol photons m⁻² s⁻¹ (12 h:12 h diurnal cycling).

Experimental measurement setup
All amperiometric and potentiometric microsensor measurements were conducted in a self-constructed Faraday cage to minimize electrical disturbance. A detailed description of the measurement setup can be found in Polerecky *et al.* (2007). Diseased corals fragments were placed in a flow chamber on top of inert sand connected to a circulation system of filtered, aerated natural seawater (1 μm mesh size, 50 l). Seawater conditions were monitored throughout the experiment and kept constant at 26 °C, salinity 35, oxygen saturation of 207.8 ± 0.4 μM (mean ± s.e.), pH (total scale) 8.062 ± 0.005 (mean ± s.e.) and a laminar flow of 1 cm s⁻¹. Illumination was provided and regulated directly from above via a fiber-optic guide from a halogen-light source (Schott KL2500, Mainz, Germany). Light intensities were monitored with a quantum irradiance meter (LI-250A, LI-COR, Lincoln, NE, USA), combined with a light sensor for photosynthetic active radiation (PAR).

Microelectrodes
Clark-type O2 microsensors with a guard cathode (tip diameter $\sim$40 μm, <1 s response time (t_{90}), detection limit 0.05 μM) were constructed and calibrated as previously described (Revsbech and Jørgensen, 1986). Fast responding H_2S sensors (tip diameter $\sim$50 μm, <1 s response time (t_{90}), detection limit 0.1 μM at pH <9) with an internal reference were prepared and used as previously described (Jeroschewski *et al.*, 1996; Kühl *et al.*, 1998). Five-point H_2S calibrations were performed in anoxic, filtered, acidified natural seawater (pH<4) and exhibiting linear responses up to 1000 μM (R^2>0.99). pH measurements were performed on the total scale, by
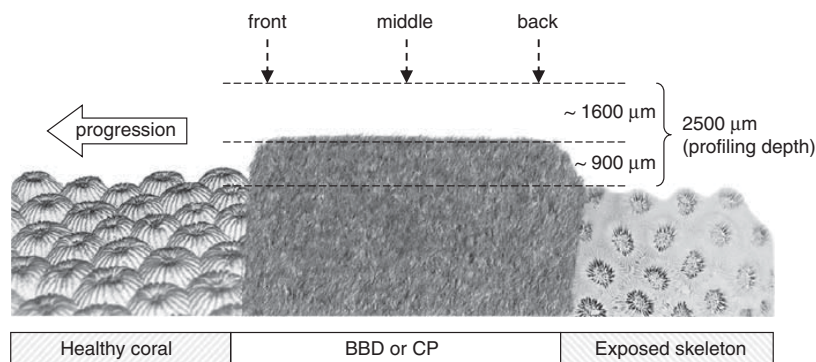
Figure 1 Schematic drawing of profile series conducted for individual disease lesions (CP and BBD). Thickness of microbial mat and profiling depth are exaggerated for clarity.

using liquid ion exchange (LIX) membrane micro-electrodes (tip diameter $20 \, \mu m$, $<2 \, s$ response time (t_{90}), detection limit 0.005) as described by de Beer (2000) and a commercial pH meter (pH 1100, Oakton, Vernon Hills, IL, USA).

Experimental procedure
Measurement series of pH and H_2S profiles were conducted in three locations across both BBD and CP lesions (lesion's front, middle and back, Figure 1) ($n = 3$) and repeated at three different irradiances (0, 40 and 250 μmol photons m^{-2} s^{-1}) to simulate *in situ* underwater light levels for night-time, transient light and day-time light regimes. Total sulphide ($S_{tot} = [H_2S] + [HS^-] + [S^{2-}]$) profiles were calculated from aligned values of pH and H_2S profiles as described by Jeroschewski *et al.* (1996) (equations (6) and (7)). The dissociation constant K_1, expressed as pK_1, was corrected for temperature and salinity according to Millero *et al.* (1988) (equation (4)) and Millero and Hershey (1989, equation (22)).

O_2 measurements were carried out at the lesion's front only, following preliminary measurements showing no horizontal gradient of O_2 across BBD and CP mats. Four different irradiances (0, 60, 125, 485 μmol photons m^{-2} s^{-1}, Table 1) were selected to estimate peak O_2 evolution at maximal *in situ* light levels (Sato *et al.*, 2009).

To determine the t_{90} value of steady-state signals of the system O_2, pH and H_2S probes were positioned at the mat surface as well as at 400 μm and at 900 μm depth within the mat for $\sim$40 min. O_2 and H_2S signals (pA) reached $>90\%$ of steady-state signals within 3–7 min, pH values (mV) took 9–13 min. To ensure steady state, light levels were applied >10 min prior to measurements for O_2 and H_2S, and >20 min for pH measurements. Microsensor tips were positioned in contact with BBD or CP mat surfaces using a stereo microscope and a 3D-manual micromanipulator (MM33, Maerzhaeuser, Germany). Profiles were conducted perpendicular to the mat surface from $\sim$1600 μm above and $\sim$900 μm into the mats covering the diffusive boundary layer (Figure 1).

Mat-migration speed was determined at the end of the experiment (after 48 h) with a digital caliper by measuring band extensions along the migration direction in a 1-cm big strip enclosing the profiling transect ($n = 5$). Developmental stages of lesions were visually classified at the start and end of the experiment on a scale from 1 to 10 (CP 1-5, BBD 6–10) by determining lesion colour, shading, surface structure and density via the stereomicroscope. Immediately after the completion of microsensor measurements, BBD and CP lesions were sampled from coral fragments with sterile forceps and subsequently weighed and preserved for molecular and pigment analyses.

Quantification of sulphate reducers
A quantitative real-time PCR (qPCR) assay targeting the dissimilatory (bi)sulphite reductase (*dsrA*) gene of sulphate-reducing bacteria (SRB) and a qPCR assay targeting the 16S rRNA gene, as detailed in Bourne *et al.* (2011), provided an estimate of SRB populations relative to total bacteria within the sampled mats. The *dsrA* gene was targeted with primers DSR1-F+ and DSR-R, adapted from Kondo *et al.* (2008) and Leloup *et al.* (2007), though modified through the use of the TaqMan chemistry and an additional internal probe (DSRtaq (HEX)-5′-CCGATAACRCYGCCGCCGTAACC GA-3′-(TAMARA)), allowing increased specificity and discrimination in quantification of *dsrA* genes within samples (Bourne *et al.*, 2011). Quantification of the bacterial abundance through targeting of the 16S rRNA gene was adapted from Nadkarni *et al.* (2002) and applied the universal primers 331-F (5′-TCCTACGGGAGGCAGCAGT-3′), 797-R (5′-GGAC TACCAGGGTATCTAATCCTGTT-3′), and the probe BacTaq ((6-FAM)-5′-CGTATTACCGCGGCTGCTGG CAC-3′-(TAMARA)), targeting almost all bacterial phyla.

Chlorophyll a concentrations
Chlorophyll *a* (Chl *a*) within the mat samples of CP and BBD was extracted by sonication in 1 ml buffered

npg

4

Table 1 O_2 concentration (mean ± s.e., μM) measured at the coral–microbial mat interphase (at 0 μm, see Figure 3) of CP and BBD in darkness and at three irradiances

Light (*μmol photons* m^{-2} s^{-1})	CP (n = 3)	BBD (n = 3)
0	23 ± 17	2 ± 2
60	247 ± 28	19 ± 19
125	468 ± 41	80 ± 73
485	1133 ± 19	467 ± 219

Abbreviations: BBD, black band disease; CP, cyanobacterial patch.

methanol (98% methanol, 2% of 0.5 M tetrabutyl ammonium acetate at pH 6.5) on ice. Samples were centrifuged and the supernatant decanted with a pipette before repeating the extraction with 0.8 ml of buffered methanol and combining both extracts. Chl *a* was determined spectrophotometrically (1 cm path length) using the equations detailed in Porra (2002).

Data analyses
Linear regressions between daily mean migration speeds and biogeochemical parameters from the front and base of the microbial mats (S_{tot}, O_2 and pH), relative abundance of SRB, developmental stages and Chl *a* contents were assessed using Pearson product–moment correlation coefficient (*R*) and a general linear-regression model. Tested values of S_{tot}, O_2 and pH used in the analyses represent daily average values calculated as means from steady-state light (125 and 250 μmol photons m^{-2} s^{-1}) and dark values from the front and base of the microbial mats. Regression analyses were performed with the statistical analyses software Origin 7.0 (OriginLab Corporation, Northampton, MA, USA).

Results

Biochemical profiles of CP and BBD lesions
CP mats were mostly devoid of H_2S and S_{tot} at all light levels, with the exception of one sample (CP no. 1) where H_2S (~ 1 μM) and S_{tot} (< 42 μM) were observed in dark and at intermediate light levels (Supplementary Figure S1 and Figure 2). In darkness, the base at the progression front of all CP mats was hypoxic (23 ± 17 μM, Table 1), with lower than ambient pH (7.73 ± 0.25, Table 2) and with profiles of decreasing O_2 and pH towards the base of the mat as exemplified in Figure 3. The base at the progression front of the CP mats was supersaturated with respect to O_2 levels $\geqslant 60$ μmol photons m^{-2} s^{-1} (Table 1). At intermediate light levels (40 μmol photons m^{-2} s^{-1}), pH at the base of the progression front was still lower than ambient (7.83 ± 0.26), although it was greater (8.61 ± 0.19) than ambient at 250 μmol photons m^{-2} s^{-1} (Table 2). At 125 μmol photons μm^{-2} s^{-1}, the front of the CP mats were O_2 supersaturated throughout as exemplified in

Figure 3. At the maximum irradiance level of 485 μmol photons m^{-2} s^{-1}, O_2 concentrations reached 1133 ± 19 μM at the front and base of the CP mats (Table 1).

The base of BBD microbial mats was anoxic in darkness (Table 1), with lower than ambient pH (Table 2) and high concentrations of H_2S at the progression front (Supplementary Figure S1). Clear vertical gradients of decreasing O_2 and pH were observed in darkness towards the BBD mat surface and of increasing H_2S towards the base (Figure 3). Also, if present, H_2S showed a horizontal gradient with highest H_2S levels at the progression front of the lesion, and lowest at the back at all light levels (Supplementary Figure S1). O_2 supersaturation was observed at 125 μmol photons m^{-2} s^{-1} at the BBD mat surface as indicated in Figure 3 and only at 485 μmol photons m^{-2} s^{-1} at the base (Table 1).

Calculations of total sulphide in BBD lesions consistently revealed strong vertical and horizontal spatial gradients from front to back of the lesions at all light levels, with large inter-colony variations in maximum H_2S and consequently S_{tot} (Supplementary Figure S1 and Figure 2). In all samples (with the exception of BBD no. 2 at intermediate light levels) sulphide accumulation was highest at the base of the progression front of BBD mats, where coral tissue was freshly covered and undergoing necrosis (Figure 2). Sulphide concentrations varied with light intensity and gradients decreased horizontally in extent with increasing light intensities (Figure 2). S_{tot} was detectable 1000 μm above the microbial mat surface in BBD no. 1 in darkness and still accumulated up to 450 μM at the base of the progression front in daylight (Figure 2).

Overall, in darkness, oxygen was depleted throughout BDD mats, while low concentrations of oxygen were still present towards the base of the CP mats (Table 1 and Figure 3). Levels of pH at the base of the mats, though highly variable, were generally lower in BBD than in CP (Table 2). Compared with CP, BBD displayed a more defined stratification into a lower (coral tissue–microbial mat interphase) anoxic-sulphidic zone and an upper phototrophic zone.

Virulence and microenvironmental correlates
BBD showed greater mean migration speeds (1.41–8.63 mm day^{-1}) than CP (0.01–1.18 mm day^{-1}), indicating an increased virulence of BBD compared with CP (Table 3). Mean migration rates were significantly correlated with developmental stages of the lesion ($P = 0.042$), presence of sulphide ($P = 0.008$) and anoxic conditions ($P = 0.024$) at the base of the progression front (Table 3). Relative quantification of the *dsrA* gene showed that the contribution of SRB to the total bacterial population increased in BBD relative to CP. However, the presence of sulphide followed trends in oxygenation and therefore the biogeochemical condition of the mats, rather
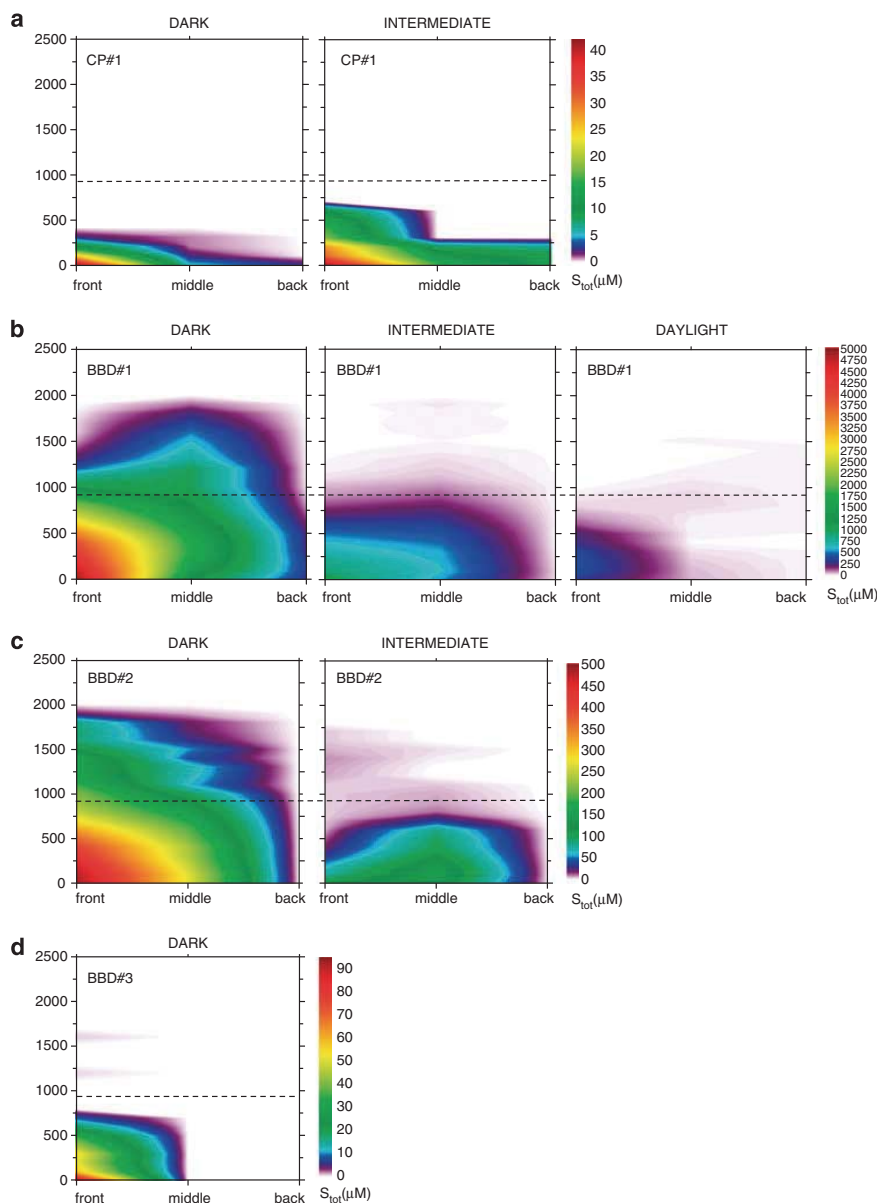
Figure 2 Spatial distribution of total sulphide (S_{tot}) concentrations for (**a**) CP no. 1, (**b**) BBD no. 1, (**c**) BBD no. 2 and (**d**) BBD no. 3 at three different light intensities (darkness = 0, intermediate = 40, daylight = 250 µmol photons m^{-2} s^{-1}). Dotted lines indicate the surface of the microbial mats. Scale bars in (**a–d**) are different to allow the representation of S_{tot} in all contour plots. Daylight contour plots for CP no. 1, BBD no. 2, as well as daylight and intermediate contour plots for BBD no. 3 were omitted as they did not contain any sulphide. All contour plots for CP no. 2 and CP no. 3 were also omitted as they did not contain any sulphide.

than the abundance of *dsrA* genes (Table 3). The linear regression analyses showed that mean migration rates were explained better by O_2 and S_{tot} concentrations at the base of the progression front of BBD and CP than by pH and SRB abundance (Table 3). Chl *a* contents also correlated significantly ($P = 0.016$) with migration speeds (Table 3), indicating the presence of high phototrophic biomass within more virulent lesions.

Discussion

Biogeochemistry of BBD and CP microbial mats
The tight coupling of pH, O_2 and total sulphide was characteristic of all disease lesion replicates. It resulted in the development of clearly defined microgradients within the BBD microbial mat, causing a clear stratification into an upper phototrophic (oxygenic) and lower anoxic-sulphidic zone

6

Table 2 pH (mean ± s.e.) measured at the coral-microbial mat interphase (at 0 μm, see Figure 3) of CP and BBD in darkness and at two irradiances

Light (μmol photons m⁻² s⁻¹)	CP			BBD		
	Front (n = 3)	*Middle* (n = 3)	*Back* (n = 3)	*Front* (n = 3)	*Middle* (n = 3)	*Back* (n = 3)
0	7.73 ± 0.25	7.53 ± 0.14	7.75 ± 0.07	7.43 ± 0.20	7.33 ± 0.11	7.49 ± 0.03
40	7.83 ± 0.26	7.74 ± 0.22	7.39 ± 0.23	7.37 ± 0.01	7.62 ± 0.11	7.49 ± 0.19
250	8.61 ± 0.19	8.58 ± 0.22	8.54 ± 0.07	7.58 ± 0.15	8.13 ± 0.27	7.83 ± 0.24

Abbreviations: BBD, black band disease; CP, cyanobacterial patch.
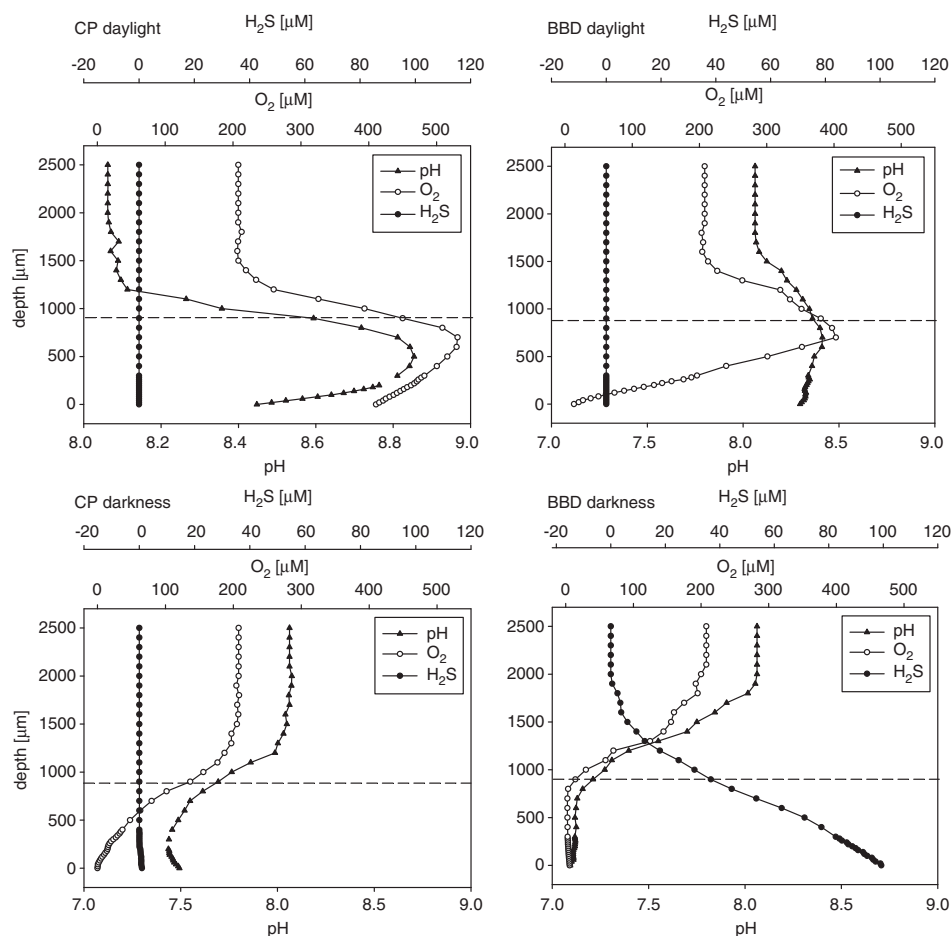
Figure 3 Exemplary dark and light profiles of H_2S and pH (measured at 250 μmol photons m⁻² s⁻¹) as well as O_2 (measured at 125 μmol photons m⁻² s⁻¹) at the front of a CP and BBD microbial lesion. The dotted lines indicate the surface of the mats, which were ~900 μm thick.

in response to varying light levels. These micro-chemical environments are shaped by the microbial community within the mat, maintaining anoxia, high levels of sulphide and low pH, especially at the coral–microbial mat interphase. Anoxia has been shown to have adverse effects on the photo-physiology of endosymbiotic algae (Ulstrup *et al.*, 2005) and overall fitness of the coral host (Shick,

1990). Furthermore, lethal concentrations of sul-phide (LC50) on invertebrates (Caldwell, 1975; Bagarinao, 1992; Knezovich *et al.*, 1996; Wang and Chapman, 1999) and coral tissue (Downs *et al.*, 2010) have been reported as low as 0.5 μM for 4 h of exposure, a factor 10⁴ lower than the maximum S_{tot} concentrations measured at the base of BBD in this study. This confirms that the measured levels of S_{tot}

Table 3 Mean migration speed, S_{tot}, O_2 and pH measured at the front and base of CP and BBD mats, along with relative quantity of sulphate-reducing bacteria, developmental stages and Chl *a* contents of individual coral lesions. Results of linear regression analyses are given with respect to migration speed

	Migration speed[a] (mm per day)	Mean S_{tot}[b] (µM)	Mean O_2[b] (µM)	Mean pH[b]	DSR (% per 10^6 16S rRNA)	Developmental stage[c]	Chl a[d] (Chl a g^{-1})
CP no. 1	1.18 ± 0.00	20	193	8.53	2.2	5	80
CP no. 2	0.04 ± 0.01	0	264	7.77	<0.01	2	212
CP no. 3	0.01 ± 0.01	0	278	8.23	0.5	2	313
BBD no. 1	8.63 ± 0.03	2654	0	7.83	9.2	10	733
BBD no. 2	4.19 ± 0.02	246	10	7.22	2.3	9	413
BBD no. 3	1.41 ± 0.02	46	113	7.47	7.8	8	267
Linear regression analyses[e]							
Intercept		1.141	5.976	18.99	0.3354	−2.120	−1.922
Slope		0.003	−0.024	−2.093	0.611	0.783	0.013
R^2		0.856	0.756	0.091	0.505	0.684	0.803
P-value		0.008*	0.024*	0.561	0.113	0.042*	0.016*

Abbreviations: BBD, black band disease; CP, cyanobacterial patch; Chl *a*, chlorophyll *a*.
[a]Mean migration speed per day ($n = 5$, ± s.e.).
[b]Mean over light (S_{tot}, pH 250 and O_2 125 µmol photons $m^{-2} s^{-1}$) and dark conditions.
[c]Developmental stage of lesions assessed by visual inspection.
[d]Stated per wet weight of mats.
[e]Significance levels at the 5% level are indicated by *.

and anoxia in BBD lesions can easily kill coral tissue on short time scales of 1–2 days, during which the microbial mat covers and progresses over the underlying coral tissue. The effects of anoxia and high levels of S_{tot} in BBD drive a high mean migration speed (i.e., virulence) of the lesions, as shown by significant positive linear correlations (Table 3). These deleterious microchemical conditions are established very fast in the dark ($t_{90} < 10$ min; owing to the mats' thinness, which facilitates diffusion), which is in accordance with the fast progression rates of BBD measured in this study *ex situ* (Table 3) and *in situ* (Richardson, 1996; Sato *et al.*, 2009).

In contrast to BBD lesions, the CP microbial mats exhibited no clear vertical stratification into phototrophic-oxygenic and anoxic-sulphidic zones. Consequently, O_2 was present throughout the mat in light (Figure 3), with only a single sample showing marginal sulphide concentrations in the dark and at intermediate irradiances (Figure 2 and Supplementary Figure S1). These conditions resulted in slower mean migration rates and hence lowered virulence of CP compared with BBD measured *ex situ* (Table 3) and *in situ* (Sato *et al.*, 2010).

As both hypoxia and Chl *a* contents increased with increasing migration speed of all lesions (Table 3), stratification of lesions into photosynthetic and anoxic-sulphidic zones became more pronounced as the lesions developed and virulence increased. This suggests that high cyanobacterial biomass facilitates the biogeochemical stratification as the lesions develop. The results thus show that stratification of the mat community into a phototrophic and anaerobic sulphate reduction zone is essential for the development of anoxia, low pH, high sulphide levels (in darkness) and therefore the increased virulence of BBD compared with CP.

Sulphate reduction and desulphuration in BBD and CP
Both bacterial sulphate reduction and desulphuration of degrading coral tissue and mucus (Hill *et al.*, 1995; Brown and Bythell, 2005) are potential sources of sulphide production at the coral-BBD microbial mat interphase. SRB typically proliferate under anoxic, sulphate-rich conditions made available by degrading tissue of BBD-infected corals. This is consistent with the strongly increased presence of SRB within BBD, representing between ∼2–9% of the bacterial population within the lesions compared with CP (Table 3). In addition to sulphide production by SRB, coral tissue and mucus desulphuration by microbes and remaining coral-derived enzymes is the most likely source of sulphide emergence (Weber, 2009). As sulphate-reduction rates were not measured in this study, distinguishing between the two sources is not feasible. Nevertheless, the BBD mat covering degrading coral tissue will strongly facilitate desulphuration and sulphate reduction and thereby considerably enhance virulence of BBD lesions compared with non-covered degrading coral tissue.

Proposed positive feedback mechanism causing BBD virulence
The stratification of BBD lesions indicates an interaction between the sulphide-tolerant phototrophic cyanobacteria (Myers and Richardson, 2009), SRB and desulphuration. Positive phototaxis in daylight and production of sulphide in darkness (negative chemotaxis) will drive motile cyanobacteria into the upper layer of BBD lesion, thereby creating a positive feedback loop for anoxic conditions at its base. Increased anoxia at the base will facilitate sulphate reduction by SRB and desulphuration and lower sulphide oxidation, which in

turn will drive negative cyanobacterial chemotaxis against increasing sulphide levels. Sulphide production, via chemical oxidation, further facilitates the presence of anoxia and indirectly lower pH, which again will increase disease virulence at the base of the mat. The three synergistic lethal factors (i.e., anoxia, high concentrations of S_{tot} and low pH) thus reciprocally enhance one another at the coral–BBD microbial mat interphase through the feedback mechanisms described above and can thereby easily create a positive feedback loop for disease virulence.

The strong horizontal and vertical gradients of sulphide in the BBD mats are in agreement with the availability of sulphate, which is limited by the presence of necrosed coral tissue at the progression front of the mat, hence its migration direction (Figure 1). The necrosed coral tissue can easily be decomposed through microbial activity (readily available within the mat of BBD) and remaining coral-derived cellular enzymes, resulting in the presence of high concentrations of sulphate. Anaerobic sulphate reduction is therefore proposed to be biogeochemically facilitated at the coral–microbial mat interphase. Desulphuration and the availability of sulphate for SRB are therefore expected to decrease along the migration gradient of the BBD mat, as suggested by the consistently observed equivalent sulphide microgradients (Figure 2). The stronger correlation of migration rates in CP and BBD with S_{tot}, anoxia and Chl *a* contents, rather than relative abundances of *dsrA* copy numbers (Table 3), indicates that the accumulation of S_{tot} by anaerobic sulphate reduction and desulphuration, rather than the presence or abundance of identified pathogenic microbial members, determines the virulence of these diseases.

The findings of this study indicate that the BBD microbial consortium as a whole establishes biogeochemical conditions at the coral–microbial mat interphase that are lethal for coral tissue. By comparing CP with BBD lesions it was shown that stratification of mats into an upper phototrophic and lower anoxic-sulphidic zone is essential for establishing such high disease virulence. The presented findings therefore indicate that steep biogeochemical microgradients, produced and maintained by the entire microbial consortium of BBD, are the major cause for the high virulence of this disease.

Acknowledgements

References

Antonius A. (1973). New observations on coral destruction in reefs. In: *10th Meeting of the Association of Island Marine Laboratories of the Caribbean*, University of Puerto Rico: Association of Island Marine Laboratories of the Caribbean: Mayaguez, Puerto Rico, p 3.

Bagarinao T. (1992). Sulfide as an environmental factor and toxicant: tolerance and adaptations in aquatic organisms. *Aquat Toxicol* **24**: 21–62.

Barneah O, Ben-Dov E, Kramarsky-Winter E, Kushmaro A. (2007). Characterization of black band disease in Red Sea stony corals. *Environ Microbiol* **9**: 1995–2006.

Bourne DG, Muirhead A, Sato Y. (2011). Changes in sulfate-reducing bacterial populations during the onset of black band disease. *ISME J* **5**: 559–564.

Brown BE, Bythell JC. (2005). Perspectives on mucus secretion in reef corals. *Mar Ecol Progr Ser* **296**: 291–309.

Caldwell R. (1975). *Hydrogen Sulfide Effects on Selected Larval and Adult Marine Invertebrates*. Water Resource Research Institute, Oregon State University: Corvallis.

Carlton RG, Richardson LL. (1995). Oxygen and sulfide dynamics in a horizontally migrating cyanobaterial mat: Black band disease of corals. *FEMS Microbiol Ecol* **18**: 155–162.

Cooney RP, Pantos O, Le Tissier MDA, Barer MR, O'Donnell AG, Bythell JC. (2002). Characterization of the bacterial consortium associated with black band disease in coral using molecular microbiological techniques. *Environ Microbiol* **4**: 401–413.

De Beer D. (2000). Potentiometric microsensors for *in situ* measurements in aquatic environments. In: Buffle J, Horvai G (eds). *In Situ Monitoring of Aquatic Systems: Chemical Analysis and Speciation*. Wiley & Sons: London, pp 161–194.

Dillon JG, Miller S, Bebout B, Hullar M, Pinel N, Stahl DA. (2009). Spatial and temporal variability in a stratified hypersaline microbial mat community. *FEMS Microbiol Ecol* **68**: 46–58.

Downs CA, Fauth JE, Downs VD, Ostrander GK. (2010). *In vitro* cell-toxicity screening as an alternative animal model for coral toxicology: effects of heat stress, sulfide, rotenone, cyanide, and cuprous oxide on cell viability and mitochondrial function. *Ecotoxicology* **19**: 171–184.

Dupraz C, Reid RP, Braissant O, Decho AW, Norman RS, Visscher PT. (2009). Processes of carbonate precipitation in modern microbial mats. *Earth-Sci Rev* **96**: 141–162.

Dupraz C, Visscher PT, Baumgartner LK, Reid RP. (2004). Microbe-mineral interactions: early carbonate precipitation in a hypersaline lake (Eleuthera Island, Bahamas). *Sedimentology* **51**: 745–765.

Fourcans A, Sole A, Diestra E, Ranchou-Peyruse A, Esteve I, Caumette P *et al.* (2006). Vertical migration of phototrophic bacterial populations in a hypersaline microbial mat from Salins-de-Giraud (Camargue, France). *FEMS Microbiol Ecol* **57**: 367–377.

Frias-Lopez J, Klaus JS, Bonheyo GT, Fouke BW. (2004). Bacterial community associated with black band disease in corals. *Appl Environ Microbiol* **70**: 5955–5962.

Glas MS, Motti CA, Negri AP, Sato Y, Froscio S, Humpage AR *et al.* (2010). Cyanotoxins are not implicated in the etiology of coral black band disease outbreaks on Pelorus Island, Great Barrier Reef. *FEMS Microbiol Ecol* **73**: 43–54.

Hill RW, Dacey JWH, Krupp DA. (1995). Dimethylsulfoniopropionate in reef corals. *Bull Mar Sci* **57**: 489–494.

Hinck S, Neu TR, Lavik G, Mussmann M, De Beer D, Jonkers HM. (2007). Physiological adaptation of a nitrate-storing beggiatoa sp to diel cycling in a phototrophic hypersaline mat. *Appl Environ Microbiol* **73**: 7013–7022.

Jeroschewski P, Steukart C, Kühl M. (1996). An amperiometric microsensor for the determination of H_2S in aquatic environments. *Anal Chem* **68**: 4351–4357.

Jonkers HM, Ludwig R, De Wit R, Pringault O, Muyzer G, Niemann H *et al.* (2003). Structural and functional analysis of a microbial mat ecosystem from a unique permanent hypersaline inland lake: 'La Salada de Chiprana' (NE Spain). *FEMS Microbiol Ecol* **44**: 175–189.

Knezovich JP, Steichen DJ, Jelinski JA, Anderson SL. (1996). Sulfide tolerance of four marine species used to evaluate sediment and pore-water toxicity. *Bull Environ Contam Toxicol* **57**: 450–457.

Kondo R, Shigematsu K, Butani J. (2008). Rapid enumeration of sulphate-reducing bacteria from aquatic environments using real-time PCR. *Plankton Benthos Res* **3**: 180–183.

Kühl M, Steuchart C, Eickert G, Jeroschewski P. (1998). A H_2S microsensor for profiling biofilms and sediments: application in an acidic lake sediment. *Aquat Microb Ecol* **15**: 201–209.

Leloup J, Loy A, Knab NJ, Borowski C, Wagner M, Jorgensen BB. (2007). Diversity and abundance of sulfate-reducing microorganisms in the sulfate and methane zones of a marine sediment, Black Sea. *Environ Microbiol* **9**: 131–142.

Ludwig R, Al-Horani FA, de Beer D, Jonkers HM. (2005). Photosynthesis-controlled calcification in a hypersaline microbial mat. *Limnol Oceanogr* **50**: 1836–1843.

Millero FJ, Hershey JP. (1989). Thermodynamics and kinetics of hydrogen sulfide in natural waters. *Mar Chem* **18**: 121–147.

Millero FJ, Plese T, Fernandez M. (1988). The dissociation of hydrogen sulfide in seawater. *Limnol Oceanogr* **33**: 269–274.

Myers JL, Richardson LL. (2009). Adaptation of cyanobacteria to the sulfide-rich microenvironment of black band disease of coral. *FEMS Microbiol Ecol* **67**: 242–251.

Nadkarni MA, Martin FE, Jacques NA, Hunter N. (2002). Determination of bacterial load by real-time PCR using a broad-range (universal) probe and primers set. *Microbiology* **148**: 257–266.

Polerecky L, Bachar A, Schoon R, Grinstein M, Jorgensen BB, de Beer D *et al.* (2007). Contribution of Chloroflexus respiration to oxygen cycling in a hypersaline microbial mat from Lake Chiprana, Spain. *Environ Microbiol* **9**: 2007–2024.

Porra RJ. (2002). The chequered history of the development and use of simultaneous equations for the accurate determination of chlorophylls a and b. *Photosynthesis Res* **73**: 149–156.

Revsbech NP, Jørgensen BB. (1986). Microelectrodes: their use in microbial ecology. *Adv Microb Ecol* **9**: 293–352.

Richardson LL. (1996). Horizontal and vertical migration patterns of Phormidium corallyticum and Beggiatoa spp associated with black-band disease of corals. *Microb Ecol* **32**: 323–335.

Richardson LL. (2004). Black band disease. In: Rosenberg E, Loya Y (eds). *Coral Health and Disease*. Springer Berlin: Berlin, Heidelberg, New York, pp 325–349.

Richardson LL, Kuta KG, Schnell S, Carlton RG. (1997). Ecology of the black band disease microbial consortium. *Proceedings of the 8th International Coral Reef Symposium*, Vol. 1. Panama City, Panama, pp 597–600.

Sato Y, Bourne DG, Willis BL. (2009). Dynamics of seasonal outbreaks of black band disease in an assemblage of Montipora species at Pelorus Island (Great Barrier Reef, Australia). *Proc R Soc B Biol Sci* **276**: 2795–2803.

Sato Y, Willis BL, Bourne DG. (2010). Successional changes in bacterial communities during the development of black band disease on the reef coral, Montipora hispida. *ISME J* **4**: 203–214.

Sekar R, Kaczmarsky LT, Richardson LL. (2008). Microbial community composition of black band disease on the coral host Siderastrea siderea from three regions of the wider Caribbean. *Mar Ecol Progr Ser* **362**: 85–98.

Shick JM. (1990). Diffusion limitation and hyperoxic enhancement of oxygen-consumption in zooxanthellate sea-anemones, zoanthids, and corals. *Biol Bull* **179**: 148–158.

Sutherland KP, Porter JW, Torres C. (2004). Disease and immunity in Caribbean and Indo-Pacific zooxanthellate corals. *Mar Ecol Progr Ser* **266**: 273–302.

Ulstrup KE, Hill R, Ralph PJ. (2005). Photosynthetic impact of hypoxia on in hospite zooxanthellae in the scleractinian coral Pocillopora damicornis. *Mar Ecol Progr Ser* **286**: 125–132.

Vismann B. (1991). Sulfide tolerance - physiological-mechanisms and ecological implications. *Ophelia* **34**: 1–27.

Voss JD, Mills DK, Myers JL, Remily ER, Richardson LL. (2007). Black band disease microbial community variation on corals in three regions of the wider Caribbean. *Microb Ecol* **54**: 730–739.

Wang F, Chapman PM. (1999). Biological implications of sulfide in sediment—a review focusing on sediment toxicity. *Environ Toxicol Chem* **18**: 2526–2532.

Weber M. (2009). How sediment damages corals. PhD thesis, University of Bremen, Bremen.

Supplementary Information accompanies the paper on The ISME Journal website (http://www.nature.com/ismej)

Supplementary Information

Figure S1: Spatial distribution of H$_2$S concentrations at the coral-microbial mat interphase (at 0 μm, see Figure 3) of all CP and BBD samples measured at three different irradiances (darkness = 0, intermediate = 40, daylight = 250 μmol photons m^{-2} sec^{-1}). Note differences in scales between CP and BBD colonies.
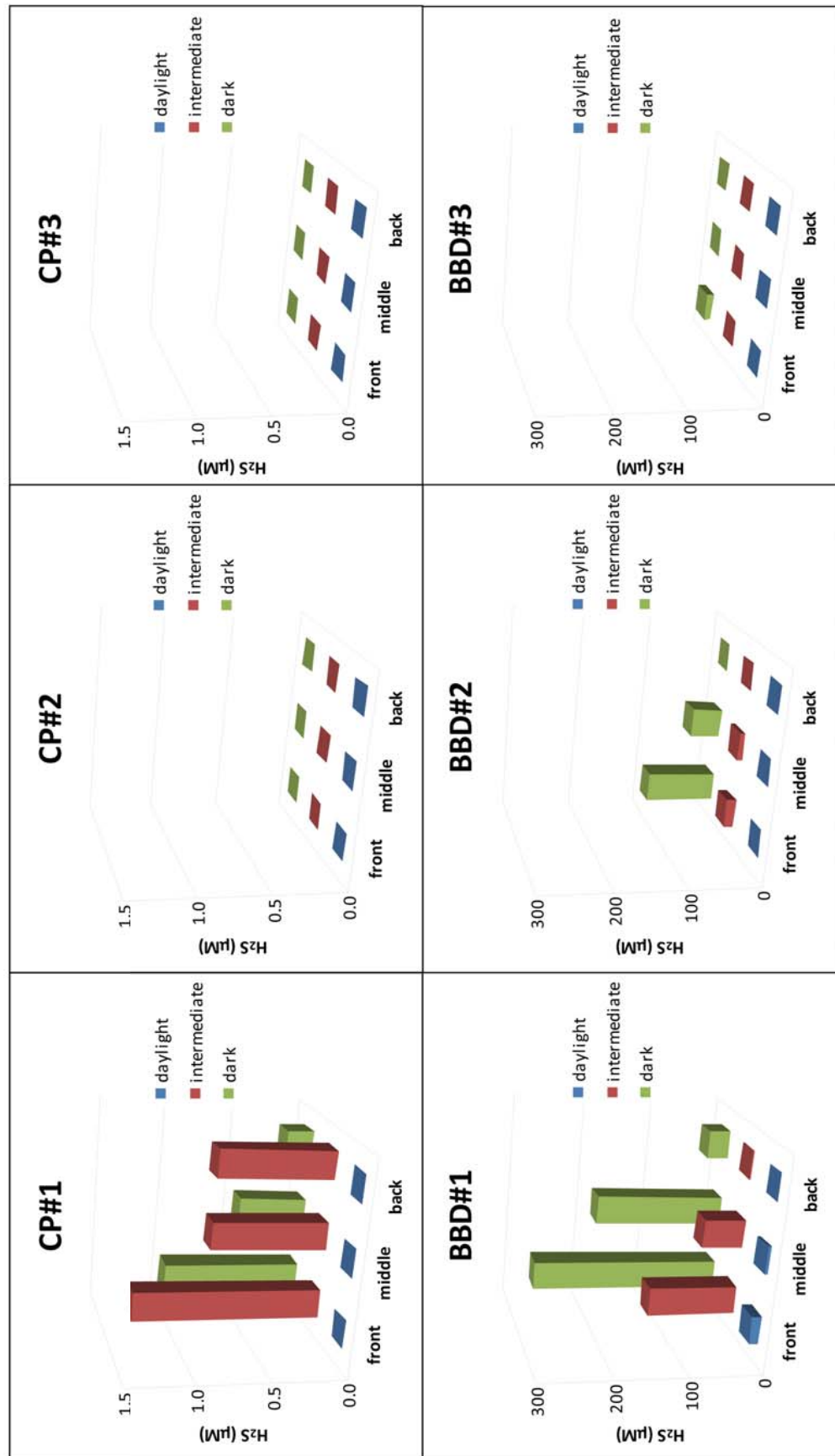
The extrapallial fluid of the bivalve *Arctica islandica* is not the site of shell formation

Abstract – a manuscript is currently in preparation

Kristina Stemmer[1*], Martin Glas[2], Dirk de Beer[2], Martin Beutler[2,3], Thomas Brey[1]

1) Alfred Wegener Institute for Polar and Marine Research, Am Handelshafen 12, D-27570 Bremerhaven, Germany
2) Max Planck Institute for Marine Microbiology, Celsiusstr. 1, D-28359 Bremen, Germany
3) bionsys GmbH, Fahrenheitstr. 1, D-28359 Bremen, Germany

Abstract

The extrapallial fluid (EPF) is an extracellular fluid, enclosed by the shell, the mantle tissue and the periostracum of bivalves. It is secreted by the outer mantle cells and is divided in most bivalves, via the pallial line, into an inner and outer section (Wilbur and Saleuddin 1983, Wheeler 1992, Vander Putten et al. 2000). The EPF was hypothesized to be the site of calcification / shell formation in bivalves (Wilbur and Saleuddin 1983, McConnoaughey and Gillikin 2008). We investigated this hypothesis by measuring pH, DIC, Ca^{2+} and Mg^{2+} levels within the EPF of the bivalve *Arctica islandica*, to determine parameters for carbonate system calculations. Using microsensors we performed long term (> 3 h) time series measurements and fluorescence-microscopy within the EPF of live bivalves (Figure 1), combined with *ex vivo* EPF Ca^{2+}, Mg^{2+} and DIC analyses, performed by atom-absorption-spectrometry (AAS) and DIC flow-injection analysis (Hall and Aller 1992), respectively.

The results showed that the outer and inner EPF had a continuously low pH (< 7.75) in both open (respiring), and closed (resting) phases of the bivalves. The pH levels fluctuated with the respiratory stages, being higher in the open- and lower in the closed-phases, and displayed a linear gradient of decreasing pH towards the mantle tissue. DIC levels followed these dynamics, being elevated (> 2000 µM) in the inner and decreased (< 2000 µM) in the outer EPF. This indicates that the carbonate chemistry of the EPF is largely determined by the respiratory state of the bivalve, and that DIC and low pH levels of both inner and outer EPF are a direct consequence of respiratory diffusional CO_2 input from the neighboring bivalve tissue. Replicated long term microsensor measurements combined with DIC analyses revealed that Ω_{Ar} was consistently too low to sustain the high rates of aragonite precipitation, which are expected for these bivalves. The EPF itself is thus not the site of calcification / shell formation in *Arctica islandica*, as previously hypothesized.
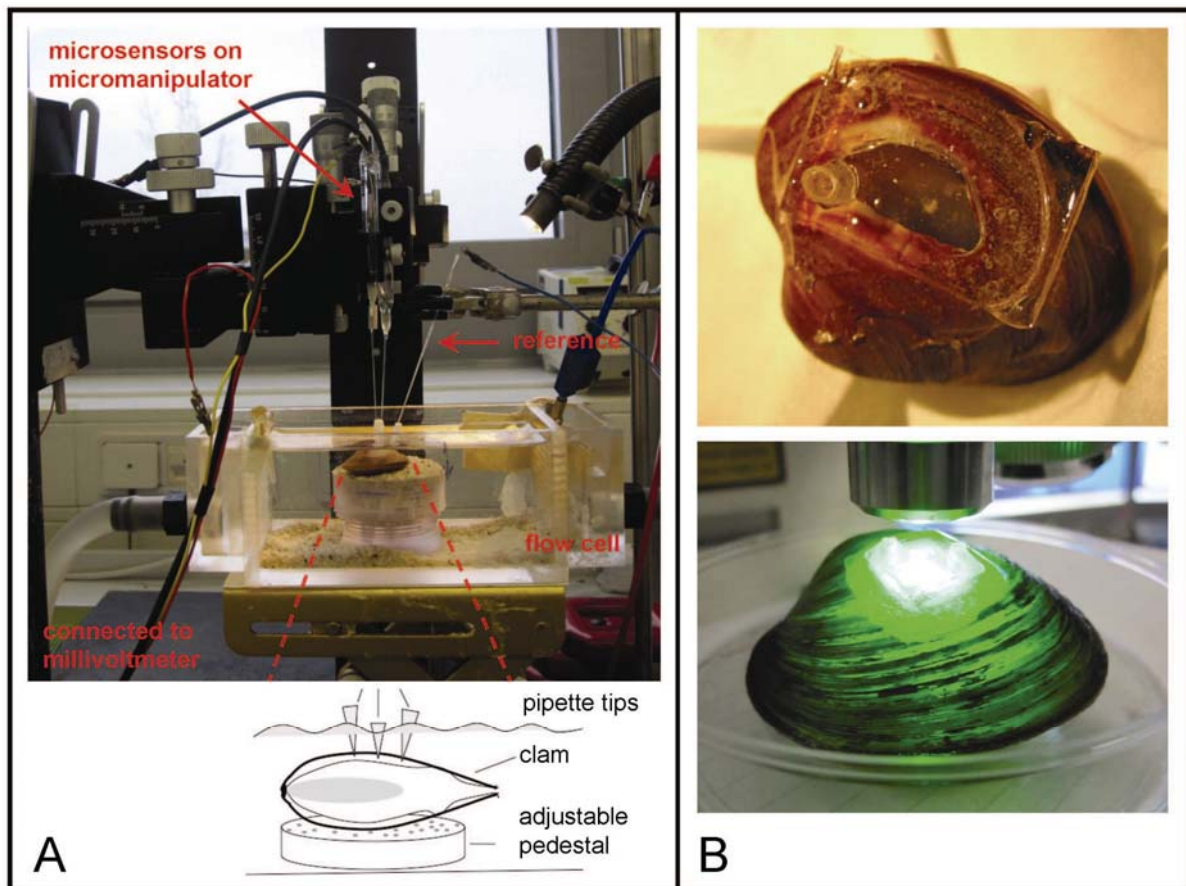
Figure 1: A) Microsensor setup for measuring simultaneous time series measurements of pH and Ca²⁺ dynamics within the extrapallial fluid (EPF) of the bivalve *Arctica islandica*. B) Individual with sealed 'shell window' for pH-fluorescence-microscopy of the inner EPF (photographs with permission from K. Stemmer).

References:

Hall OJ, Aller RC (1992). Rapid, small-volume, flow injection analysis for $\sum CO_2$ and NH_4^+ in marine and freshwaters. Limnol Oceanogr 37: 1113-1119.

McConnaughey T, Gillikin D (2008). Carbon isotopes in mollusk shell carbonates. Geo-Marine Letters 28: 287-299.

Vander Putten E, Dehairs F, Keppens E, and Baeyens W. (2000). High distribution of trace elements in the calcite shell layer of modern *Mytilus edulis*: Environmental and biological controls, Geochim. Cosmochim. Acta, 64: 997–1011.

Wheeler, A.P., 1992. Mechanisms of molluscan shell formation. In: Bonucci, E. (Ed.), Calcification in Biological Systems. CRC press: Boca Raton. pp 179–216.

Wilbur KM, Saleuddin ASM (1983). Shell formation. In: Saleuddin ASM, Wilbur KM (eds) The Mollusca. Academic: New York. pp 235–287.

The impacts of sediment-microgradients on the calcification of corals, foraminifera and crustose coralline algae

Abstract – the dataset is currently analyzed

Miriam Weber[1,2,3], Craig Humphrey[3], Martin Glas[1], Dirk de Beer[1], Katharina E. Fabricius[3]

1) Max Planck Institute for Marine Microbiology, Celsiusstr. 1, D-28359 Bremen, Germany
2) HYDRA Institute for Marine Science, Elba Field Station, 57034 Campo nell'Elba, Italy
3) Australian Institute of Marine Science, Townsville, Queensland 4810, Australia

Estuarine waters often carry high sediment load, have a relatively low pH and low carbonate saturation state. Yet, some of them do house coral reefs (Fabricius 2005). Earlier studies investigated in detail the effects of sediment cover on corals (Weber et al. 2012). However, sediments might also affect calcifiers in their vicinity, without directly covering them, through their microenvironments. *In situ* microsensor measurements on four inshore reefs of the Great Barrier Reef suggest that boundary layers around organically enriched sediments have a low pH (possibly from microbial activities and / or from metal geochemistry), and might thus affect calcification of coral recruits, small colonies and other calcifiers in their vicinity (Figure 1). We tested this hypothesis by measuring microchemical gradients of O_2, pH and Ca^{2+} on-top of calcifiers and into the sediments surrounding them (Figure 1). The laboratory experiment investigated calcification rates in each of two species of coral, foraminifera, and crustose coralline algae (CCA), situated within the boundary layer of calcareous and terrigenous sediments, the latter with and without enrichment of organic matter. The measured data are currently being analysed and are expected to be published in 2013 by Weber et al..
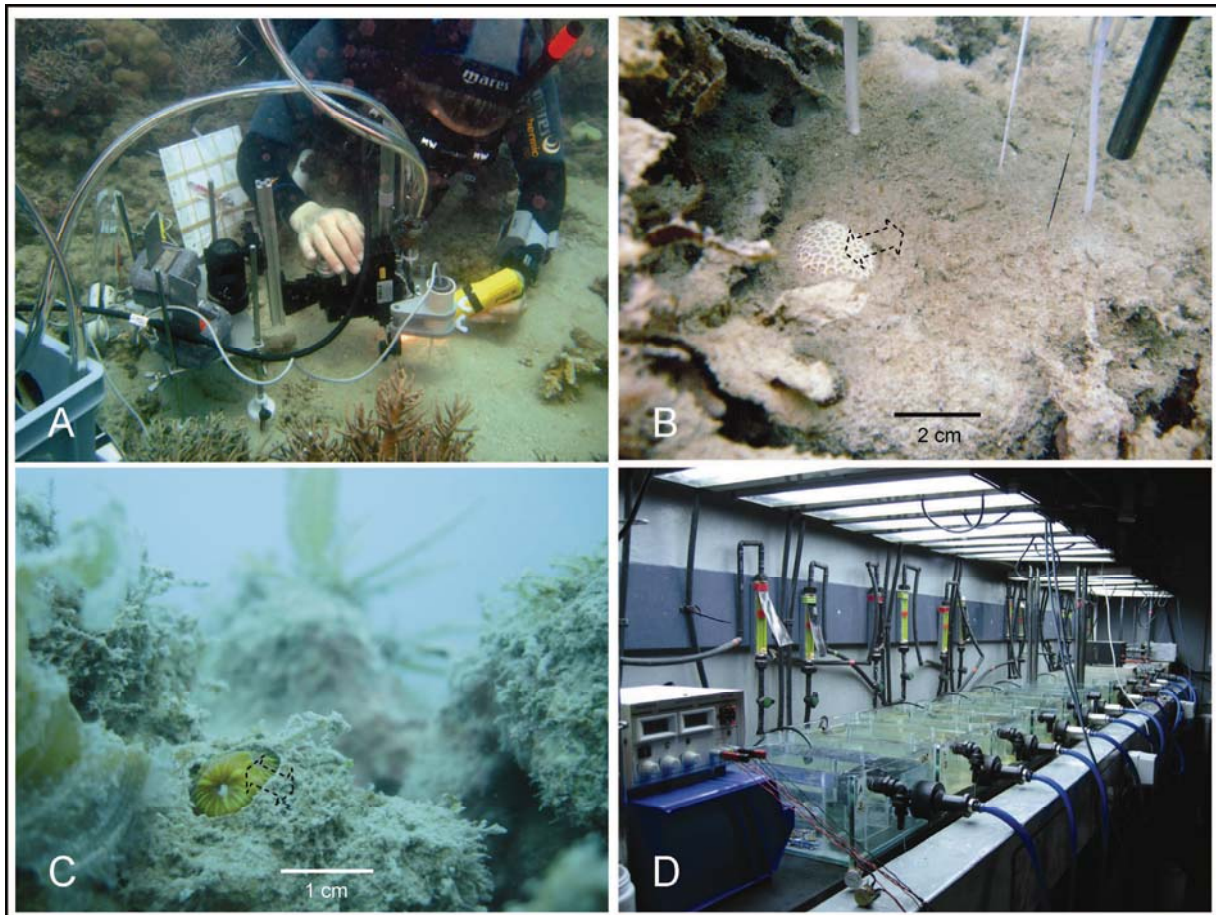
Figure 1: A) *In situ* **microsensor measurements with 'diver operated microsensor setup' (DOMS) at a near-shore reef, Whitsunday area, Great Barrier Reef.   B, C) Small coral recruits and colonies surrounded by sediment, black arrows indicate the area of possible microenvironmental interactions. D) Experimental lab setup: stirred incubation aquaria containing terrigenous sediment, with and without organic enrichments (photographs with permission M. Weber).**

References:

Fabricius KE (2005). Effects of terrestrial runoff on the ecology of corals and coral reefs: review and synthesis. Marine Pollution Bulletin 50: 125-146.

Weber M, de Beer D, Lott C, Polerecky L, Kohls K, Abed RMM et al (2012). Mechanisms of damage to corals exposed to sedimentation. Proceedings of the National Academy of Sciences 109: E1558-E1567.

Chapter 3

Ocean acidification effects on microgradients

The O_2, pH and Ca^{2+} microenvironment of benthic foraminifera in a high CO_2 world

This manuscript is currently in review with *PLosONE*

Martin S. Glas[1,2*], Katharina E. Fabricius[2], Dirk de Beer[1], Sven Uthicke[2]

Author addresses:

[1]Max Planck Institute for Marine Microbiology, Celsiusstr. 1, D-28359 Bremen, Germany

[2]Australian Institute of Marine Science, PMB 3, Townsville Qld 4810, Australia

*Corresponding Author: Martin S. Glas
Address: Max Planck Institute for Marine Microbiology, Celsiusstr. 1, D-28359 Bremen, Germany
Phone: +49 (0)421 2028 838
Fax: +49 (0)421 2028 690
Email: mglas@mpi-bremen.de

Abstract

Ocean acidification can have adverse effects on marine calcifiers. Yet, phototrophic marine calcifiers elevate their external oxygen and pH microenvironment in daylight, due to photosynthetic oxygen production and uptake of dissolved inorganic carbon (DIC). To date it has not been studied to which extent pH elevation within their microenvironments in daylight can counteract ambient seawater pH reductions, i.e. ocean acidification conditions. We measured the O_2 and pH microenvironment of four photosymbiotic and two symbiont-free benthic tropical foraminiferal species at three different ocean acidification treatments ($\sim$ 430, 1150 and 2150 μatm pCO_2). Our results showed that O_2 and pH levels were significantly elevated on photosymbiotic foraminiferal surfaces in light, compared to dark conditions, and compared to surfaces of symbiont-free foraminifera. The O_2 increase over the test surface compared with ambient seawater of photosymbiotic individuals at saturated light condition ($\Delta O_2 = 49 \pm 14$ μM (mean $\pm$ SE)), did not change significantly between ocean acidification treatments, suggesting rates of net photosynthesis were unaffected by pCO_2 (except in individuals that exhibited symbiont loss, i.e. bleaching, at elevated pCO_2). However, ΔpH (i.e. the 'pH buffering capacity') was significantly reduced at elevated pCO_2 (ΔpH = 0.067 $\pm$ 0.013 at pH 7.60, compared with 0.152 $\pm$ 0.038 at pH 8.22), due to the increased seawater acidity. The latter indicates that both photosymbiotic and symbiont-free foraminifera will experience strongly decreased microenvironmental pH conditions in daylight at elevated pCO_2. Our results, combined with previous field and laboratory studies, suggest that tropical benthic foraminifera will be quite susceptible to ocean acidification.

Introduction

Ocean acidification has become a major threat to our world's oceans [1]. From preindustrial times until today, atmospheric carbon dioxide (pCO_2) concentrations increased from $\sim$ 280 ppm to > 390 ppm, and are predicated to rise to $\sim$ 800 ppm by the end of this century under the IPCC business-as-usual emission scenario (WG 1, A2, [2]), which is likely to be exceeded [1,3]. The rate of CO_2 increase in our atmosphere is mostly due to anthropogenic induced changes from increased fossil fuel combustion, deforestation and changes in land use and is now faster than over past millions of years [4,5]. Not only is CO_2 a potent greenhouse gas in the atmosphere resulting in global warming, but about one third of the anthropogenic CO_2 increase is taken up by the oceans [1,6]. This uptake reduces pH and consequent carbonate saturation state (Ω) of the ocean surface waters, a process generally termed as 'ocean acidification' (OA). Marine calcifiers (such as coccolithophores,

foraminifera, calcareous algae and corals) account for a large fraction of the present day carbon fixation in the surface oceans [7-9] and consequent removal of CO_2 from the atmosphere into the deep sea (i.e. the 'biological pumps'). By changes in ocean chemistry ocean acidification poses a direct threat to most calcifying organisms and consequently the biological pumps [1,10,11].

However, the effect of bulk seawater pH is mediated through the diffusive boundary layer (DBL) that governs diffusive transport between the bulk seawater and the organisms' surface. Around phototrophic organisms (including most major calcifiers such as phytoplankton, foraminifera, corals and calcareous algae) DBLs can maintain substantial gradients of O_2 and consequently pH to the bulk seawater, due to their photosynthetic and respiratory exchange of dissolved inorganic carbon (DIC) [12-20]. Especially under daylight conditions, surface pH levels of phototrophic or photosymbiotic organisms can vary strongly (> 0.1 pH units) compared to the bulk seawater. It is this surface pH and the resulting gradients within the organisms' DBL, rather than the bulk seawater pH, which determines ion-availability [16] and consequently transport-kinetics between the underlying tissue and surrounding seawater. Microenvironmental pH dynamics are therefore likely to play an important role in physiological responses to ocean acidification. Understanding O_2 and pH dynamics and variability within the DBLs under both present day and future OA conditions is therefore essential for all transport involving metabolic processes such as calcification, photosynthesis or respiration.

One hypothesis could be that pH elevations within the DBL in daylight over the surface of photosymbiotic calcifiers might partly or fully counteract ambient pH decreases predicted by ocean acidification. A consequence could be that OA induced increases of seawater DIC might enhance photosynthesis and consequently aid pH elevation on their surfaces, again increasing resistance against acidification in daylight.

To date it has not been studied whether this pH elevation within their microenvironment can protect phototrophic calcifiers (or at least partly compensate) from the effects of ocean acidification in daylight and therefore lend additional resistance compared to non phototrophs. We tested this hypothesis by measuring the O_2 and pH microenvironment of 4 photosymbiotic and 2 symbiont-free benthic tropical foraminiferal species under different ocean acidification scenarios in light and dark conditions.

Material and Methods

Sampling and culturing

Specimens of the photosymbiotic species *Marginopora vertebralis*, *Amphistegina radiata, Heterostegina depressa*, and *Peneroplis* sp., and the symbiont-free species *Quinquelloculina* sp. and *Miliola* sp. were hand collected from coral rubble and other substrates containing foraminiferal assemblages by SCUBA diving during a cruise in the summer months of 2010 in the Whitsunday area, central section of the Great Barrier Marine Park. All necessary permits were obtained prior to field collection from the Great Barrier Marine Park Authority (Permit-No: G09/30237.1). Collection sites included, Bait Reef S 19°80.17' E 149°07.55', Daydream Island S 20°15.35', E 148°48.73', Shaw Island S 20°31.02' E 149°04.48' and Deloraine Island S 20°09.30', E 149°04.50' (depth 5 – 13 m, seawater temperature during collection 28.8 ± 0.2 °C (mean ± SD) and salinity 35-36). A detailed description of the sampling sites can be found in Uthicke et al. [21].

After collection, specimens were washed off substrates, cleaned by gentle washing and sieving and identified to species and genus level [22] under a dissecting-microscope (Leica MX16 A, Solms, Germany). Samples were kept in natural seawater (24° - 26 °C) under low light conditions (10 μmol photons m^{-2} s^{-1}), until they were transported to the Australian Institute of Marine Science (AIMS) in Townsville. Prior to experiments, specimens acclimatised in indoor climatic chambers > 3 weeks in natural seawater (replaced every 3 days, sediments removed) at 24° - 26 °C, 10 μmol photons m^{-2} s^{-1}, 12 h : 12 h diurnal cycling and fed with microalgae (*Isocrysis* sp.). Salinity of nearshore seawater available at the AIMS was diluted (32 - 34) due to high seasonal rainfall. During culturing and experimental treatments seawater salinity was therefore adjusted to 35 by the addition of sea salt (Sunray, Cheetham Salt, Melbourne, Australia). Salinities were measured refractometrically (S/Mill-E, Atago, Tokyo, Japan).

Experimental measurement setup

Carbon perturbations experiments were performed by the addition of CO_2 enriched air into a semi-closed circulation system of filtered (1 μm) natural seawater. CO_2 enriched air (0.2 %) was humidified via a system of Erlenmeyer flasks and bubbled into an aerated reservoir tank (30 L), connected to incubation chambers, which contained the organisms (water flow rate 0.5 – 1.0 cm s^{-1}). Gas flow rates (i.e. *pCO$_2$*) and thereby pH levels were regulated via mass flow controllers (accuracy 1.5 %, GFC17, Aalborg, Orangeburg, NY, USA). The system was allowed to equilibrate for > 48 h.

All amperometric and potentiometric microsensor measurements were conducted in a Faraday cage to minimize electrical disturbance. During measurements specimens were carefully removed with a fine brush from the incubation chambers and placed into a flow-cell (1.2 ml volume), connected to the same circulation system. Flow rates within the flow cell were adjusted volumetrically and measured before each experimental day and measured again at the end of the day (0.50 ± 0.02 cm s^{-1} (mean $\pm$ SD)). Net horizontal flow was monitored ~3 mm above the foraminiferal surface by observing particle movements via a stereo-microscope (K400, Motic, Xiamen, China).

Illumination was provided from above via a fiber-optic guide from a halogen light source (Schott KL2500, Mainz, Germany). Light intensities were monitored with a quantum irradiance meter (LI-250A, LI-COR, Lincoln, NE, USA), combined with a light sensor for photosynthetic active radiation (PAR).

Microelectrodes

Clark-type O_2 microsensors with a guard cathode (tip diameter ~20 µm, < 1 s response time (t_{90}), precision 0.05 µM) were constructed and calibrated as previously described [23]. pH measurements were performed by liquid ion exchange (LIX) membrane microelectrodes (tip diameter 5 - 20 µm, < 1 s response time (t_{90}), precision 0.001, on the NBS scale), as previously described by de Beer [24], and a commercial pH meter (pH 1100, Oakton, Vernon Hills, IL, USA). Ca^{2+} concentrations were determined with LIX microelectrodes (tip diameter 5 - 20 µm, < 2 s response time (t_{90}), precision 13 µM), which were prepared, calibrated and used as described [25,26]. A detailed description of the measurement setup can be found in Polerecky *et al*. [27].

Experimental procedure and determination of microenvironmental dynamics

Using a fine brush, foraminifera were positioned horizontally in the middle of the flow cell resting on their central elevations, with the exception of *Marginopora,* which exhibits a flat surface structure (Figure 1). Microsensor tips were positioned on the calcite shell surfaces of foraminifera, using a stereo-microscope and a 3D-manual micromanipulator (MM33, Maerzhaeuser, Wetzlar, Germany). O_2 evolution within the DBL of phototrophic species was tested under varying light intensities (data not shown). A light intensity of 30 µmol photons m^{-2} s^{-1} was found saturating, without causing photo-inhibition and used throughout all 'light' experiments (see also [28,29]). To determine the t_{90} value of steady-state signals of the system O_2, pH and Ca^{2+} probes were positioned on the test surface of photosymbiotic individuals and

recorded for ~ 30 min, while light levels were altered (light/dark changes). O_2 (pA) reached > 90 % steady-state signals ~ 2 min, pH values (mV) took < 6 min, while Ca^{2+} (mV) values did not change significantly. To ensure steady-state, light levels were applied for > 10 min prior to measurements. Steady-state profiles were measured in step sizes of 50 μm (up to 400 μm) and 100 μm about 1500 μm upward perpendicular to the foraminiferal test, through the diffusive boundary layer into the bulk seawater (Figure 1). Due to slow erecting of individuals by rhizopodial movements, gentle nudges with a fine brush were applied in between profiles to assure rhizopodial retraction, so that foraminifera and their extending DBLs remained in their horizontal position.

To illustrate the effect of zero flow (i.e. static culture) conditions on pH microenvironments, individuals of *Marginopora vertebralis* were pH profiled at the same position on the calcite shell at pH 8.22, 30 μmol photons m^{-2} s^{-1} under steady state pH and flow conditions (0.5 cm s^{-1}) and consecutively after flow was turned off after 5, 10, 20, 30, 40, 50, 60, 90 and 100 min and again after flow was re-established within 5 min. Individuals of *M. vertebralis* were chosen for these measurements since they remained attached to the bottom of the flow cell in a fixed position for extended periods of time.

To estimate spatial microenvironmental O_2 heterogeneity across the shell surfaces, specimens of every species were fine scale profiled under control pH conditions from front to back in flow direction (Figure 1).

Large scale profiling experiment

To account to some extent for spatial heterogeneity across shell surfaces (Figure 1) during the large scale profiling experiment, foraminiferal specimens (n = 2) were profiled in 2-4 locations on their calcite shell during the experiment (indicated by red crosses in Figure 1). To determine possible treatment effects on O_2 dynamics and to evaluate exact placement of microsensor tips for consecutive measurements, individuals were profiled with O_2 microsensor at pH 8.22 in light, prior to each treatment incubation. Large scale profiling experiments were conducted at pH levels of 8.22 (ambient), 7.85 and 7.60 with photosymbiotic species, and at two pH levels (8.22 and 7.60) with symbiont-free individuals (Table 1). After 24 h of incubation, microsensor measurements across the DBL of all specimens in both light (30 μmol photons m^{-2} s^{-1}) and darkness were conducted for O_2 on day 2, pH on day 3, and Ca^{2+} on day 4.
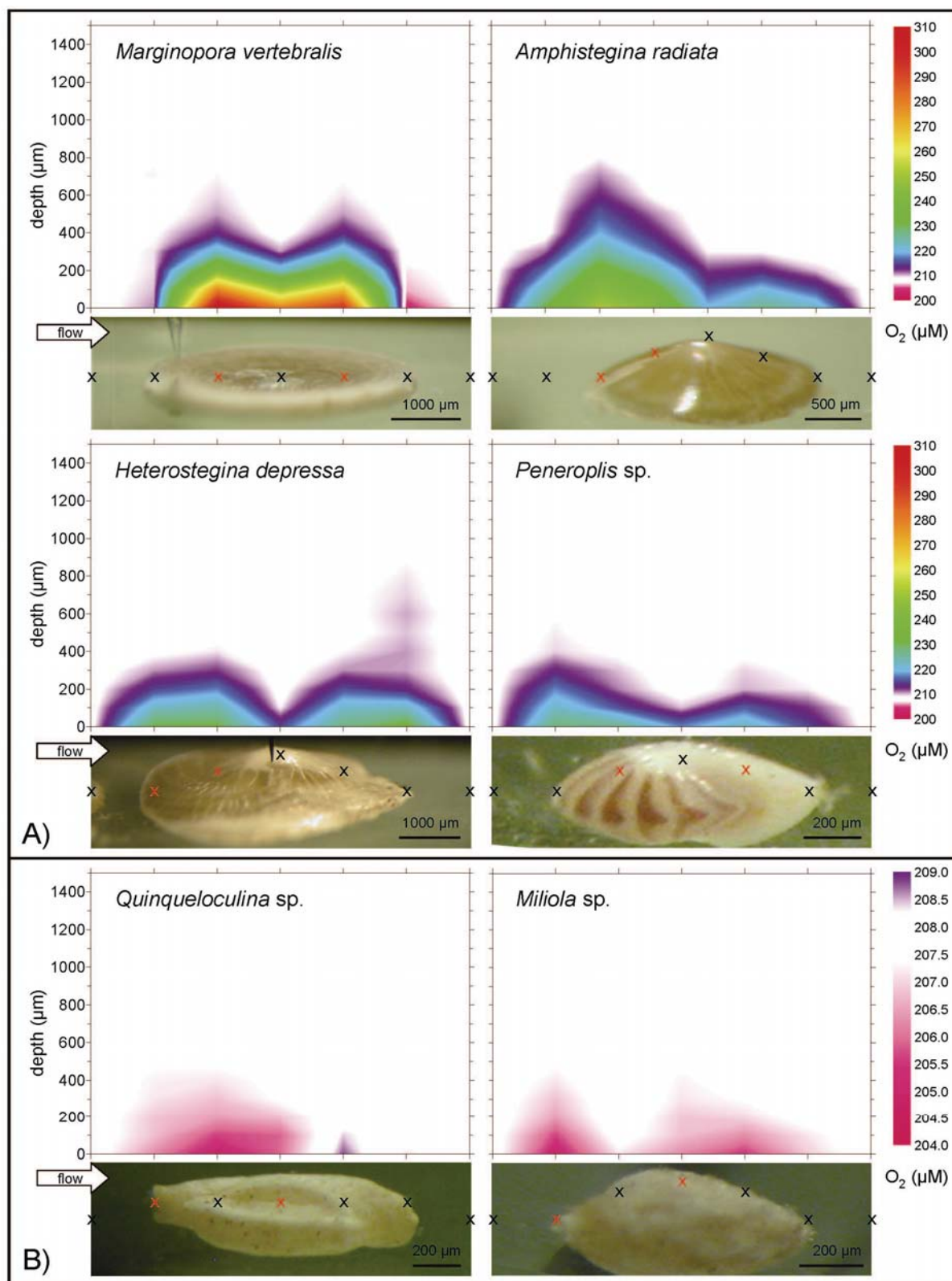
Figure 1: Microenvironmental O$_2$ heterogeneity at pH 8.22, 30 µmol photons m^{-2} s^{-1} light, and 0.5 cm s^{-1} water flow across foraminiferal shell surfaces. Data derived from fine-scale microsensor profiles at the points indicated by the crosses. Red crosses indicate the measurement positions (n = 2 - 4) used for the calculation of means per individual. Note the different contour scales between A) photosymbiotic and B) symbiont-free species.

Seawater was renewed for each experimental treatment and kept at a constant salinity (35) and pH according to the treatment (Table 1). Temperature, pH, DIC, total silicate and total phosphorus were monitored daily. DIC samples were filtered (0.2 μm nylon filters), stored gas tight, head-space free at 4 °C and analysed within a week by flow injection analysis [30]. Samples for nutrient analyses (including total silicate and phosphorus) were filtered (0.2 μm nylon filters), immediately frozen and consequently analysed with a Bran and Luebbe AA3 segmented flow analyzer (Norderstedt, Germany) following Ryle et al. [31]. Samples for total alkalinity (TA) were taken at the end of each experiment, filtered (0.2 μm nylon filters), poisoned with $HgCl_2$ and kept at 4 °C until being shipped to the University of Sydney, where they were analysed by open cell potentiometric titration [32], and calculated using linear Gran plots [33]. Corrections were applied from certified reference material (A. Dickson, Scripps Institution of Oceanography, CA, USA).

Treatment of individuals

For microsensor measurements, healthy, intact foraminiferal specimens of similar size and pigment shading were selected and liveliness confirmed in all individuals by the observation of movement. Individuals were photographed (Canon 30D, Tokio, Japan) via the dissecting microscope, before and after the experimental treatments (for complete sets, see SOM Figure 3, 4, 5). At the end of the experiments, individuals were examined and photographed under a fluorescence microscope (Axioskop mot plus, Carl Zeiss, Goettingen, Germany) equipped with a digital camera (AxioCamMRc5, Carl Zeiss, Goettingen, Germany). Fluorescence images were obtained using a halogen lamp for incident light and DAPI (excitation, G365 nm; dichroic mirror FT395; emission LP420 nm) and FITC (excitation, BP 450 - 490 nm; dichroic mirror FT510; emission LP515 nm) filter sets (Carl Zeiss, Goettingen, Germany). Foraminiferal sizes, determined as the longest diameter of individuals, were measured in small individuals from microscopic images by the software AxioVision (version 4.8.1, Carl Zeiss, Goettingen, Germany) and in large individuals via a digital calliper.

Carbonate chemistry calculations

Calculations based on measurements of DIC, pH, temperature, salinity, total-phosphate and silicate (Table 1) were performed in CO_2SYS [34], using K1 and K2 according to Millero et al. [35], with dissociations constants for H_2SO_4 detailed in Dickson [36]. Measured and calculated levels of total alkalinity deviated < 0.2 %, indicating that carbonate chemistries were in equilibrium throughout the experiments (Table 1).

Table 1: Experimental parameters (mean ± SD), monitored each day of each 4-day pCO_2 incubations (n = 4) beside TA, which was sampled at the end of each experiment (n = 1). All measured input parameters, beside TA, were used for CO₂SYS calculations.

Measured Input Parameters

Treatment	T [°C] (n = 4)	TP [µmol kg⁻¹] (n = 4)	TSi [µmol kg⁻¹] (n = 4)	pH (NBS) (n = 4)	DIC [µmol kg⁻¹] (n = 4)	TA [µmol kg⁻¹] (n = 1)
pH 8.22	25.9 ± 0.2	0.08 ± 0.01	27.19 ± 0.28	8.22 ± 0.01	2343 ± 43	2710
pH 7.85	26.0 ± 0.4	0.04 ± 0.01	23.31 ± 0.58	7.85 ± 0.01	2468 ± 21	2622
pH 7.60	25.9 ± 0.4	0.09 ± 0.01	23.51 ± 0.86	7.60 ± 0.03	2603 ± 36	2651

Calculated (n = 4)

	TA [µmol kg⁻¹]	pCO_2 [µatm]	CO₂ [µmol kg⁻¹]	HCO₃⁻ [µmol kg⁻¹]	CO₃²⁻ [µmol kg⁻¹]	Ω_{Ca}
pH 8.22	2709 ± 43	432 ± 17	12.0 ± 0.5	2060 ± 41	271 ± 5	6.52 ± 0.12
pH 7.85	2617 ± 23	1141 ± 28	31.5 ± 0.8	2307 ± 20	129 ± 3	3.11 ± 0.08
pH 7.60	2654 ± 28	2151 ± 179	59.2 ± 4.5	2465 ± 35	78.7 ± 3.7	1.90 ± 0.09

Abbreviations: TP = total phosphorus, TSi = total silicate, DIC = dissolved inorganic carbon, TA = total alkalinity, pCO_2 = partial pressure CO₂, Ω_{Ca} = saturation state of calcite

Statistical analysis

Differences in concentrations between the bulk seawater and the surface of the shells, denoted as ΔO_2, ΔpH and ΔCa^{2+}, were attained from the measured profiles. Concentration differences were calculated as the lowest and highest spatial points of the profiles respectively. At very low metabolic rates and therefore increased resolution, profile noise was balanced by a line of best fit through the seawater baseline concentrations, and DBL gradients, to attain concentration differences. Hydrogen ion activity, i.e. H^+ concentrations for dilute aqueous solutions, were calculated from pH levels. Since microsensor measurements of O_2, pH and Ca^{2+} were performed consecutively on different days, they did not depict true spatial replicates of one location (see also '*large scale profiling experiment*'). Measurement position differences of ΔO_2, ΔH^+, ΔpH and ΔCa^{2+} within individuals (Figure 1) were found to be non-significant. Consequently profiles (n = 2 - 4) were averaged for every individual for statistical analyses.

Means of ΔO_2, ΔH^+, ΔpH and ΔCa^{2+} over replicate profiles per individual were tested for normality and homogeneity of variances by normality plots and Levene's tests, respectively. Since parametric assumptions were violated, complete data sets of mean ΔO_2, ΔH^+, ΔpH and ΔCa^{2+} were analyzed by Kruskal-Wallis one way analysis of variance for different factors, and alpha levels Bonferroni corrected (Table 2). Group comparisons were performed using Wilcoxon signed rank test (WSRT) for paired samples, Kruskal-Wallis one way analysis of variance and Wilcoxon rank sum tests (= Mann Whitney U-tests) for unpaired samples, respectively. The ratios of mean ΔO_2 / ΔpH and mean ΔO_2 / ΔH^+ of all individuals were compared across *pCO₂* treatment groups, using generalized linear models (GLMs). All statistical analysis used the software R [37] or SPSS 13.0 (IBM, Armonk, NY, USA).

Results

Individual fitness

Both *Heterostegina* at pH 7.60 and *Amphistegina* individuals at pH 7.85 and 7.60 showed visual signs of symbiont loss (i.e. bleaching) at the end of the 4 day incubations (SOM Figure 4, 5). In *Amphistegina*, bleaching was accompanied by severe symbiont clumping within the cell body.

Zero-flow experiment

Within 30 sec after flow was turned off, no visible horizontal particle movement could be detected. Within 5 min after turning off flow, linear pH gradients started increasing and

after 100 min DBLs extended up to 1400 µm into the bulk seawater, reaching a maximum pH of 8.88 at the surface of the shell (Figure 2). After flow was resumed, DBLs immediately reverted back to normal steady state conditions.
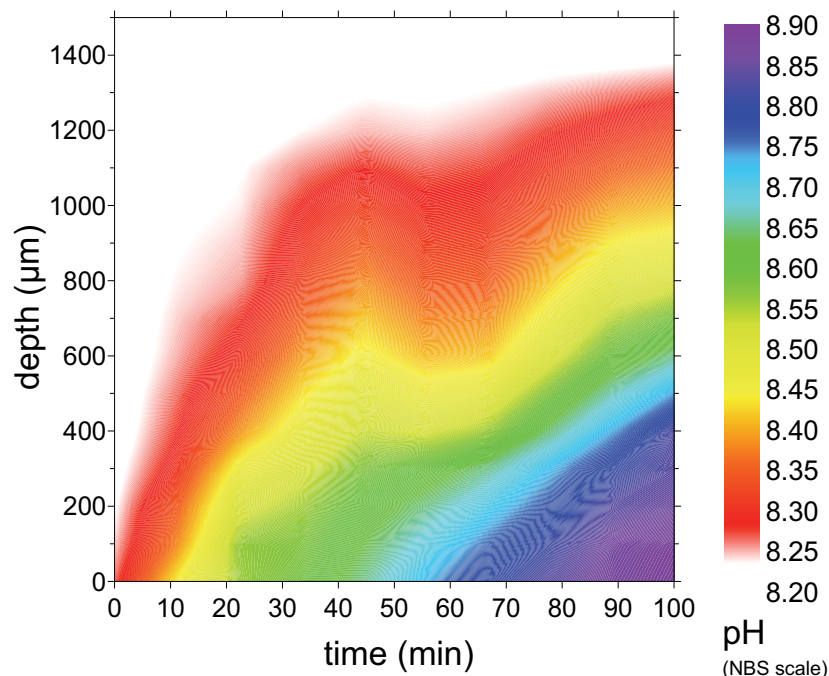
Figure 2: Temporal pH development of diffusive boundary layer (DBL) of *Marginopora vertebralis,* measured consecutively at a single position on the calcite shell at pH 8.22, 30 µmol photons m^{-2} s^{-1} under zero flow conditions after flow (0.5 cm s^{-1}) was cut off at time = 0.

O_2 microenvironment around foraminiferal tests

Due to their convex shapes, all foraminifera except for *Marginopora* had only few contact points with the bottom of the flow cell during the measurements. The effective thickness of the O_2 DBL [20] on the tests (395 ± 31 µm (mean + SE)) ranged between 150 to 850 µm (Figure 1). In phototrophic specimens, DBL thickness was laterally enlarged where symbiont densities, and therefore photosynthetic activity, was higher than at the central part of the test. In *Amphistegina, Heterostegina* and *Peneroplis,* DBLs were also enlarged at the upstream edges. Differences of O_2 between the shell surface and the bulk seawater, denoted as ΔO_2, varied across the shell and among individuals, and were generally strongly increased in photosymbiotic, and slightly decreased in symbiont-free species. The downstream edge of the *Marginopora* individual, in which symbionts were sparse, exhibited a slight O_2 under-saturation.

O_2 dynamics within individuals under illumination

Within individuals, mean ΔO_2 at pH 8.22 (control measurements) remained similar over time, between the measurements before and at the end of the incubations under illumination (WSRT, V = 33, p-value = 0.6772, Figure 4). Only in *Marginopora* at pH 8.22 and 7.60 did variation of ΔO_2 change from before to during the incubations (Figure 4). This confirms that consecutive microelectrode measurements on individuals did not affect readings under control conditions. Variation in ΔO_2 between individuals was greater for photosymbiotic, compared to symbiont-free species (Figure 4) and highest for *Marginopora* (all *pCO_2* treatments), *Amphistegina* (before incubation) and *Heterostegina* (before and during incubation) at pH 7.60. Under illumination mean ΔO_2 was significantly elevated at all *pCO_2* treatments in photosymbiotic, compared to symbiont free species (44 ± 8 µM, vs. -0.002 ± 0.753 µM (mean ± SE), U-test: W = 0, p = $1.90e^{-07}$). Beside individuals that exhibited symbiont loss, mean ΔO_2 of photosymbiotic species did not change significantly between elevated and control *pCO_2* (WSRT: V = 11, p = 0.1055). ΔO_2 was strongly decreased at pH 7.60 in *Amphistegina*, which displayed severe visual signs of bleaching (SOM Figure 5). ΔO_2 of symbiont-free individuals remained usually negative, very low and similar at both *pCO_2* treatments. Yet, some profiles of positive ΔO_2 (i.e. net production) were measured in both *Quinqueloculina* (pH 7.60, Figure 4) and *Miliola* specimens. Subsequent fluorescence imaging revealed chlorophyll autofluorescence of epiphytes on the shell surfaces of these symbiont-free individuals (Figure 3).
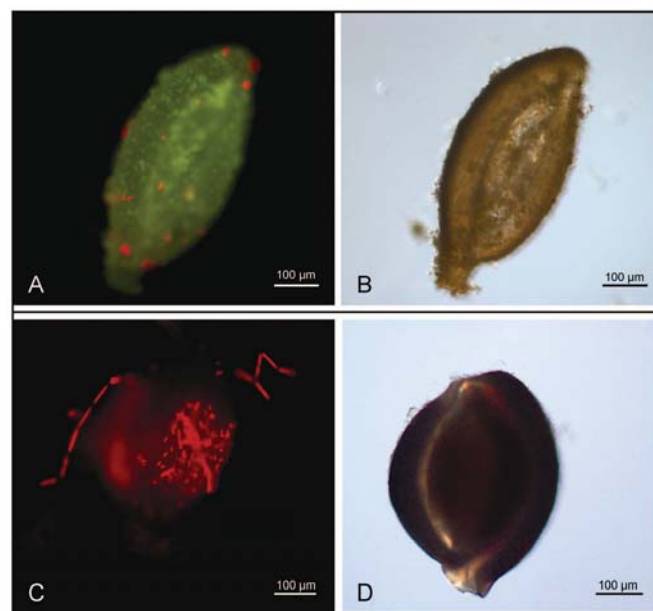
Figure 3: Exemplary microscopic images of *Quinqueloculina* (A, B) and *Miliola* (C, D) specimen profiled at pH 7.60. (A, C) Chlorophyll autofluorescence of phototrophic epiphytes on the calcite shell under green excitation light (FITC-filter set).
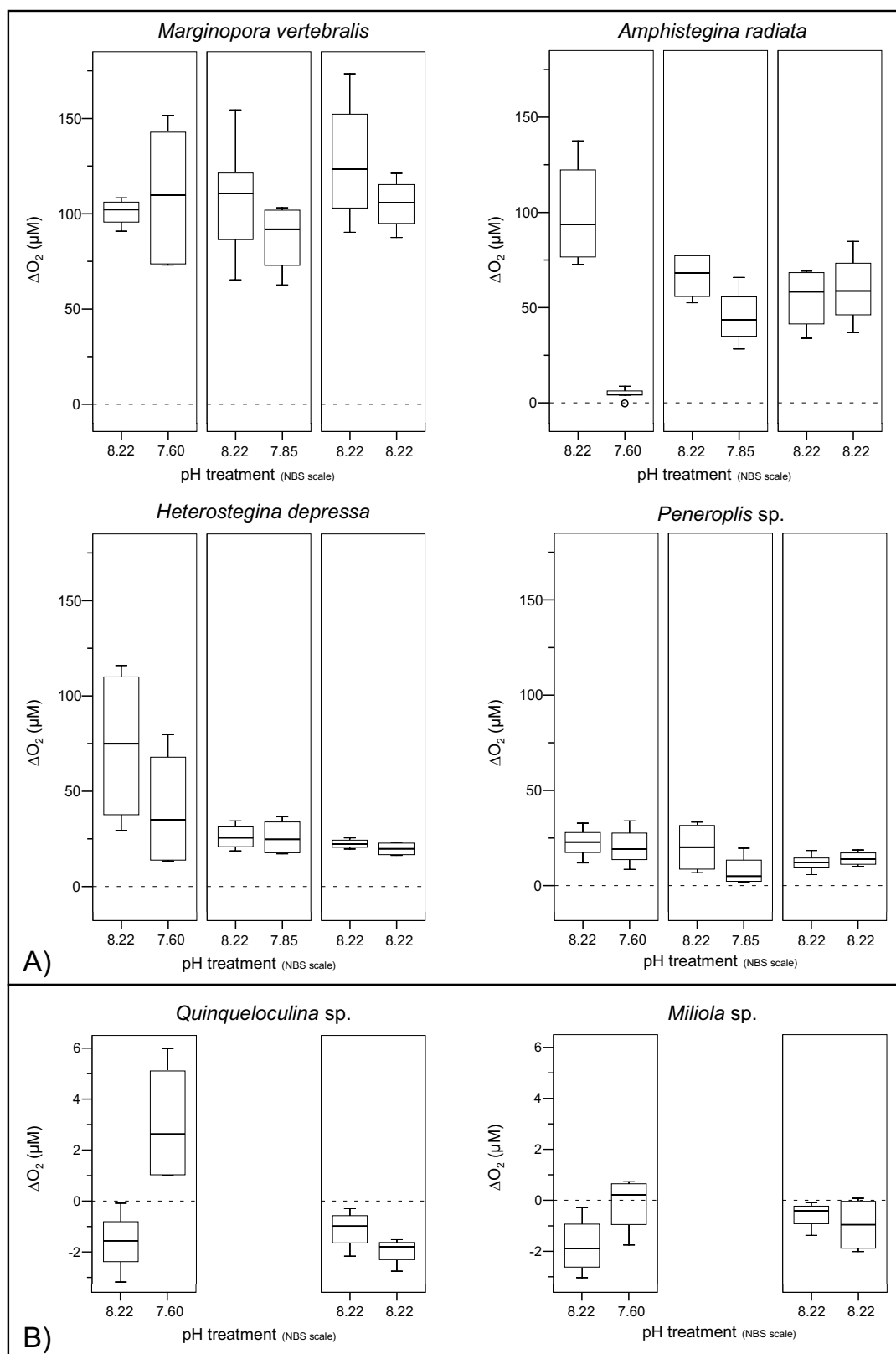
Figure 4: Box-plots representing the 25th, 50th and 75th percentiles of ΔO_2, calculated from profiles measured within individuals (n = 2) prior (at pH 8.22) and during *pCO$_2$* treatment incubations (pH 8.22, 7.85 or 7.60), under illumination (30 µmol photons m^{-2} s^{-1}) for the six foraminiferal species. Note the different scales between A) photosymbiotic and B) symbiont-free species. Outliers (> 1.5 interquartile range) are indicated by circles.

O_2, H^+, pH and Ca^{2+} dynamics within and between treatment groups

Illumination strongly affected mean ΔO_2, ΔH^+, ΔpH (Table 2), which were significantly elevated in photosymbiotic, compared to symbiont-free species at all pCO_2 and between light and dark, indicating net photosynthesis (Figure 5, 6). Beside *Amphistegina* specimens, which strongly bleached at the highest pCO_2 level (SOM Figure 5), mean ΔO_2 in light did not change significantly between pCO_2 treatments (Kruskal Wallis: $X^2 = 1.8584$, df = 2, p = 0.3949). In darkness mean ΔO_2 was negative in all photosymbiotic species indicating respiration (-11 ± 3 μM), which was enhanced in *Marginopora* and *Heterostegina* at pH 7.85 and reduced in *Amphistegina* at increased pCO_2 (Figure 5). Symbiont-free species showed net respiration in both light and dark (-1.17 ± 0.54 μM).

In contrast to ΔO_2, mean ΔH^+ was significantly affected by pCO_2 treatment, trophic level, species and symbiont-type (Table 2). Under illumination, mean ΔH^+ of all photosymbiotic species decreased with increasing pCO_2 (-1.67 ± 0.35 nM at pH 8.22 vs. -3.53 ± 0.66 nM at pH 7.60, Figure 6), beside in Peneroplis individuals, where net photosynthesis was low and variable between the pCO_2 treatments (Figure 5). In darkness at pH 8.22, mean ΔH^+ (0.070 ± 0.019 nM) of all species was slightly increased indicating net respiration. Yet, all photosymbiotic species showed a negative mean ΔH^+ at elevated pCO_2 conditions in darkness (-0.88 ± 0.21 nM, Figure 6). ΔH^+ of symbiont-free species was generally much lower in light (-0.20 ± 0.15 nM), compared to photosymbiotic species and also slightly negative at pH 7.60 at both light levels (-0.49 ± 0.17 nM).

Changes in mean ΔCa^{2+} were generally very low and exhibited high variation in space and time (39 ± 24 μM). Mean ΔCa^{2+} did not change significantly with any of the measured factors (Table 2, SOM Figure 1). At pH 7.60, mean ΔCa^{2+} was still positive (23 ± 29 μM), indicating no net $CaCO_3$ dissolution.

Table 2: Omnibus Kruskal-Wallis one way analysis of variance results of mean (n = 2 – 4) ΔO_2, ΔH^+, ΔpH and ΔCa^{2+} measured during three pH treatment incubations (8.22, 7.85 and 7.60) for different factors. Significant effects at the Bonferroni corrected 0.83 % levels are indicated in bold.

	ΔO_2 (µM)[a]			ΔH^+ (nM)[a]			ΔpH[a]			ΔCa^{2+} (µM)[a]		
	X^2	df	p	X^2	df	p	X^2	df	p	X^2	df	p
pCO_2 treatment	0.0550	2	0.9729	14.8627	2	**0.0006**	9.0712	2	0.0107	2.1433	1	0.1432
illumination	44.175	1	**$3.00e^{-11}$**	14.4391	1	**0.0001**	17.5504	1	**$2.80e^{-05}$**	0.3827	1	0.5362
trophic level[b]	0.2462	1	0.6198	13.0502	1	**0.0003**	15.2657	1	**$9.34e^{-05}$**	0.9686	1	0.3250
species	0.4675	5	0.9933	16.4631	5	**0.0056**	18.0582	5	**0.0029**	2.6097	5	0.7599
symbiont type[c]	0.3052	3	0.9591	15.6138	3	**0.0014**	17.4416	3	**0.0006**	2.5392	3	0.4682
treatment groups[d]	60.286	31	**0.0012**	58.0442	31	**0.0023**	59.4338	31	**0.0016**	12.556	23	0.9610

[a] Δ denotes the difference in O₂, pH and Ca²⁺ respectively between the surface of shell and the bulk seawater determined by microsensor profiling (n = 2 - 4), averaged over each individual.
[b] levels: photosymbiotic, heterotrophic
[c] levels: diatoms (*Amphistegina radiata, Heterostegina depressa*), dinoflagellates (*Marginopora vertebralis*), red algae (*Peneroplis* sp.), no symbionts (*Quinqueloculina* sp., *Miliola* sp.)
[d] treatment groups represent each combination of species, pCO_2, and light phase, according to box-plots represented in Figure 5, 6 and SOM Figure 1, 2.
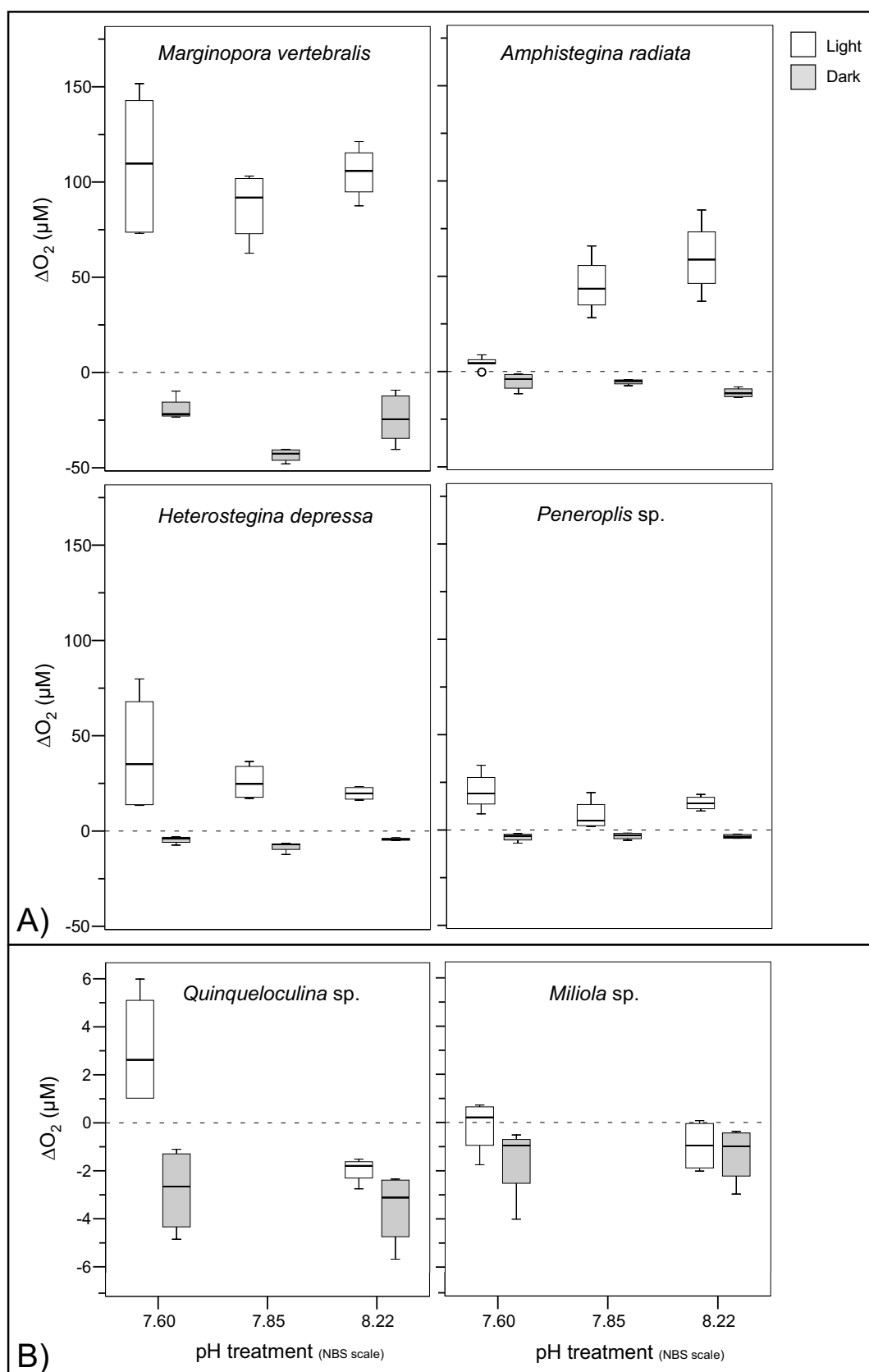
Figure 5: Box-plots representing the 25th, 50th and 75th percentiles of ΔO_2, calculated from profiles measured during the pH treatment incubations, at light (30 µmol photons m^{-2} s^{-1}) and dark conditions for the six foraminiferal species. Note the different scales between A) photosymbiotic and B) symbiont-free species. Outliers (> 1.5 interquartile range) are indicated by circles.
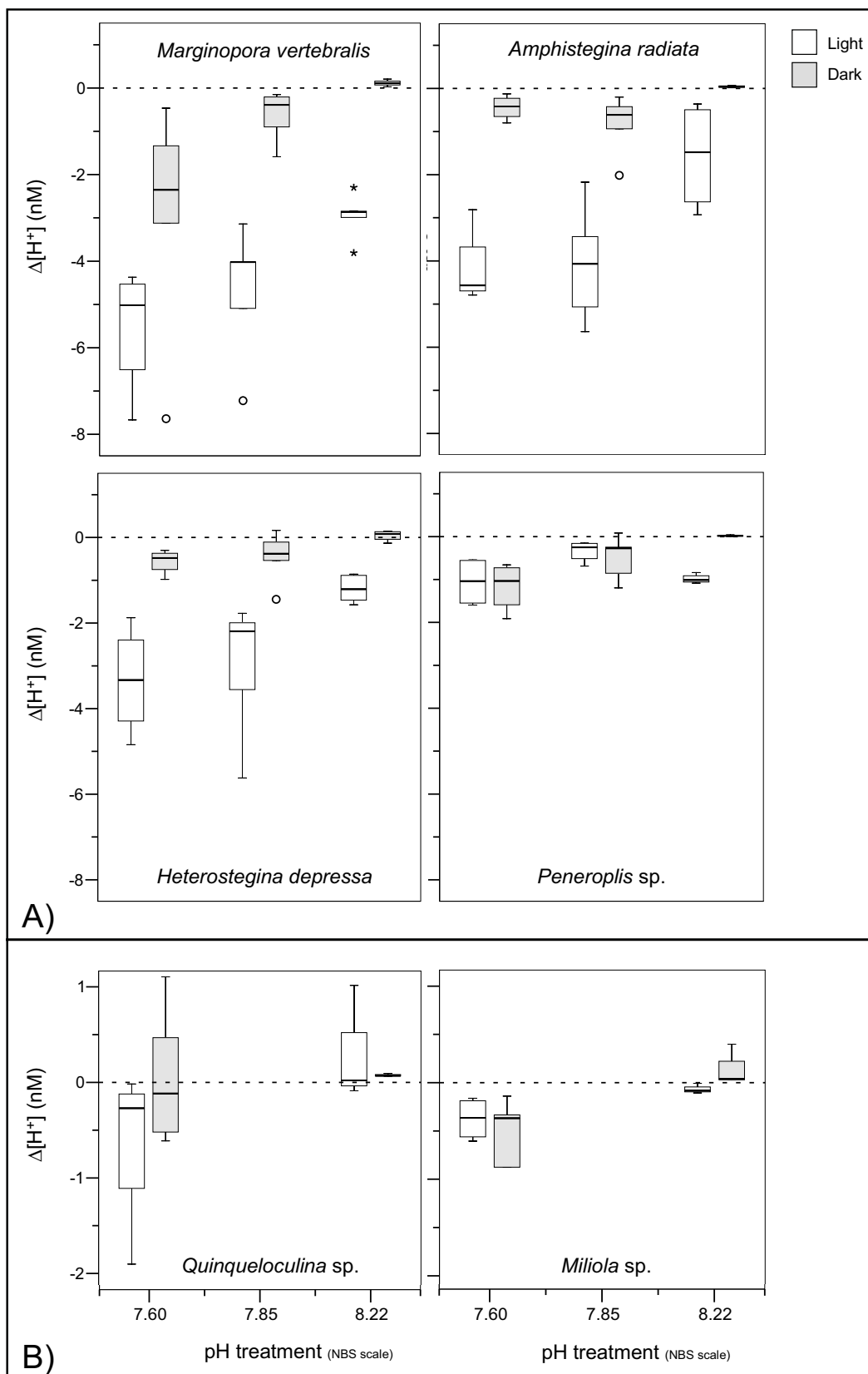
Figure 6: Box-plots representing the 25th, 50th and 75th percentiles of ΔH+, calculated from profiles measured during the *pCO₂* treatment incubation, at light (30 μmol photons m-2 s-1) and dark conditions for individual species. Note the different scales between A) photosymbiotic and B) symbiont-free species. Outliers (> 1.5 interquartile range) and extreme values (> 3 times interquartile range) are indicated by (O) and (*) respectively.

Ratios of mean $\Delta O_2 / \Delta H^+$ and mean $\Delta O_2 / \Delta pH$ across pCO_2 treatments

Mean ΔO_2 (i.e. netPS or respiration), ΔH^+ and consequently ΔpH were both quite variable across profiles within and across individuals (Figure 7). Yet, there was a significant linear correlation between mean ΔO_2 and mean ΔH^+ ($R^2 \geq 0.63$, $p_{tm} < 0.0166$) or ΔpH ($R^2 \geq 0.84$, $p_{tm} < 0.0061$) per individual for all photosymbiotic species, but not in symbiont-free species (Table 3, SOM Table 1). The slopes of the $\Delta O_2 / \Delta pH$ correlations significantly decreased at increased pCO_2, except in *Amphistegina* (Figure 7, Table 3). In symbiont-free species, mean ΔO_2 did not strongly correlate with ΔH^+ ($R^2 \leq 0.76$, $p_{tm} > 0.1006$) and ΔpH ($R^2 \leq 0.67$, $p_{tm} > 0.1780$) and slopes were inconsistent between the two pCO_2 treatments. Interestingly, ΔpH of all linear regressions at $\Delta O_2 = 0$ was positive and similar (range: 0.065 – 0.005), beside *Quinqueloculina* at pH 8.22, indicating that the foraminiferal surface has a slightly increased pH when the net O_2 flux equals zero.

Discussion

ΔO_2, ΔH^+, ΔpH and ΔCa^{2+} dynamics

In light, net O_2 evolution (photosynthesis) of photosymbiotic species remained relatively unaffected by the pCO_2 treatments, while H^+ decreased within the DBL with increasing pCO_2 (Figure 4, 6). Rates of net photosynthesis of marine phototrophs primarily depend on temperature, nutrients and light availability, as well as the efficiency of the individual carbonate concentration mechanisms (CCMs, [38-40]). Except for bleached individuals, ΔO_2 did not show a significant pCO_2 treatment effect in any species (Table 2, Figure 4). Since light levels were saturated and nutrient concentrations and temperature remained constant throughout each treatment, this may indicate either that the photosynthesis of photosymbiotic foraminifera was CO_2 saturated already at ambient pCO_2 concentrations, or that a down-regulation of DIC uptake occurred at increased pCO_2. This notion is in agreement with previous studies on diatoms [41,42] and *Symbiodinium* sp., both in culture and *in hospite* of corals [43,44] and foraminifera [45], displaying a down-regulation of CCMs and only slight effects of increased DIC on net O_2 evolution. Since there is no indication that the photosynthetic quotient (O_2 / CO_2, [46]) of the holobiont was altered at increased pCO_2, CO_2 uptake should have been constant. Increases of pCO_2 on the other hand, cause a decrease of the Revelle factor or the H^+-buffering-capacity of seawater [47]. As carbonate ion concentrations decreased < 1/3 from control to the highest pCO_2 treatment (Table 1), the H^+-buffering-capacity was significantly reduced.
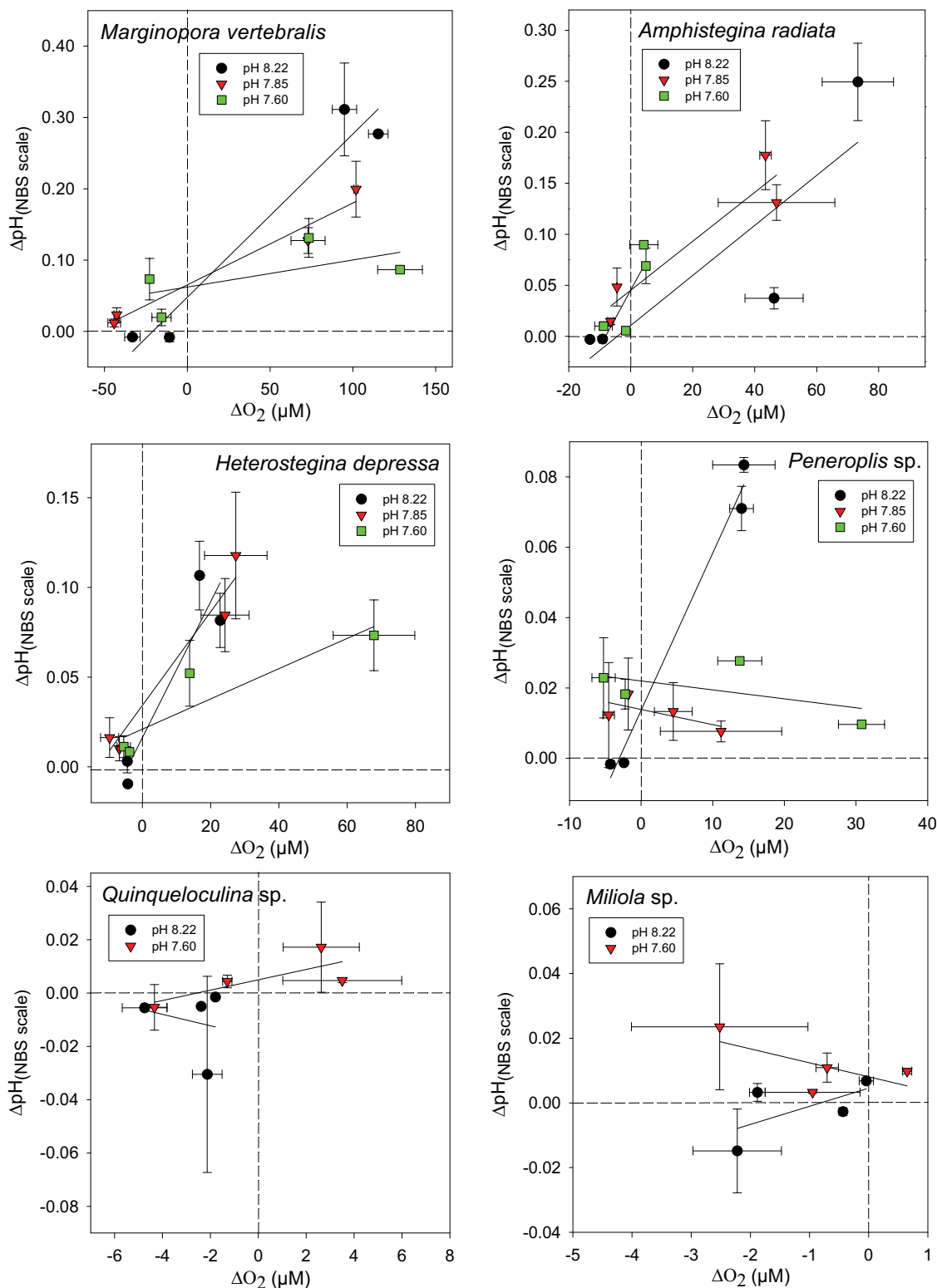
Figure 7: Relationship between mean ΔpH and ΔO$_2$ at different pH treatment groups for light (30 µmol photons m^{-2} s^{-1}) and dark conditions. Each point represents an individual foraminiferal test (mean ± SE, n = 2 – 4). Solid lines indicate linear correlations for the different pH treatment groups, dashed lines indicate the respective ΔO$_2$ and ΔpH zero-lines.

Table 3: Relationships between ΔO_2 and ΔpH per individual within each species at different pCO_2 treatments (Figure 7). Linear-model results, with significant effects at the 5 % level are indicated in bold.

	Estimate	SE	t	p	R^2	p_{tm}
Marginopora vertebralis						
Intercept	0.2570	0.3717	0.6910	0.5089	0.93	**7.20e^{-05}**
ΔO_2	-0.0231	0.0049	-4.720	**0.0015**		
pCO_2 treatment	-0.0251	0.0471	-0.5330	0.6082		
ΔO_2 : pCO_2 treatment	0.0031	0.0006	4.983	**0.0011**		
Amphistegina radiata						
Intercept	0.4521	0.4444	1.018	0.3390	0.77	**0.0061**
ΔO_2	0.0104	0.0190	0.5470	0.6000		
pCO_2 treatment	-0.0533	0.0566	-0.9420	0.3740		
ΔO_2 : pCO_2 treatment	-0.0010	0.0024	-0.4140	0.6900		
Heterostegina depressa						
Intercept	0.1522	0.2192	0.6940	0.5073	0.84	**0.0015**
ΔO_2	-0.0398	0.0109	-3.647	**0.0065**		
pCO_2 treatment	-0.0162	0.0278	-0.5840	0.5753		
ΔO_2 : pCO_2 treatment	0.0053	0.0014	3.786	**0.0053**		
Peneroplis **sp.**						
Intercept	0.0954	0.1233	0.7740	0.4614	0.86	**0.0009**
ΔO_2	-0.0559	0.0097	-5.742	**0.0004**		
pCO_2 treatment	-0.0101	0.0156	-0.6470	0.5360		
ΔO_2 : pCO_2 treatment	0.0073	0.0013	5.844	**0.0004**		
Quinqueloculina **sp.**						
Intercept	0.2691	0.2131	1.263	0.2750	0.52	0.3522
ΔO_2	0.0519	0.0706	0.7360	0.5030		
pCO_2 treatment	-0.0348	0.0277	-1.253	0.2780		
ΔO_2 : pCO_2 treatment	-0.0066	0.0092	-0.7160	0.5140		
Miliola **sp.**						
Intercept	0.0515	0.1084	0.4750	0.6590	0.67	0.1780
ΔO_2	-0.1260	0.0746	-1.688	0.1670		
pCO_2 treatment	-0.0057	0.0138	-0.4140	0.7000		
ΔO_2 : pCO_2 treatment	0.0160	0.0095	1.685	0.1670		

R^2 constitutes the multiple R^2 explaining total variance of the overall model.
p_{tm} depicts the significance of the total model.

The reduced H^+-buffering-capacity will, in return, cause stronger H^+-gradients of photosynthesis and respiration at constant CO_2 production- / consumption-rates at elevated pCO_2, as indicated by the results (Figure 6; see also [17]). Changes of ΔpH on the other hand, decreased at elevated pCO_2 concentrations (SOM Figure 2), due to their logarithmic scaling. This is also expressed by the linear regressions analyses, displaying significant interactions of main effects mainly in ΔO_2 / ΔpH and not in ΔO_2 / ΔH^+ (Table 3, SOM Table 1). It can

therefore be deduced that scaling differences outweighed changes in the buffering capacity of the seawater, when comparing ΔH^+ and ΔpH dynamics across different pCO_2.

The decreases of ΔO_2, observed between pH 8.22 and the lowered pH conditions in *Amphistegina* at 7.85 and 7.60 and *Heterostegina* at 7.60 (Figure 4), are most likely the cause of increased symbiont loss (i.e. bleaching) at lowered pH conditions (SOM Figure 4, 5). Additionally, bleaching in *Amphistegina* led to severe symbiont clumping and consequently increased heterogeneity of ΔO_2 and ΔpH across the shell. This might have led to an overestimation of ΔpH and ΔH^+ in light, in respect to ΔO_2, by profiling areas of high symbiont densities with pH sensor and areas of low symbiont density with O_2 sensors (Figure 5, 6). This might explain why $\Delta O_2 / \Delta pH$ at increased pCO_2 did not decrease significantly in *Amphistegina,* compared to all other photosymbiotic species (Figure 7, Table 3).

In dark, respiratory changes at pH 8.22 of $\Delta O_2, \Delta pH$ and consequently ΔH^+ at pH 8.22 were minor (Figure 5, 6). This is in agreement with previous microsensor measurements on foraminifera and diatoms [13,14,48], indicating that net respiratory O_2 fluxes are generally very low in these protists.

Interestingly, microenvironmental H^+ concentrations of all species were slightly decreased in darkness, compared to the bulk seawater at elevated pCO_2 (Figure 6). It can only be speculated about the cause. One possibility could be the dissolution of the calcite shell under lowered pH conditions in darkness, causing a local increase in pH [47]. However, this is unlikely since Ω_{Ca} was super-saturated at even the highest pCO_2 (Table 1), indicating no net calcite dissolution. Another possibility could be an increased uptake of CO_2 by the cell in darkness for calcification and / or internal storage. Yet, uptake of CO_2 into an intracellular DIC pool has only been shown in light for *Amphistegina lobifera* and is believed not to exist in imperforate species [49,50]. This would imply that storing DIC in intracellular DIC pools for calcification might be a wider strategy in foraminifera. A third explanation could be that foraminifera actively up-regulate their microenvironmental pH in darkness, via active proton pumping or antiporter exchange [51,52] into the cell, to compensate for decreased seawater pH and to maintain pH homeostasis for vital cellular functions.

Mean ΔCa^{2+} over the shell surface was very low, but single profiles displayed strong gradients (SOM Figure 1). Calcification in foraminifera, i.e. chamber formation, is a sensitive process which is very prone to mechanical disturbances [51,53,54]. Due to the experimental handling it can be excluded that individuals were calcifying or preparing for chamber formation > 2 h before and after the measurements. Increased Ca^{2+} uptake due to calcification was therefore not expected. The measured high variability and averaged low fluxes of ΔCa^{2+}

over the shell surface are in accordance with previous microsensor measurements on tropical (*Marginopora vertebralis*, *Amphistegina lobifera*, [14]), temperate (*Ammonia* sp., [51]) and planktonic (*Orbulina universa*, [15]) specimens. This indicates that Ca^{2+} exchange varies over time and is not evenly distributed over the shell surface for most foraminifera, but very localized. As Ca^{2+} is an important cellular ionic regulator and cytotoxic at increased cellular concentrations [55], its exchange via Ca^{2+} channels in the protoplasmic membrane must be highly regulated. Distribution of Ca^{2+} channels and Ca^{2+} fluxes over the foraminiferal surface are most likely patchy. Ca^{2+} gradients would therefore only affect a very small percentage of the total foraminiferal surface area, which would lead to the generally low total Ca^{2+} fluxes, but high variability in different profiles (SOM Figure 1).

Characterizing the foraminiferal microenvironment

O_2 and pH DBL dynamics of photosymbiotic foraminifera and other photosynthetic calcifiers correlate in response to illumination changes, with pH dynamics exhibiting a temporal time lag following O_2 dynamics [12,15,16,18].

The extent to which surface O_2 and pH on the organism's surface deviate from the bulk seawater depends on multiple factors, such as the photosynthetic activity of the organism, surrounding seawater flow, seawater H^+-buffering capacity, diffusivity / permeability of CO_2 from its source – spatial configuration of symbiont and host, diffusional transport constrains (1-3D) and the 3D surface structure of the location [14,16,20,47,56]. Since carbonate chemistry remained constant throughout the treatments (Table 1), most prominent factors during the experiment influencing DBL dynamics, included diffusional transport constrains to and from the symbionts, micro-flow surface dynamics and location specific rates of net photosynthesis and respiration. This is illustrated by the spatial extent of the DBLs (Figure 1, 2). The thickness of the ΔO_2 DBL clearly decreases along middle ridges of individuals, where laminar flow velocity was highest [57,58] and underlying photosynthesis was lower, due to decreased symbiont density in that region, compared to lateral symbiont-rich parts (Figure 1, SOM Figure 3). *Marginopora* specimens showed the steepest O_2 and pH gradients, without enlarged DBL thickness (i.e. net O_2 fluxes), indicating overall increased photosynthesis compared to all other species (Figure 1, 4, 5). Yet, ventral sides of *Marginopora* specimens locked tightly on to the inert surface of the flow chamber, thereby creating a one-dimensional diffusional barrier. The strong O_2 and pH microgradients of *Marginopora* can therefore not solely be attributed to increased photosynthesis but emerges as a combination of the

underlying photosynthesis, flat surface structure (and thereby almost laminar horizontal overlying flow), as well as one-dimensional diffusional resistance.

Variability of microsensor measurements

Measurement variability was high, but much higher between, than within individuals (Figure 4, 5, 6, 7), allowing for temporal replication of microsensor measurements. Variability was not unexpected due to the high spatial resolution of microsensor measurements (reviewed in [23]). Also, diffusive O_2 fluxes and pH dynamics across the surface of photosynthetic organisms are typically rather heterogenous (Figure 1, [14,18-20,58]). Another source of variability is due to the fact that some foraminiferal species, including *Marginopora vertebralis* and *Heterostegina depressa*, actively transport their symbionts within their cell bodies and individual chamberlets [59,60], resulting in higher variation of ΔO_2 (Figure 4) and consequently ΔpH and ΔH^+ over time for a specific spot on their shell surface. Spatial variability of ΔO_2 and consequently ΔpH (and their means), measured within and among the individuals, was therefore expected. Yet, spatial heterogeneity within individuals (Figure 1) was not represented in the sampling, since measurement positions were not significantly different. Also ΔO_2, measured before and during the pH 8.22 treatment under equal conditions (Figure 4) within the same individuals, remained relatively constant, confirming that the spatial placement of microelectrode measurements could be replicated.

Mixed responses of ocean acidification experiments

Several studies have reported contrary responses of increased *pCO₂* on both photosynthesis and calcification [10,11,61-63], even within phyla (reviewed in Doney et al. [1]). Possible causes for such variability are diverse, potentially including differences in calcifying- / carbonate concentration mechanisms and their coupling, tolerance levels, adaptation mechanisms, but also differences in the experimental designs and setups. Consequently, a comparison among ocean acidification studies, even within phyla, is difficult. Especially flow, as an important experimental parameter influencing the surface pH of organisms, has not been considered in many ocean acidification experiments. Yet, flow changes are well known to severely impact microenvironmental pH levels of photosymbiotic foraminifera (Figure 2, [14]) and other phototrophs in light [18,19,56]. The changes in surface pH are especially severe within static culture experiments, where ΔpH can change up to > 1 unit (Figure 2, [14,64]). Zero-flow conditions for ocean acidification studies should therefore

be avoided, as they are ecologically unrealistic and also confuse the carbonate chemistry of the intended pCO_2 perturbation, causing unrealistically high / low microenvironmental pH conditions in light / dark, despite increased DIC levels.

Susceptibility of foraminifera to ocean acidification

The presented results indicate that net photosynthesis will remain relatively constant at elevated pCO_2. Consequently, decreases in seawater pH will most likely not be 'buffered' at the surface of photosymbiotic foraminifera in daylight, due to the photosynthetic DIC uptake from their microenvironments. The difference between foraminiferal surface pH and bulk seawater pH in daylight (i.e. the 'pH buffering capacity'), will most likely be even more reduced, due to increased seawater acidity. Also, the fact that two photosymbiotic species showed signs of bleaching at elevated pCO_2 indicates that photosymbiotic benthic foraminifera will be quite susceptible to ocean acidification. These results are thus is in accordance with previous field studies investigating foraminiferal assemblages at natural CO_2 seeps [65,66], the latter reporting almost complete absence of larger benthic photosymbiotic foraminifera at high pCO_2 sites, compared to low pCO_2 sites.

Acknowledgments

References:

1. Doney SC, Fabry VJ, Feely RA, Kleypas JA (2009) Ocean acidification: The other CO_2 problem. Annual Review of Marine Science 1: 169-192.
2. IPCC Climate Change (2007) Synthesis report. In: Pachauri, RK, Reisinger A. editors. Cambridge Univ. Press, 2007. p. 73.
3. Feely RA, Doney SC, Cooley SR, (2009) Ocean acidification: Present conditions and future changes in a high-CO_2 world. Oceanography 22(4): 36–47.
4. Hoenisch BR., Hemming NG, Archer D, Siddall M, McManus JF (2009) Atmospheric carbon dioxide concentration across the Mid-Pleistocene transition. Science 324(5934): 1551-1554.
5. Doney SC, Schimel DS (2007) Carbon and climate system coupling on timescales from the Precambrian to the Anthropocene. Annual Review of Environment and Resources 32: 31-66.
6. Sabine CL, Feely RA, Gruber N, Key RM, Lee K, et al. (2004) The oceanic sink for anthropogenic CO_2. Science 305(5682): 367-371.
7. Gattuso JP, Buddemeier RW (2000) Ocean biogeochemistry - Calcification and CO_2. Nature 407(6802): 311-313.
8. Riebesell U, Schulz KG, Bellerby RGJ, Botros M, Fritsche P, et al. (2007) Enhanced biological carbon consumption in a high CO_2 ocean. Nature 450(7169): 545-548.
9. Ridgwell A, Schmidt DN, Turley C, Brownlee C, Maldonado MT, et al. (2009) From laboratory manipulations to Earth system models: scaling calcification impacts of ocean acidification. Biogeosciences 6(11): 2611-2623.
10. Fabry VJ, Seibel BA, Feely RA, Orr JC (2008) Impacts of ocean acidification on marine fauna and ecosystem processes. Ices Journal of Marine Science 65(3): 414-432.
11. Ries JB, Cohen AL, McCorkle DC (2009) Marine calcifiers exhibit mixed responses to CO_2-induced ocean acidification. Geology 37(12): 1131-1134.
12. De Beer D, Larkum AWD (2001) Photosynthesis and calcification in the calcifying algae *Halimeda discoidea* studied with microsensors. Plant Cell and Environment 24(11): 1209-1217.
13. Rink S, Kuehl M, Bijma J, Spero HJ (1998) Microsensor studies of photosynthesis and respiration in the symbiotic foraminifer *Orbulina universa*. Marine Biology 131(4): 583-595.
14. Koehler-Rink S, Kuehl M (2000) Microsensor studies of photosynthesis and respiration in larger symbiotic foraminifera. I The physico-chemical microenvironment of *Marginopora vertebralis*, *Amphistegina lobifera* and *Amphisorus hemprichii*. Marine Biology 137(3): 473-486.
15. Koehler-Rink S, Kuehl M (2005) The chemical microenvironment of the symbiotic planktonic foraminifer *Orbulina universa*. Marine Biology Research 1(1): 1745-1000(print) |1745-1019(electronic).
16. Wolf-Gladrow DA, Bijma J, Zeebe RE, 1999. Model simulation of the carbonate chemistry in the microenvironment of symbiont bearing foraminifera. Marine Chemistry 64(3): 181-198.
17. Flynn KJ, Blackford JC, Baird ME, Raven JA, Clark DR, et al. (2012) Changes in pH at the exterior surface of plankton with ocean acidification. Nature Climate Change: doi:10.1038/nclimate1489.
18. Kuehl M, Cohen Y, Dalsgaard T, Jorgensen BB, Revsbech NP (1995) Microenvironment and photosynthesis of zooxanthellae in scleractinian corals studied with microsensors for O_2, pH and light. Marine Ecology Progress Series 117(1-3): 159-172.
19. Shashar N, Cohen Y, Loya Y (1993) Extreme diel fluctuations of oxygen in diffusive boundary-layers surrounding stony corals. Biological Bulletin 185(3): 455-461.

20. Jorgensen BB, Revsbech NP (1985) Diffusive boundary-layers and the oxygen-uptake of sediments and detritus. Limnology and Oceanography 30(1): 111-122.
21. Uthicke S, Nobes K (2008) Benthic Foraminifera as ecological indicators for water quality on the Great Barrier Reef. Estuarine, Coastal and Shelf Science 78(4): 763-773.
22. Nobes K, Uthicke S (2008) Benthic foraminifera of the Great Barrier Reef: A guide to species potentially useful as Water Quality Indicators. Research Report.
23. Revsbech NP, Jorgensen BB (1986) Microelectrodes - Their use in microbial ecology. Advances in Microbial Ecology 9: 293-352.
24. De Beer D (2000) Potentiometric microsensors for *in situ* measurements in aquatic environments. In: Buffle J, Horvai G. editors. In situ monitoring of aquatic systems: chemical analysis and speciation. Wiley & Sons, London, pp. 161-194.
25. De Beer D, Kühl M, Stambler N, Vaki L (2000) A microsensor study of light enhanced Ca^{2+} uptake and photosynthesis in the reef-building hermatypic coral *Favia* sp. Mar. Ecol. Prog.Ser. 194: 75-85.
26. Ammann D, Bührer T, Schefer U, Müller M, Simon W (1987) Intracellular neutral carrier based Ca^{2+} microelectrode with sub-nanomolar detection limit. Pflugers Arch. 409: 223-228.
27. Polerecky L, Bachar A, Schoon R, Grinstein M, Jorgensen BB, et al. (2007) Contribution of *Chloroflexus* respiration to oxygen cycling in a hypersaline microbial mat from Lake Chiprana, Spain. Environmental Microbiology 9(8): 2007-2024.
28. Uthicke S, Vogel N, Doyle J, Schmidt C, Humphrey C (2011) Interactive effects of climate change and eutrophication on the dinoflagellate-bearing benthic foraminifer *Marginopora vertebralis*. Coral Reefs: 1-14.
29. Ziegler M, Uthicke S (2011) Photosynthetic plasticity of endosymbionts in larger benthic coral reef Foraminifera. Journal of Experimental Marine Biology and Ecology 407(1): 70-80.
30. Hall OJ, Aller RC (1992) Rapid, small-volume, flow injection analysis for $\sum CO_2$ and NH_4^+ in marine and freshwaters. Limnol. Oceanogr. 37(5): 1113-1119.
31. Ryle VD, Mueller HR, Gentien P (1981) Automated analysis of nutrients in tropical seawaters. Australian Institute of Marine Science Oceanography Series AIMS-OS-82-2(3): 24.
32. Dickson AG, Sabine CL, Christian JRE (2007) Guide to best practices for ocean CO_2 measurements. PICES Special Publication, 3 2007. 191 p.
33. Gran G (1952) Determination of the equivalence point in potentiometric titrations of seawater with hydrochloric acid. Oceanologica Acta 5: 209-218.
34. Pierrot DE, Lewis E, Wallace DWR (2006) MS Exel program developed for CO_2 system calculations, ORNL/CDIAC-105a Carbon Dioxide Information Analysis Centre. Oak Ridge National Laboratory, US Department of Energy.
35. Millero FJ, Graham TB, Huang F, Bustos-Serrano HC, Pierrot D (2006) Dissociation constants of carbonic acid in seawater as a function of salinity and temperature. Marine Chemistry 100(12): 80-94.
36. Dickson AG (1990) Standard potential of the reaction: $AgCl(s) + 12H_2(g) = Ag(s) + HCl(aq)$, and the standard acidity constant of the ion $HSO4^-$ in synthetic sea water from 273.15 to 318.15 K. The Journal of Chemical Thermodynamics 22(2): 113-127.
37. R_Development_Core_Team R: A language and environment for statistical computing (2012); available at http://www.R-project.org.
38. Falkowski PG, Raven JA (1997) Aquatic Photosynthesis, Blackwell, Oxford. 500 p.
39. Raven JA, Callow JA (1997) Inorganic carbon acquisition by marine autotrophs, Advances in Botanical Research. Academic Press. pp. 85-209.

40. Amoroso G, Sueltemeyer D, Thyssen C, Fock HP (1998) Uptake of HCO_3^- and CO_2 in cells and chloroplasts from the microalgae *Chlamydomonas reinhardtii* and *Dunaliella tertiolecta*. Plant Physiology 116(1): 193-201.

41. Burkhardt S, Amoroso G, Riebesell U, Sültemeyer D (2001) CO_2 and HCO_3^- uptake in marine diatoms acclimated to different CO_2 concentrations. Limnol Oceanogr 46(6): 1378-1391.

42. Rost B, Riebesell U, Burkhardt S, Sültemeyer D (2003) Carbon acquisition of bloom-forming marine phytoplankton. Limnology and oceanography 48: 55-67.

43. Buxton L, Badger M, Ralph P (2009) Effects of ,oderate heat stress and dissolved inorganic carbon concentration on photosynthesis and respiration of *Symbiodinium Sp* (Dinophyceae) in culture and in symbiosis. J. Phycol. 45(2): 357-365.

44. Goiran C, Al-Moghrabi S, Allemand D, Jaubert J (1996) Inorganic carbon uptake for photosynthesis by the symbiotic coral/dinoflagellate association. I. Photosynthetic performances of symbionts and dependence on seawater. J. Exp. Mar. Biol. Ecol. 199(2): 207-225.

45. Vogel N, Uthicke S (2012) Calcification and photobiology in symbiont-bearing benthic foraminifera and responses to a high CO_2 environment. Journal of Experimental Marine Biology and Ecology (in press).

46. Williams PJI, Robertson JE (1991) Overall planktonic oxygen and carbon dioxide metabolisms: the problem of reconciling observations and calculations of photosynthetic quotients. Journal of Plankton Research 13(supp1): 153-169.

47. Zeebe RE, Wolf-Gladrow D (2001) CO_2 in Seawater: equilibrium, kinetics and isotopes. Elsevier, Amsterdam. 346 p.

48. Kuehn S, Raven J (2008) Photosynthetic oscillation in individual cells of the marine diatom *Coscinodiscus wailesii* (Bacillariophyceae) revealed by microsensor measurements. Photosynthesis Research 95(1): 37-44.

49. ter Kuile B, Erez J (1987) Uptake of inorganic carbon and intrernal carbon cycling in symbiont bearing bentonic foraminifera. Marine Biology 94: 499-510.

50. ter Kuile B, Erez J (1988) The size and function of the internal inorganic carbon pool of the foraminifer *Amphistegina lobifera*. Marine Biology 99(4): 481-487.

51. Glas MS, Langer G, Keul N (2012) Calcification acidifies the microenvironment of a benthic foraminifer (*Ammonia* sp.). Journal of Experimental Marine Biology and Ecology (in press).

52. Taylor AR, Chrachri A, Wheeler G, Goddard H, Brownlee C (2011) A voltage-gated H^+ channel underlying pH homeostasis in calcifying coccolithophores. PLoS Biol 9(6): e1001085.

53. Angell RW (1967) The process of chamber formation in the foraminifer *Rosalina floridana* (Cushman). Journal of Eukaryotic Microbiology 14(4): 566-574.

54. Angell RW (1980) Test Morphogenesis Chamber Formation in the Foraminifer *Spiroloculina-Hyalina*. Journal of Foraminiferal Research 10(2): 89-101.

55. Alberts B, Johnson A, Lewis J, Raff M, Roberts K et al. (2008) Molecular biology of the cell. Mechanisms of cellular communication. 5th ed. Garland Science Taylor & Francis Group, New York. pp. 879 – 965.

56. Jorgensen BB, Des Marais D (1990) The diffusive boundary layer of sediments: oxygen microgradients over a microbial mat. Limnol. Oceanogr. 35: 1343-1355.

57. Glud R, Ramsing NB, Gundersen JK, Klimant I (1996) Planar optodes, a new tool for finescale measurements of two dimensional O_2 distribution in benthic communities. Mar. Ecol. Prog. Ser. 140: 217-226.

58. Gundersen JK, Jorgensen BB (1990) Microstructure of diffusive boundary layers and the oxygen uptake of the sea floor. Nature 345: 604-607.

59. Ross CA (1972) Biology and ecology of *Marginopora vertebralis* (Foraminiferida), Great Barrier Reef. Journal of Eukaryotic Microbiology 19(1): 181-192.

60. Roettger R (1974) Larger foraminifera: Reproduction and early stages of development in *Heterostegina depressa*. Marine Biology 26(1): 5-12.

61. Bowes G (1993) Facing the inevitable: plants and increasing Atmospheric CO_2. Annual Review of Plant Physiology and Plant Molecular Biology 44(1): 309-332.

62. Iglesias-Rodriguez MD, Halloran PR, Rickaby REM, Hall IR, Colmenero-Hidalgo E, et al. (2008). Phytoplankton calcification in a high-CO_2 world. Science 320(5874): 336-340.

63. Uthicke S, Fabricius KE (2012) Productivity gains do not compensate for reduced calcification under near-future ocean acidification in the photosynthetic benthic foraminifer species *Marginopora vertebralis*. Global Change Biology doi: 10.1111/j.1365-2486.2012.02715.x.

64. Kuehn S, Koehler-Rink S (2008) pH effect on the susceptibility to parasitoid infection in the marine diatom *Coscinodiscus* spp. (Bacillariophyceae). Marine Biology 154(1): 109-116.

65. Dias BB, Hart MB, Smart CW, Hall-Spencer JM (2010) Modern seawater acidification: the response of foraminifera to high-CO_2 conditions in the Mediterranean Sea. Journal of the Geological Society 167(5): 843-846.

66. Fabricius KE, Langdon C, Uthicke S, Humphrey C, Noonan S, et al. (2011) Losers and winners in coral reefs acclimatized to elevated carbon dioxide concentrations. Nature Clim. Change 1(3): 165-169.

Supplementary online material
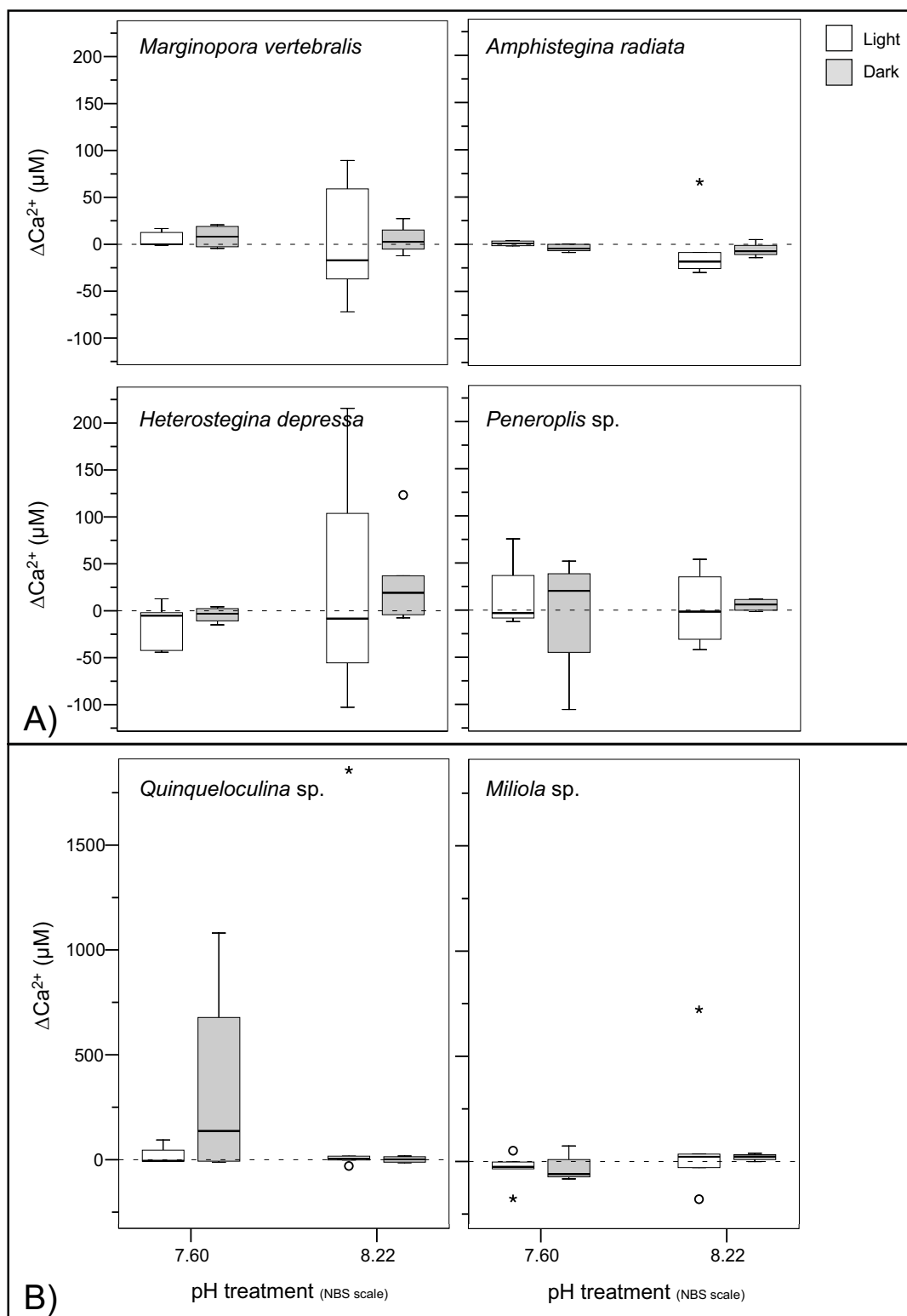
SOM Figure 1: Box-plots representing the 25th, 50th and 75th percentiles of ΔCa^{2+}, calculated from profiles measured during the pH treatment incubation, at light (30 µmol photons m[-2] s^{-1}) and dark conditions for individual species. Note the different scales between A) photosymbiotic and B) symbiont-free species. Outliers (> 1.5 interquartile range) and extreme values (> 3 times interquartile range) are indicated by (O) and (*) respectively.
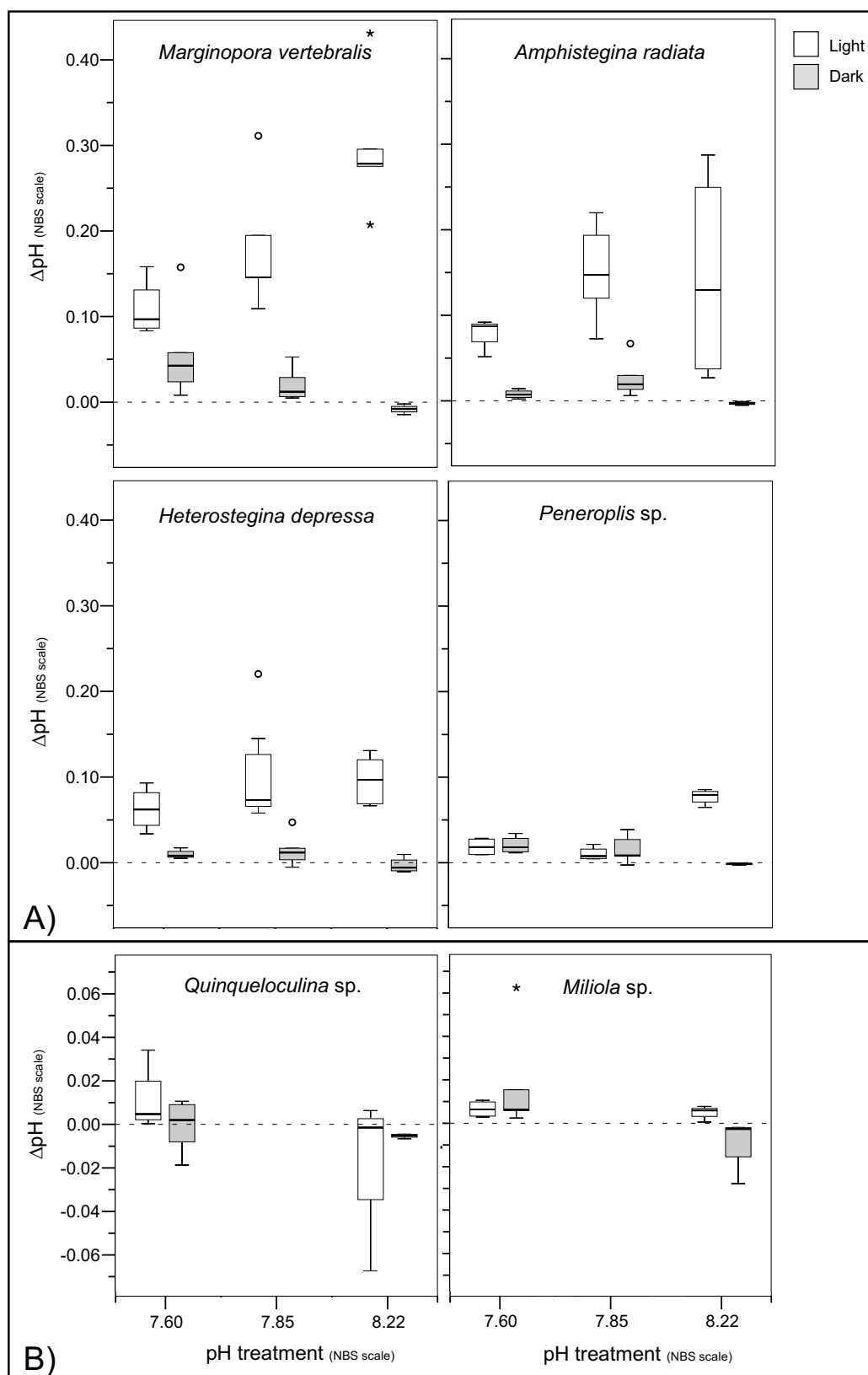
SOM Figure 2: Box-plots representing the 25ᵗʰ, 50ᵗʰ and 75ᵗʰ percentiles of ΔpH, calculated from profiles measured during the *pCO₂* treatment incubation, at light (30 µmol photons m⁻² s⁻¹) and dark conditions for individual species. Note the different scales between A) photosymbiotic and B) symbiont-free species. Outliers (> 1.5 interquartile range) and extreme values (> 3 times interquartile range) are indicated by (O) and (*) respectively.
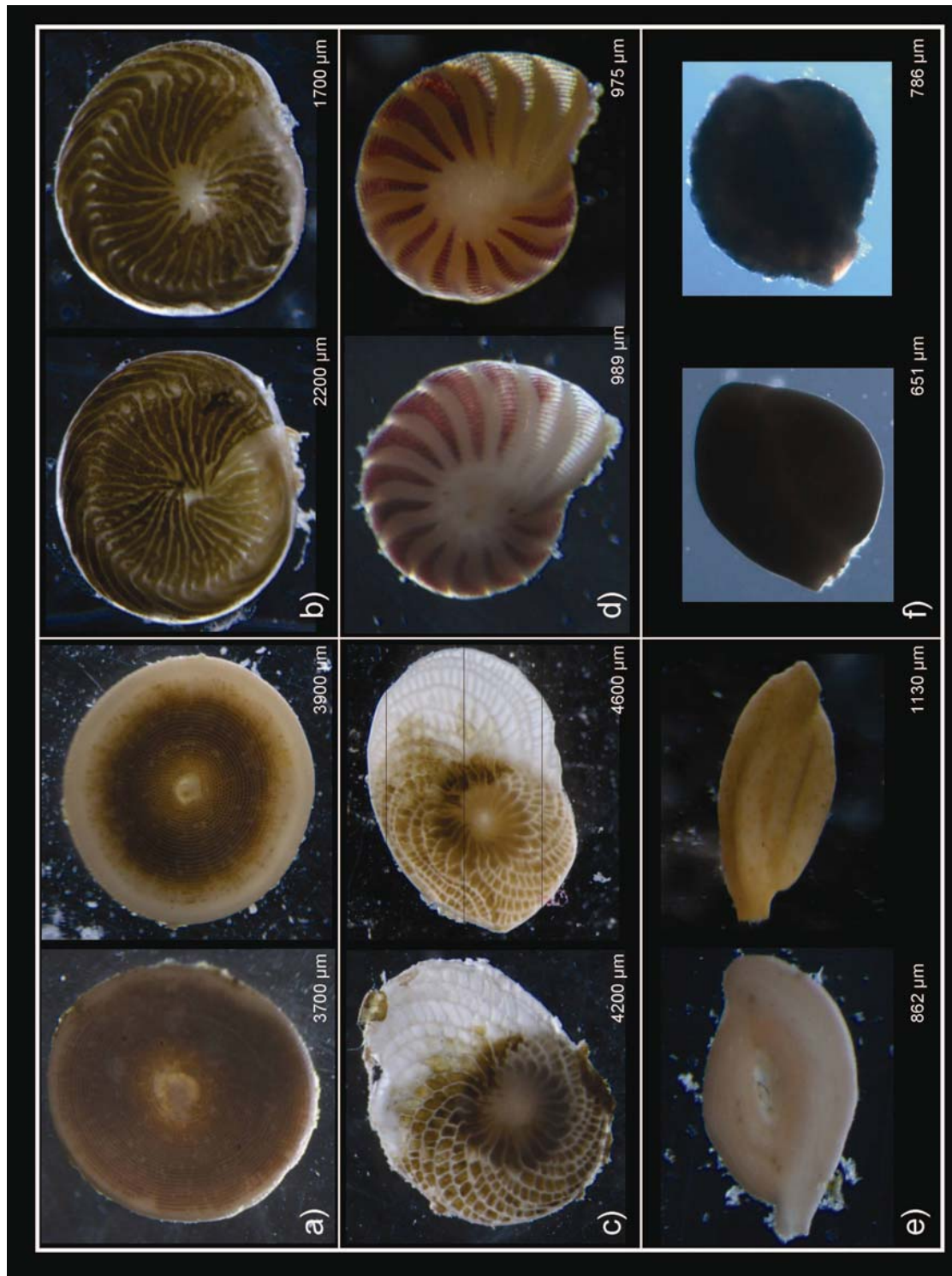
SOM Figure 3: Close up of the six foraminiferal species, photographed via dissecting microscope (a-e) and back-light microscope (f). Images were taken after control (pH 8.22) treatment incubations. a) *Marginopora vertebralis*, **b)** *Amphistegina radiata*, **c)** *Heterostegina depressa*, **d)** *Peneroplis* sp., **e)** *Quinqueloculina* sp. **and f)** *Miliola* sp. **individuals. Sizes are stated as largest possible diameter of individuals.**
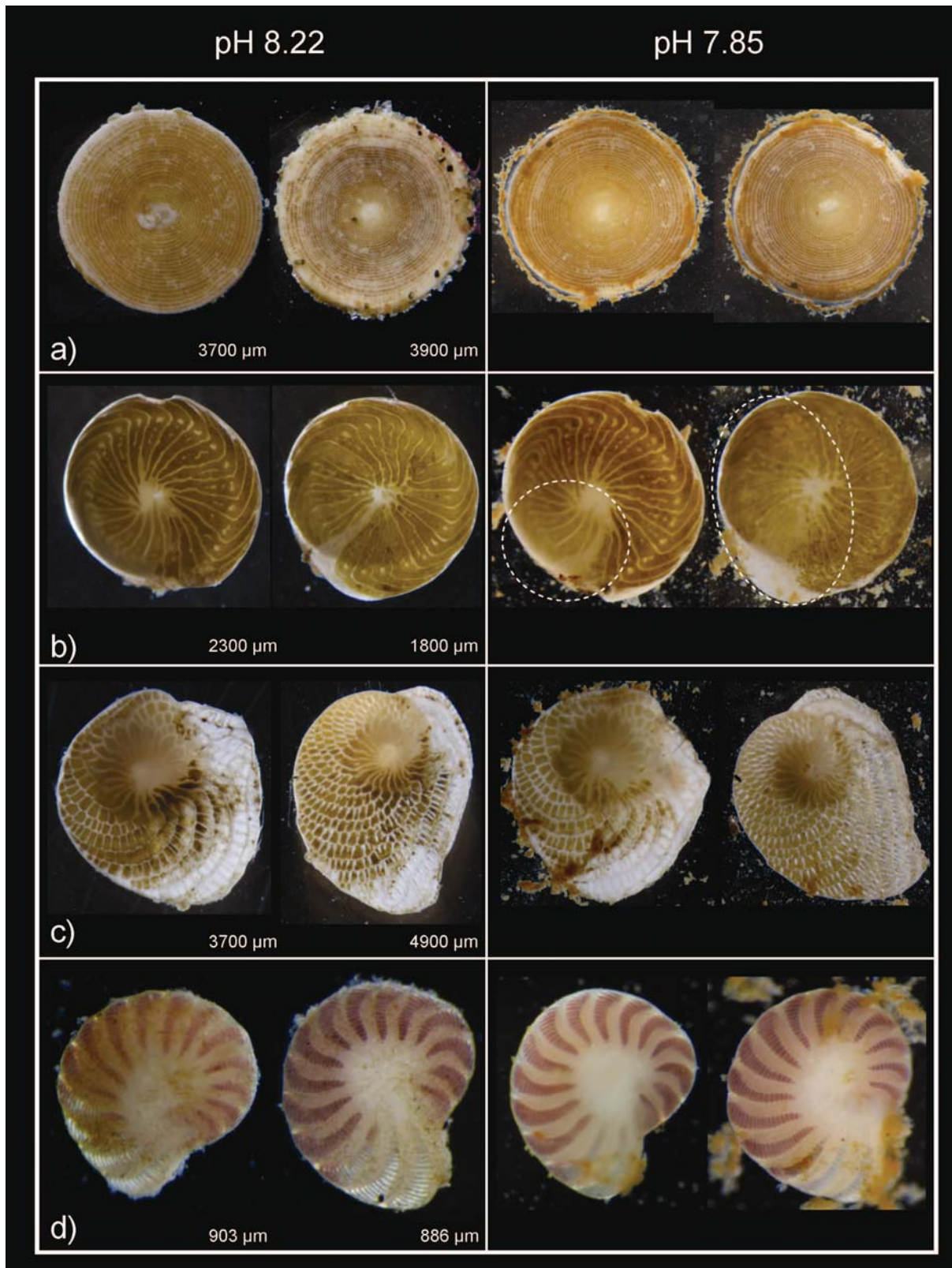
SOM Figure 4: Close up dissecting microscope images, taken before (pH 8.22) and after pH 7.85 treatment incubation. a) *Marginopora vertebralis*, **b)** *Amphistegina radiata*, **c)** *Heterostegina depressa*, **d)** *Peneroplis* **sp., individuals. Sizes are given as largest possible diameter of individuals. In** *Amphistegina*, **areas of bleaching are indicated by white dashed circles.**
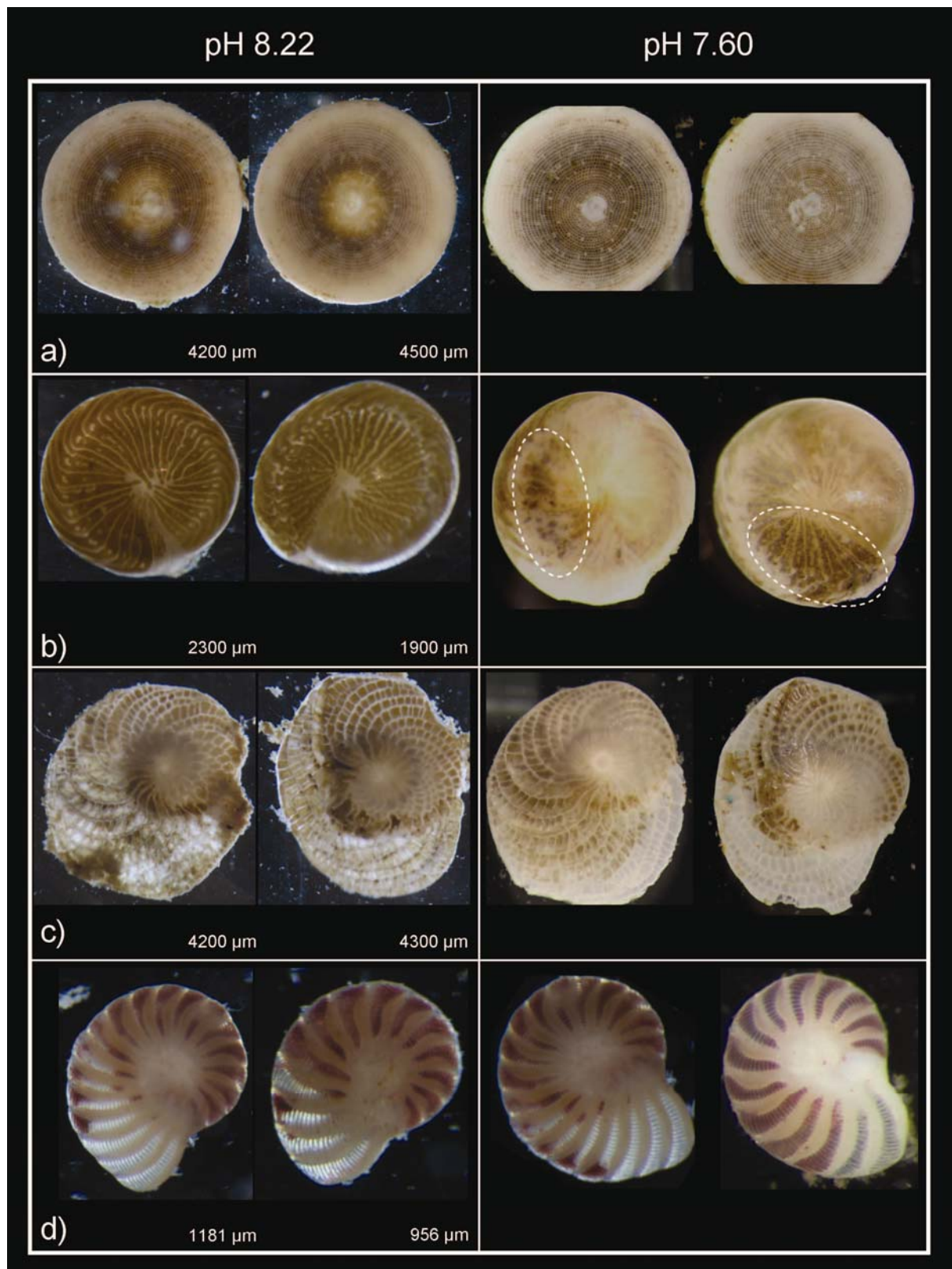
SOM Figure 5: Close up dissecting microscope images, taken before (pH 8.22) and after pH 7.60 treatment incubation. a) *Marginopora vertebralis*, **b)** *Amphistegina radiata*, **c)** *Heterostegina depressa*, **d)** *Peneroplis* **sp., individuals. Sizes are stated as largest possible diameter of individuals. Both** *Amphistegina* **and** *Heterostegina* **showed signs of bleaching. Symbiont clumping in** *Amphistegina* **is indicated by white dashed circles**.

SOM Table 1: Relationships between ΔO_2 and ΔH^+ per individual within each species at different pCO_2 treatments (Figure 7). Linear-model results with significant effects at the 5 % level are indicated in bold.

	Estimate	SE	t	p	R^2	p_{tm}
Marginopora vertebralis						
Intercept	-36.005	12.244	-2.941	**0.0187**	0.80	**0.0036**
ΔO_2	0.0116	0.1612	0.072	0.9446		
pCO_2 treatment	4.3394	1.5518	2.796	**0.0233**		
$\Delta O_2 : pCO_2$ treatment	-0.0045	0.0204	-0.222	0.8299		
Amphistegina radiata						
Intercept	-28.620	11.744	-2.437	**0.0408**	0.70	**0.0166**
ΔO_2	-1.0420	0.5022	-2.075	0.0717		
pCO_2 treatment	3.4731	1.4950	2.323	**0.0487**		
$\Delta O_2 : pCO_2$ treatment	0.1237	0.0622	1.989	0.0819		
Heterostegina depressa						
Intercept	-14.865	6.4727	-2.297	0.0507	0.85	**0.0012**
ΔO_2	0.1693	0.3218	0.526	0.6132		
pCO_2 treatment	1.7840	0.8203	2.175	0.0613		
$\Delta O_2 : pCO_2$ treatment	-0.0283	0.0417	-0.680	0.5159		
***Peneroplis* sp.**						
Intercept	-13.038	3.7634	-3.464	**0.0085**	0.63	**0.0371**
ΔO_2	0.8398	0.2972	2.826	**0.0223**		
pCO_2 treatment	1.5781	0.4768	3.310	**0.0107**		
$\Delta O_2 : pCO_2$ treatment	-0.1090	0.0382	-2.853	**0.0214**		
***Quinqueloculina* sp.**						
Intercept	-6.7470	5.7909	-1.165	0.309	0.66	0.1885
ΔO_2	-1.8837	1.9174	-0.982	0.382		
pCO_2 treatment	0.8514	0.7536	1.130	0.322		
$\Delta O_2 : pCO_2$ treatment	0.2333	0.2498	0.934	0.403		
***Miliola* sp.**						
Intercept	-5.3733	4.0374	-1.331	0.254	0.76	0.1006
ΔO_2	3.9626	2.7794	1.426	0.227		
pCO_2 treatment	0.6460	0.5145	1.256	0.278		
$\Delta O_2 : pCO_2$ treatment	-0.4918	0.3538	-1.390	0.237		

R^2 constitutes the multiple R^2 explaining total variance of the overall model.
p_{tm} depicts the significance of the total model.

Losers and winners in coral reefs acclimatized to elevated carbon dioxide concentrations

Katharina E. Fabricius[1]*, Chris Langdon[2], Sven Uthicke[1], Craig Humphrey[1], Sam Noonan[1], Glenn De'ath[1], Remy Okazaki[2], Nancy Muehllehner[2], Martin S. Glas[3] and Janice M. Lough[1]

Experiments have shown that ocean acidification due to rising atmospheric carbon dioxide concentrations has deleterious effects on the performance of many marine organisms[1-4]. However, few empirical or modelling studies have addressed the long-term consequences of ocean acidification for marine ecosystems[5-7]. Here we show that as pH declines from 8.1 to 7.8 (the change expected if atmospheric carbon dioxide concentrations increase from 390 to 750 ppm, consistent with some scenarios for the end of this century) some organisms benefit, but many more lose out. We investigated coral reefs, seagrasses and sediments that are acclimatized to low pH at three cool and shallow volcanic carbon dioxide seeps in Papua New Guinea. At reduced pH, we observed reductions in coral diversity, recruitment and abundances of structurally complex framework builders, and shifts in competitive interactions between taxa. However, coral cover remained constant between pH 8.1 and ~7.8, because massive *Porites* corals established dominance over structural corals, despite low rates of calcification. Reef development ceased below pH 7.7. Our empirical data from this unique field setting confirm model predictions that ocean acidification, together with temperature stress, will probably lead to severely reduced diversity, structural complexity and resilience of Indo-Pacific coral reefs within this century.

Rising atmospheric CO_2 from the burning of fossil fuels and deforestation affects marine systems in several ways. Through its effect on the global climate, it increases sea surface temperatures (now 0.7 °C higher than in pre-industrial times) and intensifies storm and rainfall variability, altering salinity and the terrestrial runoff of nutrients and sediments[8]. It also causes profound changes in sea water chemistry. Atmospheric CO_2 concentrations of ~390 ppm already exceed by 50–100% the historic envelope of 200–300 ppm in the past >2 million years[9]. The resulting increased partial pressure of carbon dioxide (pCO_2) in sea water has already reduced mean surface seawater pH by 0.1, thus lowering carbonate ion concentrations by 30 μmol kg^{-1}, and the saturation state of sea water for calcium carbonate minerals (Ω) by ~15%, although the magnitude of these effects varies regionally and with latitude[1,5,10,11].

The declining pH, termed 'ocean acidification', is predicted to have profound implications for marine ecosystems because carbonate ions are an essential substrate for biotic calcification. Coral reefs are of particular concern because their many tens of thousands of species ultimately depend on the structural complexity derived from the corals' carbonate skeletons[5,6]. However, specific knowledge about the capacity of reef ecosystems to acclimatize and/or adapt to long-term exposure to lowered pH (increased pCO_2

and reduced Ω) remains inadequate. Much of our understanding stems from short-term laboratory perturbation experiments of individual organisms or from deterministic models. Perturbation experiments report variable and sometimes severe responses in many marine plants, invertebrates and vertebrates at lowered pH, such as declining calcification, altered physiologies and some effects on survival[2-4]. Although laboratory experiments are indispensable, most are too brief for full organism acclimatization to occur, and co-limiting factors (for example nutrients, currents and irradiance) are difficult to simulate *ex situ*[12,13]. Experiments also provide little information about processes leading to ecosystem adaptation, such as altered reproduction, competition, food webs and disease susceptibility, or genetic adaptation. There is therefore a great need for empirical data documenting the long-term effects of ocean acidification on marine ecosystems acclimatized to high pCO_2, as found around submarine CO_2 vents. Recently, changes in shallow-water marine rocky shore ecosystems have been investigated at volcanic CO_2 vents in the Mediterranean, documenting major declines in many calcifying and non-calcifying organisms and increases in macroalgae and seagrasses at reduced seawater pH (refs 7,14).

Here we report the effects of natural *in situ* exposure to elevated seawater pCO_2 on tropical coral reef communities, coral growth, recruitment, seagrasses and sedimentary properties. The study is based on field investigations of clear-water coral reefs and seagrass communities around three cool volcanic seeps of ~99% CO_2 gas, and at three adjacent control sites with similar geomorphology, seawater temperature and salinity, that fringe the D'Entrecastraux Islands, Milne Bay Province, Papua New Guinea (Supplementary Figs S1, S2, Table S1).

Coral communities at 3 m depth were compared between control sites ('low pCO_2': bubble streams >5 m from the transect lines, medians per site 7.97–8.14 pH at total scale, 296–494 ppm pCO_2) and reef sections with moderate seep activity ('high pCO_2': bubble streams <5 m from the transect lines, pH 7.73–8.00, 444–953 ppm pCO_2; Fig. 1a,b, Supplementary Fig. S3, Table S2). The median saturation state of sea water for the calcium carbonate mineral aragonite (Ω_{arag}) was 3.5 at the control sites and 2.9 at the seeps. The zones of most vigorous venting were covered by sand or rocks with individual coral colonies, macroalgae or dense seagrass (Fig. 1c, Supplementary Fig. S4). No reef development was found at a pH less than 7.70 (>1,000 ppm CO_2), and hence the most intensely venting zones were excluded from the reef assessment.

The field surveys showed that at high compared with low pCO_2 sites, hard coral cover was similar (33% versus 31%; Fig. 2a, Supplementary Table S3). However, the cover of massive *Porites*

[1]Australian Institute of Marine Science, PMB 3, Townsville, Queensland 4810, Australia, [2]University of Miami Rosenstiel School of Marine and Atmospheric Science, 4600 Rickenbacker Causeway, Florida 33149, USA, [3]Max-Planck Institute for Marine Microbiology, Department of Biogeochemistry, Celsiusstr. 1, 28395 Bremen, Germany. *e-mail: k.fabricius@aims.gov.au.
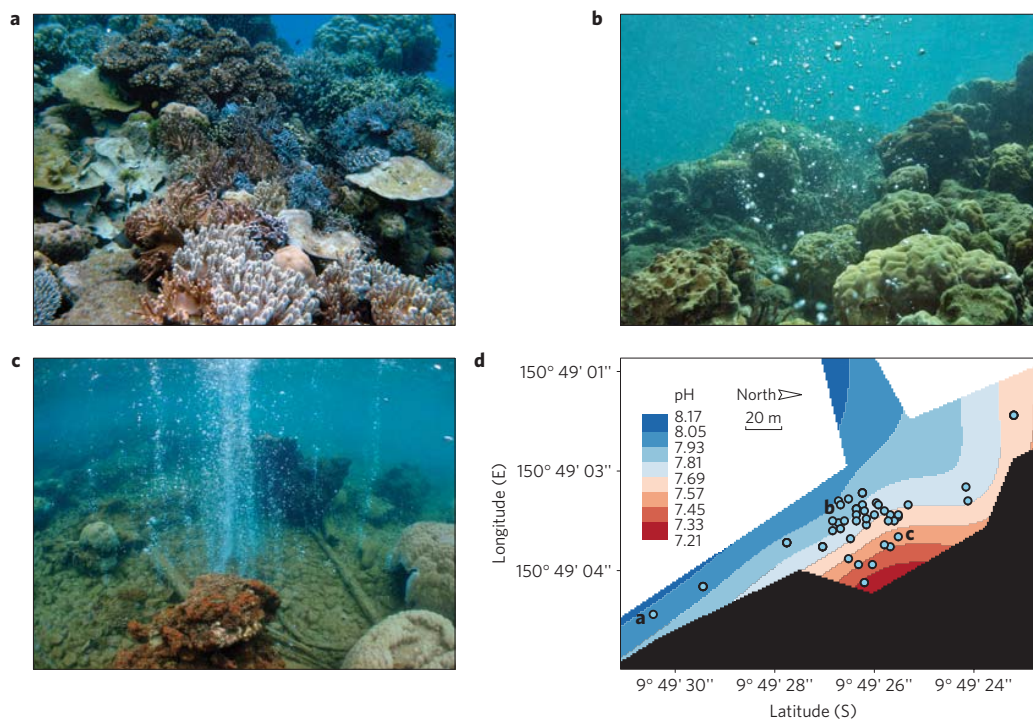
Figure 1 | Volcanic CO₂ seeps of Milne Bay. Seascapes at **a**, control site ('low pCO$_2$': pH ∼ 8.1), **b**, moderate seeps ('high pCO$_2$': pH 7.8–8.0), and **c**, the most intense vents (pH < 7.7), showing progressive loss of diversity and structural complexity with increasing pCO$_2$. **d**, Map of the main seep site along the western shore of Upa-Upasina (marked as grey; map: Supplementary Fig. S1). Colour contours indicate seawater pH, and the letters indicate the approximate locations of seascapes as shown in **a**–**c**.

corals doubled, whereas the cover of structurally complex corals (with branching, foliose, and tabulate growth forms, that is, excluding massive, submassive and encrusting growth forms) was reduced three fold. The taxonomic richness of hard corals was reduced by 39%. The cover of fleshy non-calcareous macroalgae doubled and seagrass increased eight fold, whereas the cover of crustose coralline algae (important calcareous substrata for coral settlement) and of other red calcareous algae was reduced seven fold. Cover and richness of soft corals and sponge cover were also significantly reduced. The density and taxonomic richness of hard coral juveniles were reduced 2.8- and 2-fold, respectively, and of soft coral juveniles 18- and 12-fold, at the high pCO$_2$ sites (Fig. 2b). Even juvenile densities of massive *Porites* declined >fourfold at high pCO$_2$, despite the high representation of this taxon in the adult community.

The pH for each 10-m section along the study transects at the largest seep site (Upa-Upasina) was spatially predicted from the observed pH data (Supplementary Fig. S3). As seawater pH declined from 8.1 to 7.8, reef communities gradually changed, without a clear threshold (Fig. 3, Supplementary Table S4). In particular, hard coral richness, coral juveniles, and crustose coralline algae progressively declined with declining pH.

Differences in rates of calcification and tissue thickness in massive *Porites* between the high and low pCO$_2$ sites were small (Fig. 2c, Supplementary Table S3). However, massive *Porites* colonies were paler at high pCO$_2$, and had almost twice the density of externally visible macrobioeroders in their living surfaces compared to low pCO$_2$ sites. Similarly, *in situ* growth measurements found small differences in linear extension in the ubiquitous coral *Pocillopora damicornis*. Clades of endosymbiotic dinoflagellate algae did not change in response to high pCO$_2$ in *P. damicornis* (90% with clade D1, 10% with C1 at both seeps and controls) and *Acropora millepora* (100% with clade C3).

At both the high and low pCO$_2$ sites in Milne Bay, mean calcification rates of massive *Porites* over the past 12 years were 30% lower than expected given their latitude[15] (Fig. 4). This finding is in agreement with an increasing body of data that show that rates of calcification in massive *Porites*, *P. damicornis* and other corals have declined by 14–30% over the past ∼2 decades in large geographic regions around the world, with the two global factors, temperature stress and/or ocean acidification, considered the most likely cause(s)[16,17]. Milne Bay summer maximum sea surface temperatures have exceeded the long-term averages in 9 of these last 12 years[18]. Severe coral bleaching occurred in the region in 1996, followed by minor bleaching in 1998 and 2000–2001 (Supplementary Information). The similar and low calcification rates at the high and low pCO$_2$ sites suggest that calcification in massive *Porites* is relatively insensitive to a reduction to pH 7.8, and that another factor (possibly temperature stress) has had a stronger effect on calcification. Nevertheless, even massive *Porites* were infrequent near the most intense vents where seawater pH was <7.7, in agreement with experiments showing a 55–75% reduction in *Porites* calcification at pH 7.49 and 7.19 compared to that at ambient pH (ref. 19).

Seagrass communities at the intense seeps (>500 ppm pCO$_2$) had three to four times higher shoot densities and below-ground biomass compared with those at the control site, but reduced diversity (Fig. 2d). On seagrass blades, calcareous epiphyte cover and densities of the large foraminifera *Marginopora vertebralis* were both nearly zero near the seeps. The increases in seagrass and macroalgal cover and reductions in epiphytes and carbonate organisms are similar to the findings reported from volcanic CO₂ vents in the Mediterranean[7].

Surface sediments at high pCO$_2$ sites were almost free of inorganic carbon, calcareous biota and their remains (foraminifera, small gastropods and calcareous spicules; Fig. 2e), whereas

LETTERS
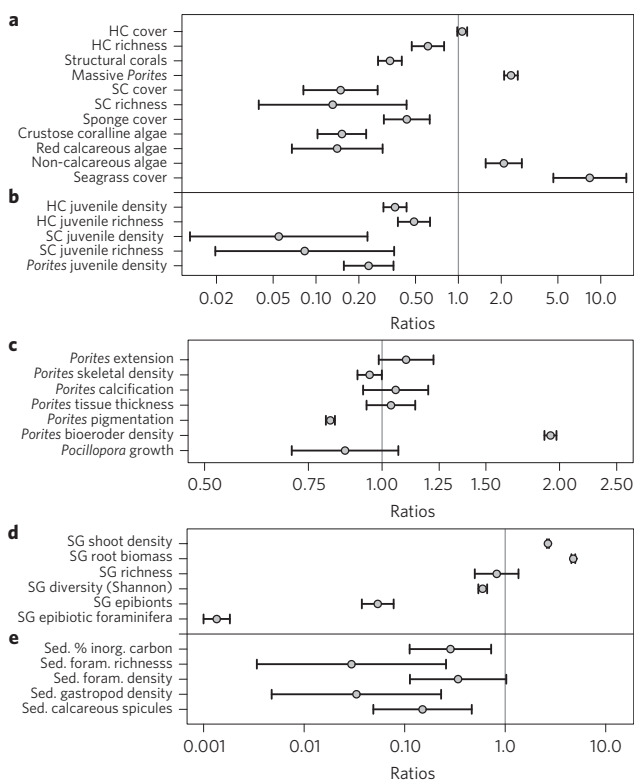
Figure 2 | Response ratios (high pCO$_2$/low pCO$_2$, averaged across the three reefs), summarizing the observed biotic changes. Differences are significant at the 5% level if the error bars (upper and lower 2 SE) do not include the value 1.0. The panels include **a**, reef communities including hard and soft corals (HC, SC); **b**, juvenile corals; **c**, skeletal extension, density and calcification, tissue thickness, colony pigmentation and densities of externally visible macrobioeroders in massive *Porites*, and linear extension in *Pocillopora damicornis*; **d**, seagrass (SG) shoot density, below-ground biomass, diversity, epibiont cover, densities of foraminifera; **e**, sediment properties and associated calcifying biota. Foram. is Foraminera, sed. is sedimentary and inorg. is inorganic.

organic carbon, nitrogen and siliceous spicules did not change along the pH gradient. Indeed, across the high pCO$_2$ sites, total seawater alkalinity was elevated by ~50 µEquiv kg^{-1} sea water (Supplementary Table S2), suggesting continued net carbonate dissolution. The more sparsely seeping Esa'Ala high pCO$_2$ site sediments still contained ~5% inorganic carbon (controls: 6–10%), however many foraminifera tests were corroded or pitted.

The implications of the observed ecological changes for the future of coral reefs are severe. The decline in structurally complex framework-forming corals at lowered pH is likely to reduce habitat availability and quality for juvenile fish and many invertebrates[20]. The low coral juvenile densities (including those of *Porites*) probably slows coral recovery after disturbance, suggesting reduced community resilience. The loss of crustose coralline algae that serve as settlement substratum for coral larvae probably impedes larval recruitment, and the doubling of non-calcareous macroalgae reduces the available space for larvae to settle. Susceptibility to storm breakage would also increase, if internal macrobioeroder densities in massive *Porites* are indicative of borer densities in other coral taxa and reef substrata. Indeed, high bioerosion rates have been reported from reefs where deepwater upwelling reduces Ω_{arag} (ref. 21). However, the causal mechanisms and implications of these and many other of the observed changes, such as
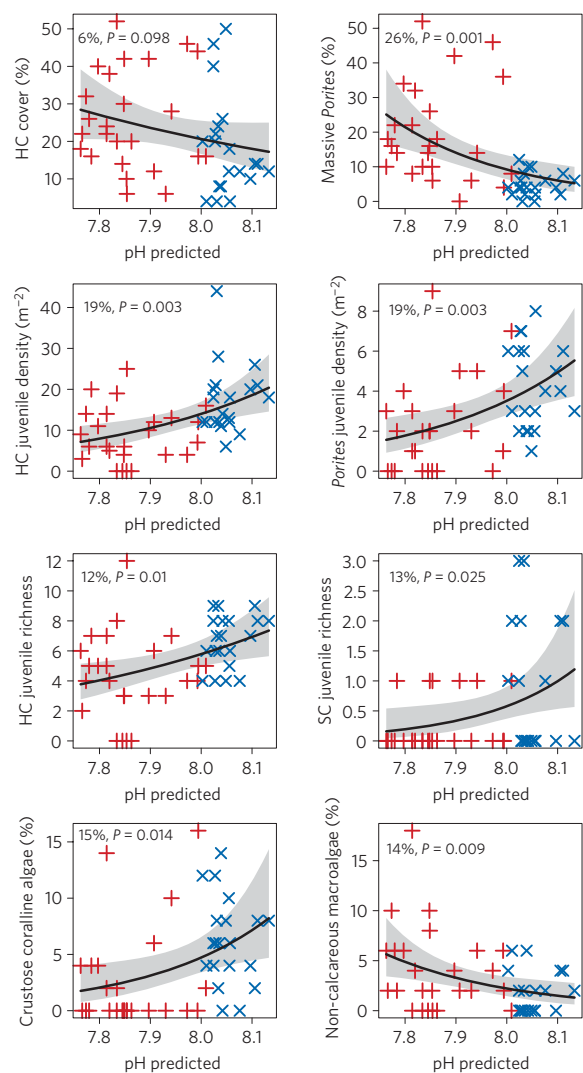
Figure 3 | Progressive changes in reef biota along a pH gradient at Upa-Upasina Reef. Red and blue symbols indicate high and low pCO$_2$ transect sections respectively, and mean pH was predicted from seawater measurements ($N = 74$; Supplementary Fig. S3A and B). The black lines indicate the log-linear fits and the grey bands indicate upper and lower 2 SE. Also presented are the percentage variance explained by pH, and the significance of the relationships. Abbreviations as in Fig. 2.

increased macroalgal cover and bioeroder densities, and declines in sponges, soft corals and numerous other taxa at lowered pH remain poorly understood.

Natural limitations exist in using the Milne Bay CO$_2$ seeps as proxies to assess the future of coral reefs. The seeps are surrounded by areas with ambient pH, supplying larvae of sensitive taxa for recolonization, and hence partly offsetting the negative effects of ocean acidification on recruitment. As a result of wave mixing, pCO$_2$ approaches background values during windy periods, providing respite from low pH, especially during the trade-wind seasons. The Milne Bay seeps are located within the coral triangle at 9° latitude, where conditions for reef development are ideal; reefs at higher latitudes with low Ω_{arag} may be more susceptible to ocean acidification. Reefs around the seeps are also under relatively low anthropogenic pressures (Supplementary Information), and it is likely that ocean acidification may affect reefs more severely if they are already stressed from terrestrial runoff or overfishing.
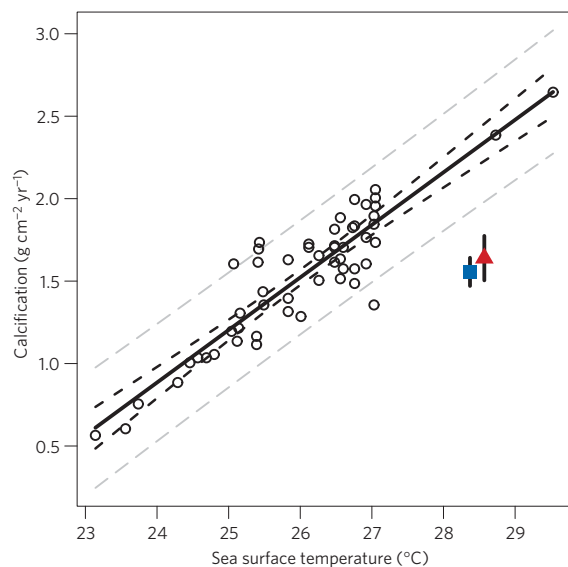
Figure 4 | Mean rates of calcification of massive *Porites* at the Milne Bay seep sites and other Indo-Pacific regions as a function of mean annual sea surface temperature. Circles represent colonies from many Indo-Pacific regions (averaged over 1961–1990; $N = 10$–15 colonies per point; from ref. 15). Solid line: linear regression fit, black and grey dashed lines: upper and lower 95% confidence and prediction intervals, respectively. Red triangle and blue square: calcification of massive *Porites* at high- and low-$p\text{CO}_2$ sites, respectively ($N = 17$ and 12 colonies; vertical bars: upper and lower SE).

Bearing in mind these caveats, our data nevertheless suggest that tropical coral reefs with high coral cover can still exist at seawater pH of 7.8 (750 ppm $p\text{CO}_2$, 150 µmol kg^{-1} carbonate ions, or Ω_{arag} 2.5), albeit with severe losses in biodiversity, structural complexity and resilience. As pH declines from 8.1 to 7.8, the loss of the stenotopic fast-growing structurally complex corals progressively shifts reef communities to those dominated by slow-growing, long-lived and structurally simple eurytopic massive *Porites* (Fig. 1a,b). As a result of this shift in species composition, coral cover seems to be unaltered during the transition from 8.1 to ~7.8 pH units. Reef development ceases at 7.7 pH units (980 ppm $p\text{CO}_2$, 125 µmol kg^{-1} carbonate ions, 2.0 Ω_{arag}), suggesting these values are terminal thresholds for any form of coral reef development. This threshold is higher than those previously derived from global spatial correlations between aragonite saturation state and reef development[5], possibly because the high latitude reefs and upwelling sites where low aragonite saturation states are naturally found are also exposed to very low or fluctuating temperatures, which is not the case at the Milne Bay seep sites. The threshold is also higher than those derived from deterministic model predictions, possibly because these models assess pH changes and projected increases in temperature stress simultaneously[6] (the seeps are not yet subjected to the projected warming of >2 °C).

The rate of atmospheric CO_2 increase continues to accelerate, with emission scenarios predicting CO_2 concentrations of 540–970 ppm and a decline in seawater pH by 0.14–0.35 units globally (to 7.9–7.7 units, $\Omega_{\text{arag}} = 3.0$–2.1) for 2100 (refs 8,22). The range of exposures of the seep sites are therefore comparable to end-of-century $p\text{CO}_2$ projections (however, without the additional stress due to the predicted warming). Our study demonstrates that many ecological properties in coral reefs will gradually change as pH declines to 7.8, and that it would be catastrophic for coral reefs if seawater pH dropped below 7.8 (at 750 ppm $p\text{CO}_2$). We have shown here that large differences in sensitivity between organisms to

declining pH result in complex changes in tropical ecosystems, with a few taxa and processes winning, but many more losing prominence. Temperature stress leading to reduced coral calcification (for example in massive *Porites*) has the potential to further accelerate and exacerbate the losses. Our data add to the mounting body of evidence that shows a rapid transition to a low CO_2 emissions future is necessary to minimize the risk of profound losses of coral reef ecosystem functions and services, not only due to climate change, but also due to ocean acidification.

Methods

Chemical analyses. Volcanic gas samples were collected by pooling gas from 10 separate bubble streams in replicate 250 ml glass bottles, and analysed with a micro gas chromatograph (Hewlett Packard M200; Supplementary Table S1). A small boat deployable $p\text{CO}_2$ monitoring system (showerhead equilibrator, LiCOR 820 Infrared Gas Analyser linked to a GPS, and submersible pump) was used to measure $p\text{CO}_2 \sim 1$ m above the benthos. Water samples were taken with a Niskin bottle or by divers. One aliquot was immediately analysed for temperature and salinity with a YSI Model 30 Portable Conductivity, Salinity and Temperature Meter. Another aliquot was analysed for pH (within 1 h) using a Mettler Toledo pH probe and meter, and converted to the total pH scale[23]. Two more aliquots were fixed with mercuric chloride and stored in 125 ml PET bottles for later determination of total alkalinity ('open-cell' Gran titration[23]) and dissolved inorganic carbon (UIC Coulometer). Other seawater parameters (Ω_{arag}, $p\text{CO}_2$) were calculated from pH, total alkalinity, salinity and temperature using CO2SYS (ref. 24). Salinity was measured with a Guildline 8410A Portable Salinometer. Seawater elemental composition was analysed with an inductively coupled plasma-optical emission spectrometer (ICP-OES) (Varian).

Biotic responses. Fifty-metre-long transects were laid shore-parallel at 3 m depth (5 and 4 transects at the seep and control sites of Upa-Upasina, respectively, 2 each at the seep and control sites of Esa'Ala and Dobu). Photographs were taken every metre along the transects for later analysis of benthic cover and reef community composition[25], and all scleractinian and octocoral juveniles (<5 cm diameter) were recorded *in situ* within a 0.30 m wide belt. Proximity to seeps (<5 m or >5 m) was used to classify each 10-m transect section as high or low $p\text{CO}_2$.

For retrospective analyses of growth rates in massive *Porites*, short cores (~25 cm long, 3.5 cm diameter) were extracted from the upper surfaces of >0.5 m tall colonies at 3 m depth ($N = 29$; 4–8 cores from each site). Cores were sliced, X-rayed to identify annual density bands, and skeletal density was measured with an americium-241 gamma densitometer[15]. The rate of calcification was defined as the product of annual linear extension (growth between adjacent density minima) and skeletal density, and averaged over the past 12 years for each core (the period common to all but one of the cores). Tissue thickness was determined along the core cross-sections. Macrobioeroder densities (counts of all externally visible orifices), and colony surface pigmentation (colour chart readings[26]) were investigated *in situ* on 20–29 massive *Porites* colonies per site.

In-situ short-term skeletal growth rates of the coral *Pocillopora damicornis* were determined with an optical micrometer (Keyence 7,000 LED/CCD). *P. damicornis* was chosen for this study because, unlike in many other structurally complex corals, sufficient replicates were found even at the high $p\text{CO}_2$ sites. One 40–50 mm branch was collected from each of 15 colonies at the high and low $p\text{CO}_2$ sites of Upa-Upasina (3 m depth). These were glued to base plates, and their height in relation to a reference rod determined before and after a 6-day deployment at the collection sites.

Denaturing gradient gel electrophoresis (DGGE) fingerprinting of the second ribosomal internally transcribed spacer (ITS2), in combination with sequencing[27], was used to identify the endosymbiotic algae associating with *A. millepora* and *P. damicornis* corals from high and low $p\text{CO}_2$ sites at both Dobu and Upa-Upasina (15 replicate colonies per site and species). ITS2 products were separated using 8% poly-acrylamide gels with a 35–65% denaturant gradient (formamide and urea) in an INGENYphorU DGGE unit for 15 h at 75 V. A representative of each band was cut, re-amplified, sequenced (Macrogen Ltd, Korea), and compared with sequences in the public library GenBank (http://www.ncbi.nlm.nih.gov).

Seagrass shoot density and species composition (dominated by *Cymodocea rotunda* and *Cymodocera serrata*) were quantified in fifteen 400 cm^2 quadrats at <1 m depth at the high and low $p\text{CO}_2$ sites of Esa'Ala. Below-ground biomass was harvested, dried at 60 °C and weighed. Calcareous epibiont cover and foraminifera densities (*Marginopora vertebralis*) on seagrass blades were analysed using photography and *in situ* measurements at the high and low $p\text{CO}_2$ sites of Upa-Upasina and Esa'Ala.

Sediment geochemistry and foraminiferal assemblages in the upper 1 cm sediment layer were assessed along the benthic transects and seagrass sites (20 samples in total). Sediments were wet-sieved (63 µm mesh), dried, weighed, sorted (200 foraminifera per sample), and the abundances of siliceous, calcareous and echinoid spicules, *Halimeda* segments and small gastropods were estimated. Total carbon was analysed in dried and ground sediment samples (LECO Truspec CN Analyzer), and organic carbon and nitrogen were analysed after dissolving

LETTERS

inorganic carbon with 1 M HCl (Shimadzu TOC-V Analyzer, calibrated with the certified reference MESS-1, and two in-house standards).

Statistical methods. Generalized additive models[28] were used to predict pH values from the field observations to each 10-m section of the transects (see below) and to spatial grids of the three reefs for the purposes of display. The degree of smoothness of the spatial smoothers was selected by cross-validation. Despite the patchiness in seawater chemistry, the spatial models explained 44%, 74% and 59% of deviance in the pH data of Upa-Upasina, Dobu and Esa'Ala, respectively (Supplementary Fig. S4). Ratios of observed variables for low to high pCO_2 sites (Fig. 2) were estimated using generalized linear models (GLMs). The models used a log link function to constrain estimated ratios to be non-negative, and their variance was taken to be proportional to the mean[29]. The models also included the effects of reefs, and the reported ratios (Fig. 2, Supplementary Table S3) represent weighted averages across the three reefs. GLMs were also used to assess changes in biota along the pH gradient at Upa-Upasina (Fig. 3, Supplementary Table S4). All statistical analyses used the software R (ref. 30).

References

1. Feely, R. *et al*. Impact of anthropogenic CO_2 on the $CaCO_3$ system in the oceans. *Science* **305**, 362–366 (2004).
2. Doney, S. C., Fabry, V. J., Feely, R. A. & Kleypas, J. A. Ocean acidification: The other CO_2 problem. *Annu. Rev. Mar. Sci.* **1**, 169–192 (2009).
3. Kroeker, K. J., Kordas, R. L., N, C. R. & Singh, G. G. Meta-analysis reveals negative yet variable effects of ocean acidification on marine organisms. *Ecol. Lett.* **13**, 1419–1434 (2010).
4. Hendriks, I. E., Duarte, C. M. & Alvarez, M. Vulnerability of marine biodiversity to ocean acidification: A meta-analysis. *Estuar. Coast. Shelf Sci.* **86**, 157–164 (2010).
5. Kleypas, J. A. *et al*. Geochemical consequences of increased atmospheric carbon dioxide on coral reefs. *Science* **284**, 118–120 (1999).
6. Hoegh-Guldberg, O. *et al*. Coral reefs under rapid climate change and ocean acidification. *Science* **318**, 1737–1742 (2007).
7. Hall-Spencer, J. *et al*. Volcanic carbon dioxide vents show ecosystem effects of ocean acidification. *Nature* **454**, 96–99 (2008).
8. IPCC *Climate Change 2007: Synthesis Report* (eds Pachauri, R.K. & Reisinger, A.) (Cambridge Univ. Press, 2007).
9. Hönisch, B. *et al*. Atmospheric carbon dioxide concentration across the mid-Pleistocene transition. *Science* **324**, 1551–1554 (2009).
10. Orr, J. C. *et al*. Anthropogenic ocean acidification over the twenty-first century and its impact on calcifying organisms. *Nature* **437**, 681–686 (2005).
11. Key, R. M. *et al*. A global ocean carbon climatology: Results from Global Data Analysis Project (GLODAP). *Glob. Biogeochem. Cycles* **18**, GB4031 (2004).
12. Langdon, C. & Atkinson, M. Effect of elevated pCO_2 on photosynthesis and calcification of corals and interactions with seasonal change in temperature/irradiance and nutrient enrichment. *J. Geophys. Res.* **110**, C09S07 (2005).
13. Atkinson, M. J. & Cuet, P. Possible effects of ocean acidification on coral reef biogeochemistry: Topics for research. *Mar. Ecol. Prog. Ser.* **373**, 249–256 (2008).
14. Cigliano, M. *et al*. Effects of ocean acidification on invertebrate settlement at volcanic CO_2 vents. *Mar. Biol.* **157**, 2489–2502 (2010).
15. Lough, J. M. Coral calcification from skeletal records revisited. *Mar. Ecol. Prog. Ser.* **373**, 257–264 (2008).
16. De'ath, G., Lough, J. M. & Fabricius, K. E. Declining coral calcification on the Great Barrier Reef. *Science* **323**, 116–119 (2009).
17. Manzello, D. P. Coral growth with thermal stress and ocean acidification: Lessons from the eastern tropical Pacific. *Coral Reefs* **29**, 749–758 (2010).
18. Reynolds, R. W. *et al*. An improved *in situ* and satellite SST analysis for climate. *J. Clim.* **15**, 1609–1625 (2002).
19. Krief, S. *et al*. Physiological and isotopic responses of scleractinian corals to ocean acidification. *Geochim. Cosmochim. Acta* **74**, 4988–5001 (2010).
20. Wilson, S. K. *et al*. Habitat degradation and fishing effects on the size structure of coral reef fish communities. *Ecol. Appl.* **20**, 442–451 (2010).
21. Manzello, D. *et al*. Poorly cemented coral reefs of the eastern tropical Pacific: Possible insights into reef development in a high-CO_2 world. *Proc. Natl Acad. Sci. USA* **105**, 10450–10455 (2008).
22. Feely, R. A., Doney, S. C. & Cooley, S. R. Ocean acidification: Present conditions and future changes in a high-CO_2 world. *Oceanography* **22**, 36–47 (2009).
23. Dickson, A. G., Sabine, C. L. & Christian, J. R. (eds) *Guide to Best Practices For Ocean CO_2 Measurements* 191 (PICES Special Publication 3, 2007).
24. Lewis, E. & Wallace, D. W. R. Program developed for CO_2 system calculations'. Report No. ORNL/CDIAC-105, (US Department of Energy, Oak Ridge, Tennessee, 1998).
25. Jonker, M., Johns, K. & Osborne, K. Surveys of benthic reef communities using underwater digital photography and counts of juvenile corals. (Australian Institute of Marine Science, 2008).
26. Siebeck, U. E., Marshall, N. J., Klueter, A. & Hoegh-Guldberg, O. Fine scale monitoring of coral bleaching using a colour reference card. *Coral Reefs* **25**, 453–460 (2007).
27. Sampayo, E. M., Dove, S. & Lajeunesse, T. C. Cohesive molecular genetic data delineate species diversity in the dinoflagellate genus *Symbiodinium*. *Mol. Ecol.* **18**, 500–519 (2009).
28. Wood, S. N. *Generalized Additive Models: An Introduction with R* (Chapman and Hall/CRC Press, 2006).
29. McCullagh, P. & Nelder, J. A. *Generalized Linear Models* (Chapman and Hall, 1989).
30. R_Development_Core_Team R: *A Language and Environment for Statistical Computing* (2011); available at http://www.R-project.org.

Author contributions

All authors were involved with either fieldwork or data analyses. K.E.F. initiated and designed the study and wrote the manuscript, with contributions from all others. C.L. and R.O. analysed the seawater chemistry, C.H., S.N., K.E.F. and J.M.L. collected and analysed the *Porites* data, C.L. the *in situ* coral growth data, K.E.F. and S.N. the reef community data, S.U. the sediments and foraminifera, N.M. and S.U. the seagrass and epibiont data, and G.D. and K.E.F. conducted the statistical analyses.

Supplementary Information to "Losers and winners in coral reefs acclimatized to elevated carbon dioxide concentrations"

by Katharina E. Fabricius, Chris Langdon, Sven Uthicke, Craig Humphrey, Sam Noonan, Glenn De'ath, Remy Okazaki, Nancy Muehllehner, Martin Glas, and Janice M. Lough

Study sites

The study was conducted at three volcanic seep sites at Normanby and Dobu Islands, D'Entrecasteaux Island group, Milne Bay Province, Papua New Guinea (Fig. S1). At each reef, a high CO_2 site around the seeps and a control site were investigated.

Upa-Upasina Reef (north-western Normanby Island) is the largest site with thousands of bubble streams emerging along ~200 x 40 m of reef slope (Fig. S2). Seeps are most intense near the shore at <0.5 m depth, but dense bubble streams are found down to 5 m depth. Village elders confirm these seeps have existed at that location throughout their life (the local traditional site name "Illi Illi Bua Bua" translates to "Blowing Bubbles"). Currents were weak, longshore and tidal, ranging from 2–4 cm s^{-1} during the study; mixing may be much greater during the trade wind season, reverting pH to near background levels. The control site was located 500 m south of the seep site, with a topography similar to the seep site.

Dobu Reef has several intense vents surrounded by dispersed seeps (~120 x 30 m), and experiences periods of high turbidity. It was more wave-exposed than the other sites, and currents ranged from 6–15 cm s^{-1} during the study, suggesting rapid removal and dilution of the CO_2. For the water chemistry, the control samples were taken from the perimeter of the seep, while for the benthic study, the control site was a patch reef 2.5 km from the seep on the western side of Dobu Island.

Esa'Ala Reef (north-eastern Normanby Island) has sparse bubble streams within an area of ~150 x 50 m, and an area of moderate seep activity at the north-eastern edge in a seagrass meadow at 0.5 m depth. Currents were weak, longshore and tidal, ranging from

$4–8$ cm s^{-1} during the study. The control site was 130 m south of the seeps along a reef slope, while the high CO_2 site is slightly recessed and near a boat jetty.

Environmental data for this extremely remote location are sparse. Severe coral bleaching occurred in the Milne Bay region in 1996, followed by minor bleaching in 1998 and 2000–2001 [1,2]. Besides this, the relatively high coral cover and reports by the local communities suggest that reefs in the D'Entrecasteaux Islands region have had a history of relatively low disturbance since the 1996 bleaching event. Tropical cyclones are rare at this latitude, customary fishing tenures may somewhat moderate fishing pressure, and nearly 100% vegetation cover on both islands minimizes terrestrial runoff.

References:

[1]   Davies, J. M., Dunne, R. P., and Brown, B. E., *Marine and Freshwater Research* **48** (6), 513 (1997).

[2]   Munday, P. L., in *Global Coral Reef Monitoring Network (GCRMN) Report 2000*, edited by C. Wilkinson (Australian Institute of Marine Science, Townsville, 2000).

2
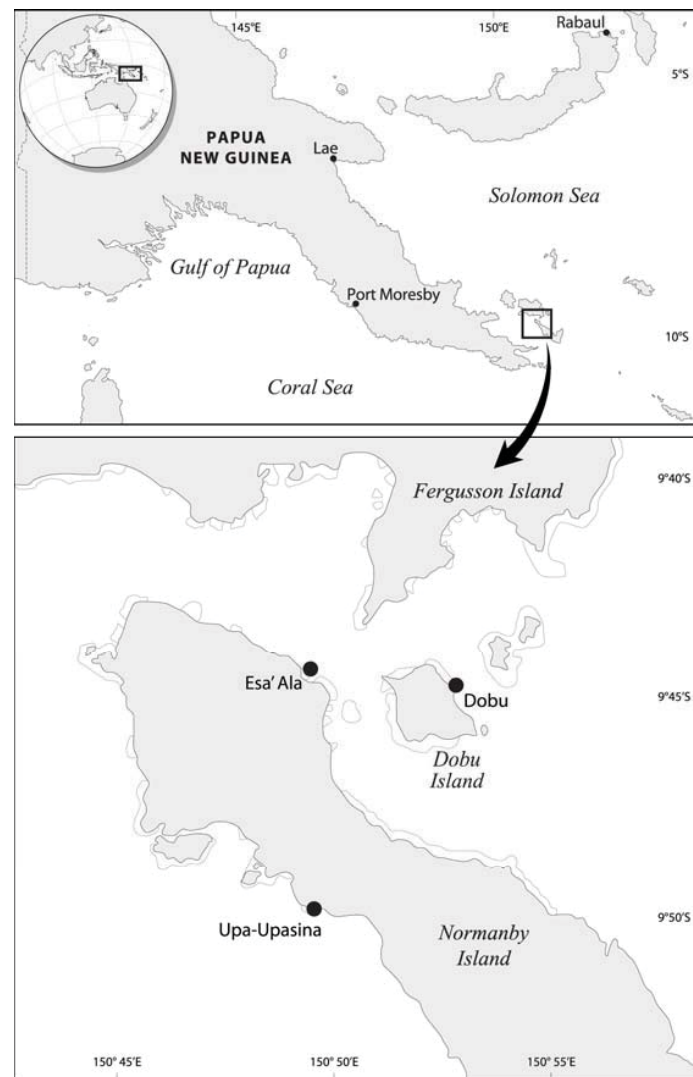
Figure S1: Maps of Papua New Guinea and the three study reefs on Normanby and Dobu Islands, Milne Bay Province.

a

b

c

d

e

f

4

g

h

i

j

k

l

5
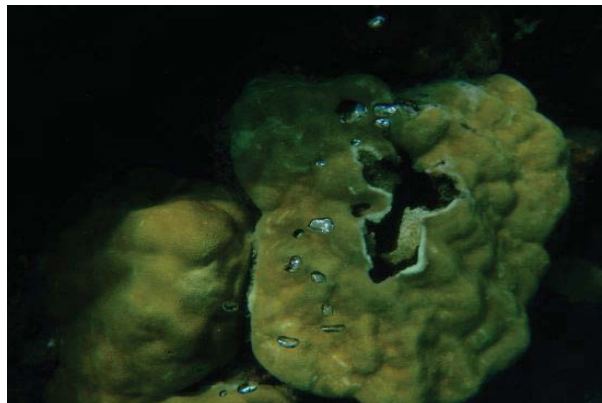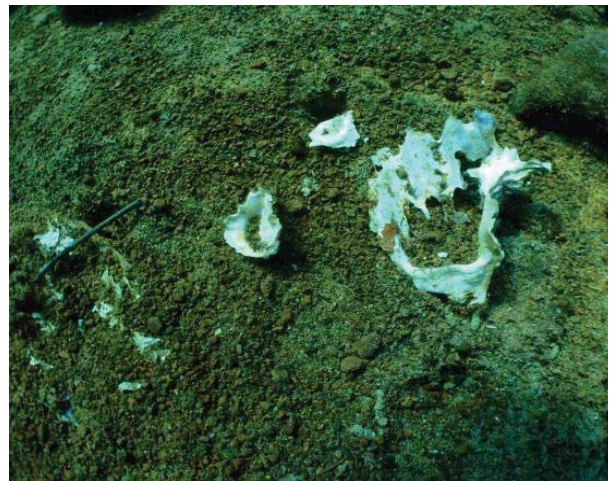
Figure S2 (previous 2 pages): Features of coral reefs at CO_2 seeps and control sites. **a, c, e, f, and g:** Seascapes at the CO_2 seeps, PNG. **b, d:** Massive *Porites* colonies directly in contact with bubbles; their skeletons dissolve from underneath but tissues appear to be unblemished. **h:** Seagrasses within coral reefs; **i:** seagrass meadows with very high biomass at >600 pCO_2. **j:** Heavily etched and eroded shells of oysters and other mollusks. **k, l:** Adjacent coral reefs away from the CO_2 seeps (control sites) with high cover of structurally complex corals and soft corals.

Gas composition

At the Dobu seep site, gas contained 163 ppm H_2S (Table S1) and the smell of hydrogen sulfide was noticeable from the surface. However, seawater concentrations of sulphur were 896-909 mg/L at this and the other sites (Table S2), which is typical for oceanic waters. This suggests that only a small proportion of the H_2S traces entered into the aquatic phase, where it would be oxidized to non-toxic sulfate due to the ~100% O_2 saturation present the site. Corals in contact with bubble streams showed no signs of discoloration, lesions or tissue necrosis (Fig. S2), confirming that the gas is non-toxic to these corals.

Table S1: Composition of the volcanic gases at the three seep sites.

	CO_2 (%)	O_2 (%)	N_2 (%)	CH_4 (ppm)	C_2H_4 (ppm)	H_2S (ppm)	N_2O (ppm)
Upa-Upasina	>99	0.50	0.10	87	0	0	0
Dobu	>99	0.11	0.14	4,360	0	163	0
Esa'Ala	>98	1.22	0.71	3,983	0	0	0

Seawater carbonate chemistry

In the field, seawater pH steeply increased away from each bubble stream, reaching ambient values within <0.1 m of a gentle bubble steam and <5 m at more intense vents. The seep sites are therefore a mosaic of patches with reduced pH, with the local pH depending on the proximity and intensity of bubble streams, surrounded by normal pCO_2 for remnant populations of the more sensitive taxa. At the seep sites of Upa-Upasina and Dobu, median seawater pH was 7.77 and 7.73 units, respectively, compared with values from the control sites (7.97– 8.02) (Table S2, Figs. S3, S4). The reductions in pH were less on windy than on calm days, due to mixing. At the seep site of Esa'Ala, mean pH was only slightly reduced (median = 8.00).

Table S2: Seawater parameters at the three study reefs. Values for the Esa'Ala seep site are split into reef sites and those from the shallow NW seagrass bed (SG).

Reef	Exposure	N	Temperature (°C)			Salinity (PSU)		
			Median	5%ile	95%ile	Median	5%ile	95%ile
Upa-Upasina	Control	6	27.7	27.4	28.6	34.5	34.5	34.6
Upa-Upasina	Seep	31	27.6	27.4	28.1	34.5	34.4	34.6
Dobu	Control	3	28.4	28.2	28.5	34.4	34.4	34.4
Dobu	Seep	7	28.6	28.2	29.1	34.4	34.4	34.4
Esa'Ala	Control	4	27.9	27.9	27.9	34.7	34.6	34.7
Esa'Ala	Seep	11	27.7	27.6	28.0	34.7	34.5	34.7
Esa'Ala	SG Control	2	29.0	27.8	30.1	33.3	33.3	33.3
Esa'Ala	SG Seep	7	27.8	27.7	28.4	34.3	33.6	34.7

Reef	Exp	pH (total scale)			TCO_2			CO_3 (µmol kg^{-1} SW)		
		Med	5%ile	95%ile	Med	5%ile	95%ile	Med	5%ile	95%ile
U	C	8.01	7.99	8.02	2001	1969	2007	212.5	207.2	222.0
U	S	7.77	7.02	7.99	2141	2003	2571	139.3	30.37	208.7
D	C	7.97	7.88	7.97	2016	2014	2061	200.0	171.2	204.5
D	S	7.73	7.09	7.89	2183	2066	2401	134.0	39.3	177.1
E	C	8.02	8.02	8.02	1978	1968	1980	219.5	218.1	223.4
E	S	8.00	7.99	8.02	1999	1990	2004	214.0	207.5	220.0
E	SG-C	8.14	8.1	8.18	1884	1873	1895	274.0	264.1	283.9
E	SG-S	7.99	7.13	8.06	1972	1902	2397	203.0	63.6	235.4

7

Reef	Exp	pCO$_2$ (µatm)			Equilibr. CO$_2$ (ppm)			Ω_{arag}		
		Med	**5%ile**	**95%ile**	**Med**	**5%ile**	**95%ile**	**Med**	**5%ile**	**95%ile**
U	**C**	443	416	456	419	401	436	3.48	3.35	3.66
U	**S**	846	454	5737	502	377	992	2.28	0.49	3.37
D	**C**	494	485	628	1000	631	1157	3.24	2.79	3.48
D	**S**	953	606	5213	1545	819	1747	2.20	0.64	2.89
E	**C**	418	409	423	382	379	390	3.62	3.58	3.69
E	**S**	444	423	460	425	374	605	3.53	3.39	3.66
E	**SG-C**	296	262	330	NA	NA	NA	4.31	4.15	4.47
E	**SG-S**	492	379	9007	602	495	652	3.37	1.02	3.75

Reef	Exp	TA (µmol kg^{-1} SW)			Ca^{2+} (mg L^{-1})			Ba (mg L^{-1})		
		Med	**5%ile**	**95%ile**	**Med**	**5%ile**	**95%ile**	**Med**	**5%ile**	**95%ile**
U	**C**	2296	2277	2305	421	419	426	0.002	0.001	0.002
U	**S**	2319	2292	2480	421	418	424	0.001	0.000	0.004
D	**C**	2293	2293	2298	419	415	434	0.002	0.002	0.005
D	**S**	2319	2302	2360	417	415	419	0.002	0.001	0.003
E	**C**	2288	2277	2291	428	425	428	NA	NA	NA
E	**S**	2298	2286	2304	430	422	434	NA	NA	NA
E	**SG-C**	2288	2286	2289	NA	NA	NA	NA	NA	NA
E	**SG-S**	2272	2190	2349	428	427	430	NA	NA	NA

Reef	Exp	Cl (mg L^{-1})			K (mg L^{-1})			Mg (mg L^{-1})		
		Med	**5%ile**	**95%ile**	**Med**	**5%ile**	**95%ile**	**Med**	**5%ile**	**95%ile**
U	**C**	22428	18827	23597	365.0	364.2	368.2	1366	1362	1384
U	**S**	21702	19300	24632	364.8	362.4	367.4	1364	1355	1376
D	**C**	22236	20307	23526	362.0	362.0	369.2	1357	1348	1380
D	**S**	21933	19832	25014	363.0	361.9	364.2	1350	1347	1357
E	**C**	22326	21477	23892	366.9	365.1	369.4	1388	1379	1391
E	**S**	24983	23104	27892	369.6	361.9	371.3	1394	1365	1405
E	**SG-C**	NA	NA	NA	NA	NA	NA	NA	NA	NA
E	**SG-S**	25841	21963	26854	370.2	367.2	372	1394	1384	1395

Reef	Exp	Na (mg L⁻¹)			S (mg L⁻¹)			Sr (mg L⁻¹)		
		Med	5%ile	95%ile	Med	5%ile	95%ile	Med	5%ile	95%ile
U	C	10151	10130	10300	901.0	899.5	908.2	8.58	8.54	8.68
U	S	10151	10062	10235	899.4	895.8	905.2	8.60	8.51	8.76
D	C	10105	10039	10327	896.0	894.2	908.6	8.55	8.47	9.27
D	S	10059	10023	10106	895.2	894.0	899.5	8.50	8.48	8.55
E	C	10286	10212	10307	906.0	901.6	909.6	8.67	8.62	8.69
E	S	10345	10106	10410	911.2	888.1	916.8	8.72	8.57	8.84
E	SG-C	NA	NA	NA	NA	NA	NA	NA	NA	NA
E	SG-S	10379	10272	10387	909.3	901.8	910.4	8.70	8.70	8.75
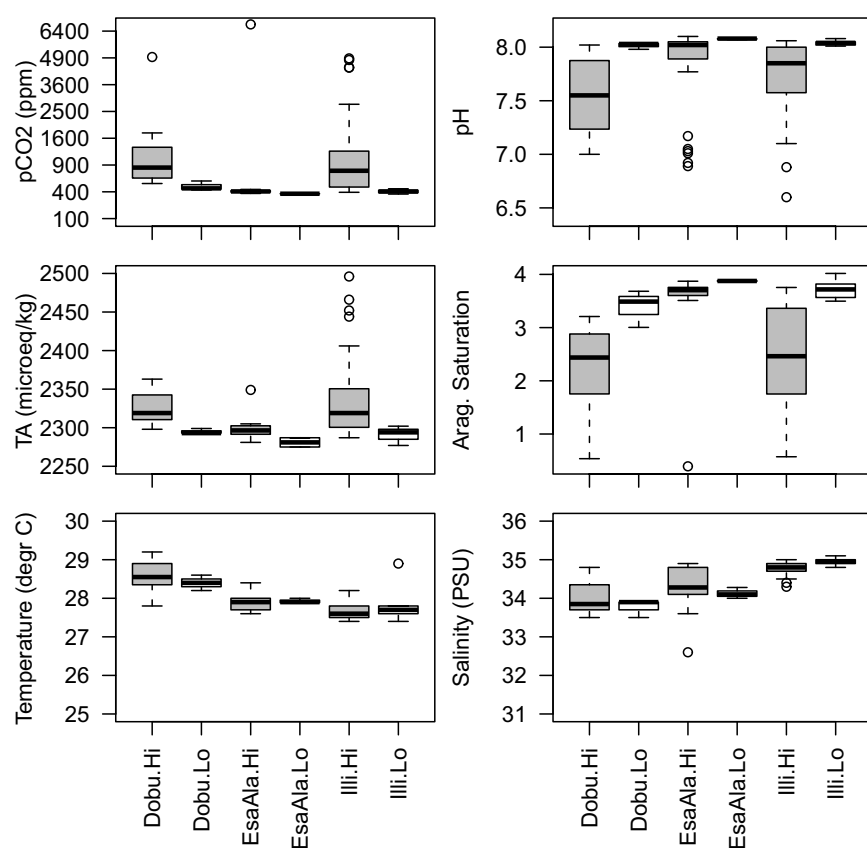
Figure S3: Observed seawater chemistry data at the three volcanic CO_2 seep sites of Milne Bay. Grey bars = High pCO_2, white bars = Low pCO_2 (control sites).

9
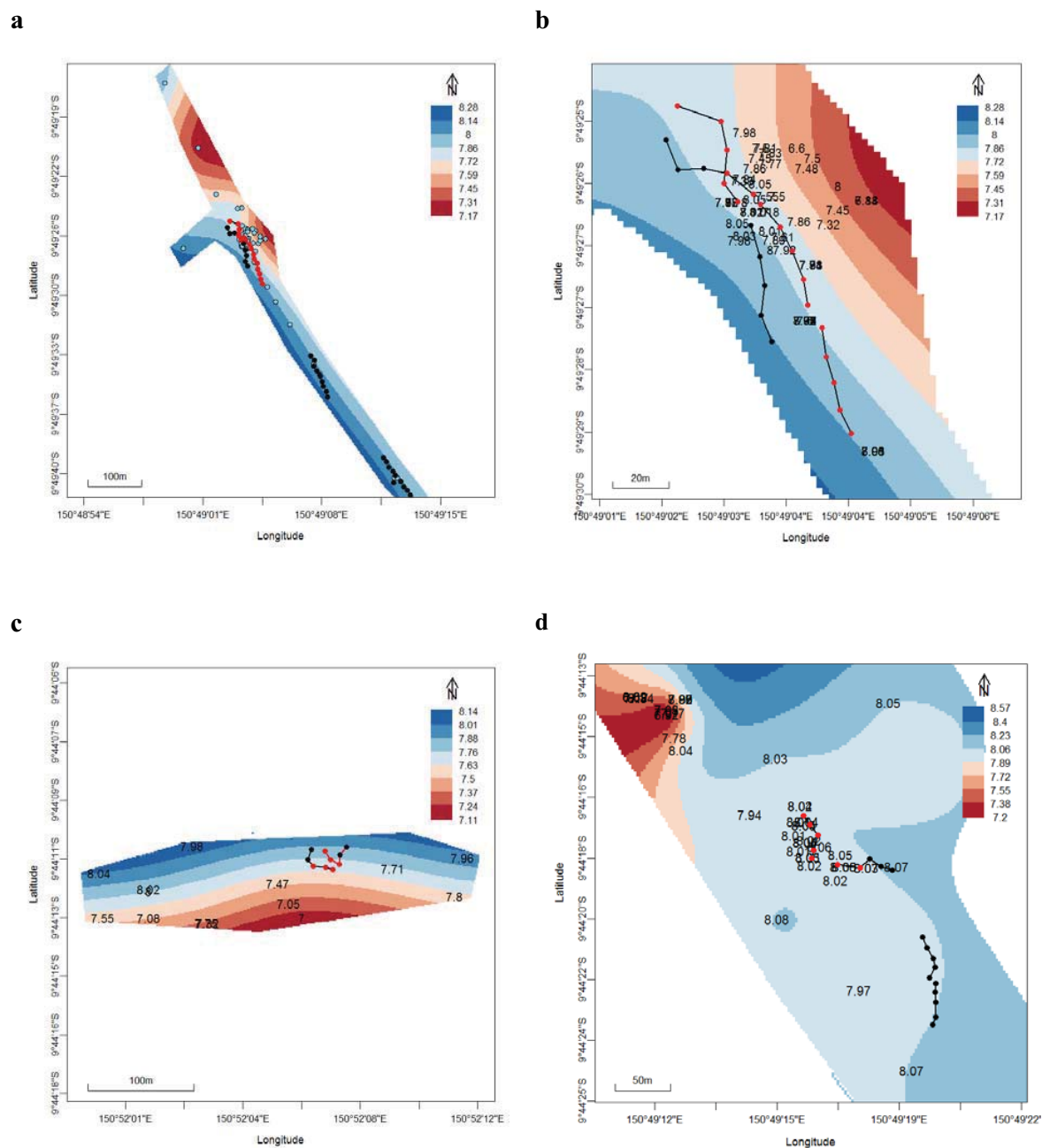
Figure S4: Location of transects and predicted seawater pH (total scale, ambient temperature) at the volcanic CO_2 seeps of Milne Bay. (**a** and **b**) Upa-Upasina($R^2 = 0.44$, N=74 seawater samples), (**c**) Dobu ($R^2 = 0.74$, N=9); (**d**) Esa'Ala ($R^2 = 0.59$, N=17). Red and black dots: Red and black dots indicated High and Low pCO_2 sections along the 50-m transects. Blue dots (**a**) and pH values (**b–d**): locations of seawater samples.

Biotic responses

Table S3: Log ratios of physiological and ecological variables measured at the High and Low pCO_2 reef sections (Fig. 2). Means are back-transformed logged values. N = Number of sampling units (transect sections, *Porites* cores, *Pocillopora* colonies, seagrass plots and sediment samples).

	N	Mean Low pCO₂	Mean High pCO₂	Ratio H/L	Ratio +2SE	Ratio − 2SE
Reef benthic cover and richness:						
Hard coral (% cover)	85	30.8	32.8	1.06	1.15	0.98
Massive *Porites* (% cover)	85	10.7	24.9	2.3	2.61	2.09
Hard coral richness (taxa transect^{-1} section)	85	4.25	2.60	0.61	0.79	0.47
Structural coral (% cover)	85	12.9	4.27	0.33	0.40	0.27
Pocillopora damicornis (% cover)	85	0.58	0.33	0.57	2.27	0.15
Crustose coralline algae (% cover)	85	6.15	0.93	0.15	0.23	0.10
Macroalgae red calcareous (% cover)	85	1.89	0.27	0.14	0.29	0.07
Macroalgae non-calcareous (% cover)	85	1.60	3.33	2.08	2.79	1.56
Soft coral cover (% cover)	85	2.69	0.40	0.15	0.27	0.08
Soft coral richness (taxa transect^{-1})	85	0.76	0.10	0.13	0.43	0.04
Sponges (% cover)	85	2.76	1.20	0.43	0.63	0.3
Seagrass (% cover)	85	0.25	2.13	8.38	15.12	4.65
Coral juveniles:						
Hard coral juvenile density (m^{-2})	85	12.7	4.57	0.34	0.43	0.30
Hard coral juvenile richness (taxa transect^{-1})	85	5.13	2.50	0.49	0.63	0.38
Soft coral juvenile density (m^{-2})	85	1.22	0.07	0.06	0.23	0.01
Soft coral juvenile richness (taxa transect^{-1})	85	0.80	0.07	0.08	0.35	0.02
Porites juvenile density (m^{-2})	85	3.98	0.93	0.23	0.35	0.16
P. damicornis juvenile density (m^{-2})	85	0.31	0.23	0.76	2.17	0.26

Coral colonies:						
Porites linear extension (cm yr^{-1})	27	1.11	1.22	1.10	1.22	0.99
Porites skeletal density (g cm^{-3})	27	1.39	1.33	0.95	1.00	0.91
Porites rate of calcification (g cm^{-2} yr^{-1})	27	1.55	1.63	1.06	1.20	0.93
Porites tissue thickness (mm)	27	3.63	3.76	1.04	1.14	0.94
Porites pigmentation (color chart score)	150	3.8	3.1	0.82	0.83	0.80
Porites macrobioeroder density (m^{-2})	150	149	288	1.93	1.98	1.89
P. damicornis growth rate (µm day^{-1})	30	38.0	32.8	0.87	1.07	0.70
Seagrass and epibionts:						
Seagrass shoot density (m^{-2})	15	1367	3641	2.66	2.73	2.60
Seagrass below-ground biomass (g m^{-2})	15	342	1628	4.8	4.98	4.55
Seagrass richness (plot^{-1})	15	4.72	3.88	0.82	1.36	0.50
Seagrass Shannon (plot^{-1})	15	138	83	0.60	0.66	0.54
Seagrass epibionts (%)	51	21.9	1.19	0.05	0.08	0.04
Seagrass epibiotic foraminifera (m^{-2})	51	1206	1.63	0.001	0.002	0.001
Sediments and calcareous biota:						
Sediment inorganic carbon (%)	20	7.39	2.10	0.29	0.73	0.11
Sediment nitrogen (%)	20	0.03	0.04	1.47	2.91	0.75
Sediment organic carbon.(%)	20	0.17	0.40	2.34	6.14	0.89
Sediment foraminfera density (g^{-1})	10	55.3	1.64	0.03	0.26	0.003
Sediment foraminifera richness (taxa g^{-1})	10	20.0	6.80	0.34	1.03	0.11
Sediment gastropods density (g^{-1})	10	12.3	0.41	0.03	0.23	0.01
Calcareous spicules density (g^{-1})	10	5.89	0.89	0.15	0.47	0.05

Table S4: Gradual changes of reef biota along the pH gradient in Upa-Upasina Reef. Results of generalized linear models (Fig. 3).

	Estimate	SE	t-value	P	R2	% Change pH 8.1 to 7.7
Hard coral (% cover)	-1.36	0.80	-1.69	0.098	0.064	+65%
Massive *Porites* (% cover)	-4.23	1.23	-3.44	0.001	0.262	+378%
Hard coral juvenile richness (taxa transect^{-1})	1.87	0.75	2.50	0.016	0.132	-50%
Structural coral (% cover)	3.59	2.47	1.45	0.154	0.068	-74%
Hard coral w/out *Porites* (% cover)	2.58	1.31	1.98	0.055	0.086	-62%
Hard coral juvenile density (m^{-2})	2.83	0.90	3.13	0.003	0.19	-65%
Porites juvenile density (m^{-2})	3.41	1.08	3.15	0.003	0.189	-72%
Hard coral juvenile richness (taxa transect^{-1})	1.80	0.67	2.69	0.010	0.124	-49%
Soft coral juvenile density (m^{-2})	5.17	2.59	1.99	0.053	0.111	-85%
Soft coral juvenile richness (taxa transect^{-1})	5.44	2.35	2.32	0.025	0.128	-87%
Crustose coralline algae (% cover)	4.16	1.63	2.56	0.014	0.148	-79%
Macroalgae non-calcareous (% cover)	-3.94	1.44	-2.74	0.009	0.145	+331%

13

Conclusions and perspectives

Conclusions and perspectives

The chapters presented in this thesis investigate microenvironments of marine calcifiers in comparison to bulk seawater conditions. Chapters are first discussed individually and later merged to a common conclusion. Perspectives on future research will be given at the end.

1. Chapter 1 - Calcification in foraminifera

In this chapter, chamber formation in a benthic symbiont-free foraminifer (*Ammonia* sp.) was studied. The results show that calcification during chamber formation strongly acidifies the extracellular microenvironment around the foraminifera, and that the acidification is a direct consequence of calcite precipitation to maintain pH homeostasis. The foraminifera exert tight control over the external acidification and thus the H^+-transport-pathways. The results further provide indirect evidence that the site of calcification must be a small volume ($<$ 3 µm thick) and delineated, via protoplasmic membranes, from the surrounding seawater. These findings are not in contradiction with the notion of high-pH vesicles or a high-pH calcification site (Introduction - Figure 10), but rather support this idea, with the addendum, that the site of calcification must be delineated from the cytosol and surrounding seawater. This is in accordance with earlier observations on the chamber formation process of benthic foraminifera (Angell 1979, Be et al. 1979, Erez 2003, Hemleben et al. 1986). By creating a high pH site for calcification, compared to the surrounding seawater and the neighboring cytosol, an efficient DIC trap would be created, facilitating bilateral diffusion of CO_2 into such a compartment. Transport of DIC to the calcification site is therefore thought to occur via CO_2 diffusion and not via HCO_3^- or CO_3^{2-} pumps. Additionally, pH elevation in such a compartment will increase super saturation with respect to calcite, which facilitates $CaCO_3$ precipitation. Calcification in *Ammonia* thus shows many similarities with calcification mechanisms of corals (Jokiel 2011) and coccolithophores (Taylor et al. 2011). All of them calcify in very small delineated compartments and display a strict control over the saturation state of their calcifying fluids and thus H^+-transport-pathways.

The results suggest that the trans-membrane transport of H^+ during calcification to the extracellular space could be a widespread mechanism in unicellular calcifiers, since transport pathways are short and H^+ expulsion thus represents an energy efficient way to maintain pH homeostasis. It is therefore anticipated that external acidification during calcification is also measurable in other calcareous symbiont-free species of foraminifera.

The building blocks for calcification, i.e. Ca^{2+}, DIC and the co-incorporated (trace) elements and stable isotopes must originate from the foraminiferal microenvironment. One implication of the results is thus related to the interpretation of foraminiferal shell proxy signals. Recent results indicate that Ca^{2+} - and therefore quite likely also DIC - are actively taken up during chamber formation in *Ammonia* sp. (Nehrke et al. unpublished data), and not stored in intracellular pools as previously suggested for *Amphistegina lobifera* and *Amphisorus hemprichii* (ter Kuile et al. 1989). Yet, long lasting microenvironmental acidification has a significant effect on ion speciation (e.g. boric acid / borate) and carbonate ion concentrations within the foraminiferal microenvironment (Wolf-Gladrow et al. 1999). Carbonate ion concentrations have been shown to affect both $^{18}O/^{16}O$ and $^{13}C/^{12}C$ ratios in the calcareous shells of different unicellular organisms including foraminifera (Spero et al. 1997, Ziveri et al. 2011). All relationships described to date between carbonate ion concentration of seawater and oxygen isotope fractionation are linear, but slopes between species differ considerably (Ziveri et al. 2011). Assuming that the carbonate chemistry in the microenvironment around the growing chamber of *Ammonia* is the carbonate chemistry relevant for oxygen isotope fractionation, the effect of a pH drop from 8.08 to 6.31 (measured pH minimum) on oxygen isotope fractionation can be estimated. Using the shallowest slope, the measured pH minimum of pH 6.31 would cause a 0.33 ‰ difference, while using the steepest slope would yield a 3.67 ‰ difference of $d^{18}O_{calcite}$-$d^{18}O_{water}$ (Ziveri et al. 2011). Additionally, within their natural habitats, i.e. sediments with decreased diffusivity, compared to natural seawater, this pH effect is expected to be more pronounced. Calcification itself might thereby constitute a strong "vital effect" for carbonate chemistry and pH dependent proxy interpretations. This hypothesis could be tested by measuring microenvironmental pH and O_2 dynamics around calcifying and non calcifying foraminifera, together with subsequent shell proxy analyses. Techniques applied should combine pH and O_2 fluorescence imaging and microsensor pH and O_2 measurements of the foraminiferal microenvironments, with subsequent NanoSIMS or laser ablation coupled mass spectrometry analyses of foraminiferal shells, to test for $^{18}O/^{16}O$, $^{13}C/^{12}C$ and boric-acid/borate ratios.

2. Chapter 2 - Microenvironmental conditions in black band disease and cyanobacterial patch lesions

This chapter investigated the biogeochemistry of the coral lesions black band disease (BBD) and cyanobacterial patch (CP) in relation to their virulence. The results from this study indicate that biogeochemical microgradients (mainly hypoxia, high sulphide and low pH),

shaped by the complex microbial communities of BBD and CP mats as a whole, are the trigger for the virulence of these lesions, rather than a defined pathogen (according to Koch's postulate). By covering and trapping deleterious microchemical conditions close to the coral tissue, BBD strongly aids degradation of coral tissue, which contributes to the progression of these lesions across coral colonies.
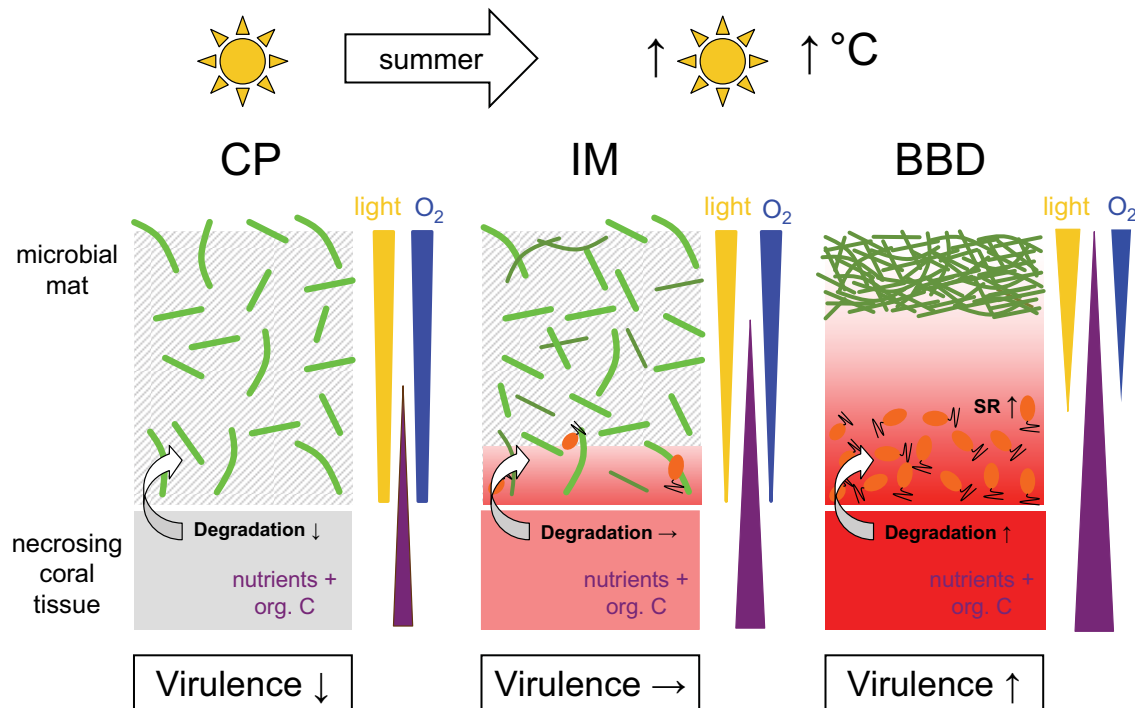
Figure 1: Functional model describing the transition from the coral lesion 'cyanobacterial patch' (CP), via an intermediate stage (IM), to fully developed BBD lesions. CP associated cyanobacterial *Blennothrix* spp. are indicated in light green, BBD associated *Oscillatoria* spp. in darker green and sulphate reducing bacteria in orange. Red shading indicates the increasing presence of sulphide. SR = anaerobic sulphate reduction.

We propose a model, functionally characterizing the transition from CP to BBD (Figure 1), which is based on our cumulative knowledge of the lesions (Glas et al. 2010, Chapter 2, Sato et al. 2009, 2010, 2011). In this model, seasonally elevated light and temperature levels drive a shift in the cyanobacterial community within CP, towards an intermediate stage (Figure 1, IM). Growth or increased cyanobacterial cell densities develop a vertical light gradient within the mat, which will trigger positive phototaxis of motile cyanobacteria towards the surface. This distribution will in addition create vertical O_2 gradients within the mat, resulting in increased hypoxia at its base. Hypoxic to anoxic conditions at the coral-microbial mat interphase will enhance fermentation and desulphuration of degrading coral tissue and lower pH, thus creating favorable conditions for sulphate

reducing bacteria (SRB) at its base. Negative cyanobacterial chemotaxis against increasing sulphide levels will enhance microchemical stratification and consequently disease virulence, resulting in fully developed BBD (Figure 1, BBD). BBD thereby creates a positive feedback loop for its own virulence.

Information that is lacking, but would be required to validate the proposed model, is the inter-migration pattern of the motile cyanobacteria within BBD and CP. Future investigations will combine *in situ* field and controlled laboratory experiments, applying microsensor tools together with hyperspectral measurements of the lesions. By this approach we hope to determine microchemical dynamics, while imaging the migration speed and the inter-migration of associated cyanobacterial filaments, to elucidate the interplay between negative chemotaxis and positive phototaxis on a small scale (< 2 cm^2) within the lesions. Experiments will compare illumination vs. dark, BBD vs. CP, combined with temperature changes and time replicated measurements as the lesions develop. Using this approach, we hope to functionally answer differences in migration speed of CP and BBD, associated with diurnal cycling, light, as well as temperature changes (Sato et al. 2010), and thus gain an holistic understanding of the lesions' etiology.

Another crucial stage in BBD etiology (as in most coral diseases) is the actual onset of the lesions. It is still not clear how BBD infects corals and especially, what factors cause the formation of the complex microbial communities (reviewed in Bourne et al. 2009). Corals naturally suffer from tissue damages, such as predation, fish scrapings, wind-wave breakage, or tissue necrosis. Such lesions often heal or develop into (turf) algae colonized patches (Bak et al. 1977). The above mechanism might indicate that BBD expansion generally originates from micro-algal dominated patches, adjacent to coral tissue. Increases in light and temperature would favor BBD associated cyanobacterial species, leading to the observed transition of microbial communities and ensuing establishment of deleterious microchemical gradients.

3. Chapter 3 - Microchemical conditions around foraminifera at elevated *pCO₂*

This chapter investigated the effects of elevated pCO_2, i.e. ocean acidification conditions, on O_2, pH and Ca^{2+} microgradients around benthic photosymbiotic and symbiont free foraminifera. The results show that both photosymbiotic and symbiont-free species experience strongly decreased microenvironmental pH conditions in light and darkness at elevated pCO_2. Net photosynthesis of photosymbiotic species was not increased at elevated

$CO_{2(aq)}$ concentrations, but microenvironmental pH changes and H^+ concentrations were significantly decreased, as a result of the increased acidity and consequently decreased H^+-buffering-capacity of the seawater. Foraminifera are thus not able to compensate for water column pH decreases within their microenvironment. These results are in accordance with very recent modeling data on pH and H^+ microenvironments of marine phytoplankton (Flynn et al. 2012), suggesting increased microenvironmental H^+ variability around phytoplankton at elevated pCO_2. Increased microenvironmental H^+ variability will most likely exert additional stress on foraminifera. The presented field study investigating natural CO_2 seeps within coral reefs in Papua New Guinea showed almost complete absence of photosymbiotic foraminifera at low pH (7.73-8.00) sites, which supports the idea that foraminifera are quite susceptible to ocean acidification. However, apart from the presented results of this study, there is currently no knowledge of the impacts of lowered seawater pH conditions on foraminiferal cell-physiology, and associated energy demands to maintain pH homeostasis.

O_2 and pH DBL dynamics of photosymbiotic foraminifera and other phototrophic calcifiers, qualitatively correlate in response to illumination changes, with pH dynamics exhibiting a temporal time lag following O_2 dynamics (Kühl et al. 1995, Wolf-Galdrow et al. 1999, de Beer and Larkum 2001, Köhler-Rink and Kühl 2000, 2005). The exact quantitative correlation between O_2 and pH, thus H^+ changes, has to date not been measured and only modeling data exists (Wolf-Gladrow and Riebesell 1997, Wolf-Gladrow et al. 1999). Several of the measured pH profiles exhibited almost linear DBL gradients (Chapter 1-3, Kühl et al. 1995, Rink et al. 1998, Köhler-Rink and Kühl 2000, 2005). The linearity of pH DBL gradients is however not directly intuitive, considering their logarithmic scaling and the fact that protons are buffered in seawater (for extensive discussion see Wolf-Gladrow and Riebesell 1997, Wolf-Gladrow et al. 1999). We aim to disentangle the O_2/pH and O_2/H^+ relationship in more detail, to maintain robust data for DIC-flux-transport-, and consequent H^+-emergence-modeling. Yet, marine calcifiers exhibit a high spatial variability of O_2 and consequently pH DBL development over their surfaces (e.g. Chapter 3, Shashar et al. 1993, Kühl et al. 1995, Köhler-Rink et al. 2000). To establish robust quantitative correlations of O_2/pH for accurate modeling, O_2 and pH microsensor measurements should be conducted simultaneously at a single spot (< 10 µm interspace of sensor-tips) on phototrophic tissue, i.e. time and space aligned. We are currently performing such measurements in the abundant reef coral *Pocillopora damicornis*, in combination with fine scale chlorophyll-a (hyperspectral) imaging and back-reflectance measurements, to characterize the photosynthetic spatial heterogeneity of the tissue (Glas et al. in prep.).

The field study in Papua New Guinea additionally showed dominance of unstructured corals (massive and encrusting growth forms), compared to structured corals (branching, foliose and tabulate growth forms) at high pCO_2. This may hint that beside genus specific differences in tolerance levels, morphology might play an important role in the overall performance of photosymbiotic calcifiers to ocean acidification. In structured corals, like *Pocillopora damicornis,* longitudinal growth occurs mainly via their branching tips. The coral tips are often lightly shaded, have low symbiont densities and photosynthetic rates, compared to the inner parts of the colony, which contribute mostly to secondary thickening of the skeleton (reviewed in Jokiel 2011). The pH microenvironment around branching tips is therefore less elevated in daylight, due to photosynthetic $CO_{2(aq)}$ uptake, compared to other parts of the coral (Glas et al. in prep.). Net calcification decreases, due to increased pCO_2 (Chapter 3, reviewed in Hoegh-Guldberg et al. 2007) are therefore likely to stronger impact on branching tips than on the inner part of the coral colony. It is thus hypothesized that ocean acidification enhances secondary growth (thickening) over longitudinal growth, and consequently un-structured over structured coral growth forms. We are currently addressing this second hypothesis with the approach described above, by comparing O_2/pH ratios across different parts of *Pocillopora damicornis* colonies at different pCO_2 levels.

4. Common conclusion

Many studies have investigated the effects of calcification, respiration, photosynthesis, diseases or sediment exposure on marine calcifiers at the macro-scale. Microenvironmental O_2 and pH dynamics depict the sum of all these metabolic and microenvironmental influences on the surface of marine calcifiers. Even if all of the above parameters are quantified in perturbation experiments for an entire organism, modeling of O_2 and pH DBL dynamics only yield rough approximations, due to their high spatial heterogeneity and many dependencies, such as the local photosynthetic activity, surrounding seawater flow, diffusional transport constrains or tissue surface structure. However, it is often the small scale interactions (< 1 cm in distance) that impose transport limitations, and thus determine the performance of calcifiers (Chapter 2, Wangpraseurt et al. 2012, Weber et al. 2012). Hence, to understand how the above processes functionally connect and impact on marine calcifiers, one must resolve to the microscale level and measure DBL and viscous sublayer dynamics, to characterize transport- and chemical-limitations for the organism.

It can also be concluded that it is largely the metabolism of calcifiers (Chapter 1-3), rather than bulk seawater carbonate system changes (Chapter 3), which determine

microenvironmental O_2, pH and Ca^{2+} dynamics. Yet, as shown, increased pCO_2 levels and ensuing carbonate system changes, are likely to severely alter microenvironmental H^+ concentrations and variability.

There is little known about the physiological effects of lowered pH conditions on marine calcifiers and the associated energy demands to maintain pH homeostasis. However, evidence is growing that prolonged periods of low pH, combined with anoxia, are lethal for coral tissue and that high levels of total sulphide amplify this virulence (Chapter 2, Wangpraseurt et al. 2012, Weber et al. 2012). It is hypothesized that under lowered extracellular pH conditions, energy demands of calcifiers significantly increase to maintain pH homeostasis between their tissues and the surrounding seawater. It is secondly hypothesized that calcifiers meet these increased energy demands by enhancing respiration. The severe shift of pH equilibria over their tissue surfaces for extended periods of time, e.g. by internal calcification (Chapter 1), sediment-exposure (Chapter 2, Weber et al. 2012), microbial-mat cover (Chapter 2) or elevated pCO_2 (Chapter 3), thus stresses marine calcifiers. Hence, if microenvironmental oxygen is depleted, e.g. by microbial mat cover (Chapter 2) or sediment exposure (Chapter 2), corals can if capable revert to fermentation pathways to maintain pH homeostasis, though such a switch yields little energy for the animal (Weber et al. 2012). If lowered pH conditions and anoxia prevail for extended periods of time, failing pH homeostasis of the tissue would result in mortality. This view would explain why anoxia or low pH conditions alone (Chapter 1, Chapter 3) do not harm calcifiers, if conditions are reversed back normal within hours or a few days. In addition, photosymbiotic calcifiers regularly experience prolonged periods of microenvironmental hypoxia and low pH conditions at night, to which they are naturally adapted (e.g. Shashar et al. 1993, Kühl et al. 1995, Köhler-Rink and Kühl 2000, 2005, Weber et al. 2012). Hence, diffusional O_2 transport constrains seem to play an important role in the O_2 supply of the tissues. If diffusional resistance is too high to fulfill respiratory demands, e.g. by microbial mat- or sediment-cover, pH homeostasis may not be maintained and organisms ultimately suffocate. It was recently shown that sediment dwelling, benthic calcareous foraminifera and other non-calcareous protists, which naturally experience low pH and anoxic conditions for extended periods of time, can respire nitrate, via denitrification and thus overcome oxygen limitations (Piña-Ochoa et al. 2010). The evolution of such respiratory pathways to adapt to hypoxic and low pH habitats is in accordance with the above hypothesis that maintaining pH homeostasis demands a lot of energy and is crucial for most calcifiers. Testing such a hypothesis would require an integrated approach, which should consist of perturbation experiments, testing

single and combined effects of low pH and anoxia on microenvironmental dynamics, calcifier's physiology, and their ecological performances. In practice, such experiments should combine microenvironmental microsensor measurements of O_2 and pH, standard metabolic rate (SMR) measurements, quantification of energy-metabolites such as ATP, ADP and AMP within the exposed tissues, as well as growth-, calcification-, $CaCO_3$-dissolution-, and mortality-rate-measurements.

5. References

Angell RW (1979). Calcification during chamber development in *Rosalina floridana*. Journal of Foraminiferal Research 9: 341-353.

Bak RPM, Brouns JJWM, Heys FML (1977). Regeneration and aspects of spatial competition in the scleractinian corals *Agaricia agaricites* and *Montastrea annularis*. Proceedings of Third International Coral Reef Symposium 1: 143-148.

Be AWH, Hemleben C, Anderson OR, Spindler M (1979). Chamber formation in planktonic foraminifera. Micropaleontology 25: 294-307.

Bourne DG, Garren M, Work TM, Rosenberg E, Smith GW, Harvell CD (2009). Microbial disease and the coral holobiont. Trends in Microbiology 17: 554-562.

de Beer D, Larkum AWD (2001). Photosynthesis and calcification in the calcifying algae *Halimeda discoidea* studied with microsensors. Plant Cell and Environment 24: 1209-1217.

Erez J (2003). The source of ions for biomineralization in foraminifera and their implications for paleoceanographic proxies. Biomineralization 54: 115-149.

Flynn KJ, Blackford JC, Baird ME, Raven JA, Clark DR, Beardall J et al (2012). Changes in pH at the exterior surface of plankton with ocean acidification. Nature Climate Change, advanced online publication: doi:10.1038/nclimate1489

Glas MS, Motti CA, Negri AP, Sato Y, Froscio S, Humpage AR et al (2010). Cyanotoxins are not implicated in the etiology of coral black band disease outbreaks on Pelorus Island, Great Barrier Reef. Fems Microbiology Ecology 73: 43-54.

Hemleben C, Anderson OR, Berthold W, Spindler M (1986). Calcification and chamber formation in foraminifera - a brief overview. In: Leadbeater BSC, Riding R (eds). Biomineralization in lower plants and animals. Oxford University Press: Oxford. pp 237-249.

Hoegh-Guldberg O, Mumby PJ, Hooten AJ, Steneck RS, Greenfield P, Gomez E et al (2007). Coral Reefs Under Rapid Climate Change and Ocean Acidification. Science 318: 1737-1742.

Jokiel PL (2011). The reef coral two compartment proton flux model: A new approach relating tissue-level physiological processes to gross corallum morphology. Journal of Experimental Marine Biology and Ecology 409: 1-12.

Köhler-Rink S, Kühl M (2000). Microsensor studies of photosynthesis and respiration in larger symbiotic foraminifera. I The physico-chemical microenvironment of *Marginopora vertebralis*, *Amphistegina lobifera* and *Amphisorus hemprichii*. Marine Biology 137: 473-486.

Köhler-Rink S, Kühl M (2005). The chemical microenvironment of the symbiotic planktonic foraminifer *Orbulina universa*. Marine Biology Research 1: 68-78.

Kühl M, Cohen Y, Dalsgaard T, Jørgensen BB, Revsbech NP (1995). Microenvironment and photosynthesis of zooxantella in scleractinian corals studied with microsensors for O_2, pH and light. Marine Ecology Progress Series 117: 159-172.

Piña-Ochoa E, Hogslund S, Geslin E, Cedhagen T, Revsbech NP, Nielsen LP et al (2010). Widespread occurrence of nitrate storage and denitrification among Foraminifera and *Gromiida*. Proceedings of the National Academy of Sciences of the United States of America 107: 1148-1153.

Rink S, Kühl M, Bijma J, Spero HJ (1998). Microsensor studies of photosynthesis and respiration in the symbiotic foraminifer *Orbulina universa*. Marine Biology 131: 583-595.

Sato Y, Bourne DG, Willis BL (2009). Dynamics of seasonal outbreaks of black band disease in an assemblage of *Montipora* species at Pelorus Island (Great Barrier Reef, Australia). Proceedings of the Royal Society B-Biological Sciences 276: 2795-2803.

Sato Y, Willis BL, Bourne DG (2010). Successional changes in bacterial communities during the development of black band disease on the reef coral, *Montipora hispida*. ISME Journal 4: 203-214.

Sato Y, Bourne D, Willis B (2011). Effects of temperature and light on the progression of black band disease on the reef coral, *Montipora hispida*. Coral Reefs: 1-9.

Shashar N, Cohen Y, Loya Y (1993). Extreme diel fluctuations of oxygen in diffusive boundary-layers surrounding stony corals. Biological Bulletin 185: 455-461.

Spero HJ, Bijma J, Lea DW, Bemis BE (1997). Effect of seawater carbonate concentration on foraminiferal carbon and oxygen isotopes. Nature 390: 497-500.

Taylor AR, Chrachri A, Wheeler G, Goddard H, Brownlee C (2011). A voltage-gated H^+ channel underlying pH homeostasis in calcifying coccolithophores. PLoS Biol 9: e1001085, advanced online publication: doi:10.1371/journal.pbio.1001085

ter Kuile B, Erez J, Padan E (1989). Mechanisms for the uptake of inorganic carbon by two species of symbiont-bearing foraminifera. Marine Biology 103: 241-251.

Wangpraseurt D, Weber M, Røy H, Polerecky L, de Beer D, Suharsono et al (2012). *In situ* oxygen dynamics in coral-algal interactions. PLoS ONE 7: e31192, advanced online publication: doi:10.1371/journal.pone.0031192

Weber M, de Beer D, Lott C, Polerecky L, Kohls K, Abed RMM et al (2012). Mechanisms of damage to corals exposed to sedimentation. Proceedings of the National Academy of Sciences 109: E1558-E1567.

Wolf-Gladrow D, Riebesell U (1997). Diffusion and reactions in the vicinity of plankton: A refined model for inorganic carbon transport. Marine Chemistry 59: 17-34.

Wolf-Gladrow DA, Bijma J, Zeebe RE (1999). Model simulation of the carbonate chemistry in the microenvironment of symbiont bearing foraminifera. Marine Chemistry 64: 181-198.

Ziveri P, Thoms S, Probert I, Geisen M, Langer G (2011). A universal carbonate ion effect on stable oxygen isotope ratios in unicellular planktonic calcifying organisms. Biogeosciences Discuss 8: 7575-7591.

Schriftliche Erklärung

Gem. § 6(5) Nr.1-3 PromO

Ich erkläre, dass ich

1. die Arbeit ohne unerlaubte, fremde Hilfe angefertigt habe,

2. keine anderen, als die von mir angegebenen Quellen und Hilfsmittel benutzt habe, und

3. die den benutzen Werken wörtlich und inhaltlich entnommenen Stellen als solche kenntlich gemacht habe.

(Datum, Ort) (Unterschrift)

Written declaration

Corr. § 6(5) Nr.1-3 PromO

I state that I

1. have finished this work without illegal help,

2. have used no other sources and aid, than stated, and

3. have cited any references.

(Date, Location) (Signature)